A MULTILEVEL DECISION ANALYSIS METHOD FOR REMEDIATION OF CONTAMINATED SITES UNDER CONDITIONS OF UNCERTAINTY

By

TODD A. WANG

Associate of Science
Dodge City Community College
Dodge City, Kansas
1983

Bachelor of Science
Colorado School of Mines
Golden, Colorado
1986

Submitted to the Faculty of the
Graduate College of the
Oklahoma State University
in partial fulfillment of
the requirements for
the Degree of
MASTER OF SCIENCE
December, 1995

DISCLAIMER NOTICE

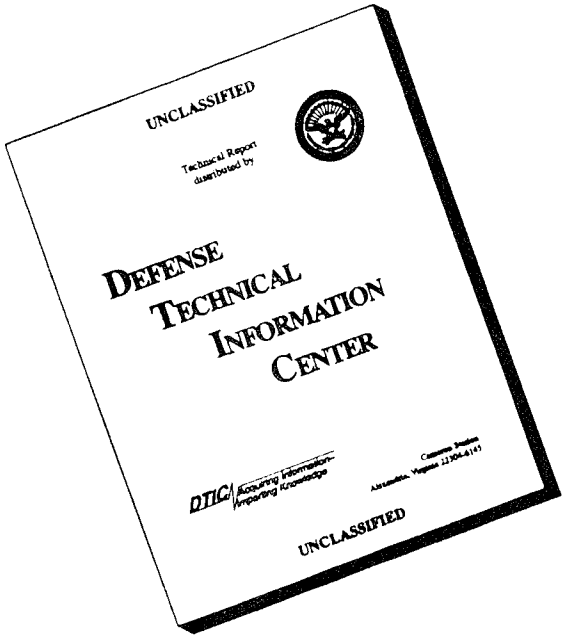

THIS DOCUMENT IS BEST QUALITY AVAILABLE. THE COPY FURNISHED TO DTIC CONTAINED A SIGNIFICANT NUMBER OF PAGES WHICH DO NOT REPRODUCE LEGIBLY.

A MULTILEVEL DECISION ANALYSIS METHOD FOR REMEDIATION OF CONTAMINATED SITES UNDER CONDITIONS OF UNCERTAINTY

By

TODD A. WANG

Associate of Science
Dodge City Community College
Dodge City, Kansas
1983

Bachelor of Science
Colorado School of Mines
Golden, Colorado
1986

Submitted to the Faculty of the
Graduate College of the
Oklahoma State University
in partial fulfillment of
the requirements for
the Degree of
MASTER OF SCIENCE
December, 1995

A MULTILEVEL DECISION ANALYSIS METHOD

FOR REMEDIATION OF CONTAMINATED

SITES UNDER CONDITIONS OF

UNCERTAINTY

Thesis Approved:

William F. McKenna

Thesis Advisor

Gregory J. Wilber

Dean of the Graduate College

PREFACE

This study was conducted to provide a decision analysis methodology for military commanders and their staffs when confronted with an environmental contamination problem. The methodology was based on an established problem solving foundation that was adapted to incorporate uncertainty analysis of imperfect data and quantify the uncertainty with respect to time. The methodology provided a link between the uncertainty analysis and a decision optimization model which can be applied to strategic, operational or tactical level decision making.

I wish to express my sincere appreciation to my primary advisor and mentor, Dr. William F. McTernan for his guidance, assistance and friendship. I also would like to express gratitude towards the other members of my thesis committee; Dr. Samir M. Ahmed, Dr. Gregory G. Wilber and Dr. Keith D. Willett for their assistance and pertinent commentary during the course of this work.

I would like to give special appreciation to Colonel Otis Williams, Commander of the Tulsa District, United States Army Corps of Engineers as well as his staff for their support, suggestions and friendship. This research would not have been possible without the data and resources made available by Major Patrick Caraway, Cliff Murry and Ken Kebble.

TABLE OF CONTENTS

Chapter Page

LIST OF TABLES

LIST OF FIGURES

Figure Page

Figure Page

NOMENCLATURE

AT123D	analytical transport one-, two- or three-dimensional model
COA	course of action
CORA	Cost of Remediation Alternative software program
CSC	United States Command and Staff College, Fort Leavenworth, Kansas
C(t)	remedial action cost function
DAM	decision analysis methodology
DNAPL	dense non-aqueous phase liquid
DOD	United States Government Department of Defense
EMV	estimated monetary value
EPA	United States Environmental Protection Agency
FCAP	capital cost for failure
FOM	operational and maintenance cost for failure
FM	United States Army field manual
HH&E	human health and environment
i	index rate for money
LHAAP	Longhorn Army Ammunition Plant
MCL	maximum contaminant level
MOM	operation and maintenance cost for monitoring groundwater

M(t)	monitoring cost function
MW	monitoring well
NEPA	National Environmental Policy Act
NPDES	National Pollutant Discharge Elimination System
O&M	operation and maintenance costs
POC	plane of compliance
$P(sn_x)$	probability for n state of nature
RACAP	capital cost for remedial action
RAOM	operation and maintenance cost for remedial action
R(t)	failure cost function
t	time unit
TCAP	capital cost for testing
TCE	Trichloroethylene
TOM	operation and maintenance cost for testing
T(t)	additional testing cost function
UB 90 CI	upper boundary of the 90% confidence interval
UB 95 CI	upper boundary of the 95% confidence interval
UEP	unlined evaporation pond
USACE	United States Corps of Engineers
VOC	volatile organic compound

CHAPTER I

INTRODUCTION

Defining the Problem

Need for Methodology

It is no secret that the number of federal facilities requiring environmental cleanup is large and the money available for their remediation is getting increasingly tighter. Within the U.S. Army's Installation Restoration Program there are over 15,000 sites identified, 30 of which are listed on the national priority list (Brown, 1993). Under these circumstances the need for optimizing resources and making the right decisions has never been greater. In recent years there has been a general consensus that cleanup of all contaminated sites to their previous pristine level is monetarily infeasible (Hellman and Hawkins, 1988). This has become very apparent within the Department of Defense (DOD) effort to remediate a large number of facilities with increasing budgetary constraints. Therefore a management approach has been to optimize resources and reduce the risk to human health and environment (HH&E) to a level acceptable to the general public and regulators. The approach may seem simple but the problems involve uncertainty of the situation and numerous decisions which can make solving the problem a very complex and monumental task. Decisions concerning level of risk, criteria for site evaluation, remediation alternatives, uncertainty of data and other parameters are very complex issues that decision makers must incorporate into a decision making process.

Decision making is problem solving, and most often it is done with some degree of uncertainty. As the complexity and uncertainty of a problem increases, the decision maker's ability to keep it all in perspective and analyze a myriad number of factors is lessened. Decision making was once considered an art but has since been developed into a science called decision analysis (Baird 1978). Decision analysis provides a rational step-by-step approach to aid in the decision-making process (Ossenbruggen, 1984). Judgment, rather than intuition, is used and it implies a process of forming an opinion or estimate by prudent discernment and comparison (Baird, 1978). Decision analysis allows the decision maker to compartmentalize the problem and think through it in a rational and structured method. The decision analysis methodology (DAM) presented within this thesis uses the fundamentals of decision analysis and links a decision model to stochastic models that quantify uncertainty within economic and environmental frameworks.

A decision tree as shown in Figure 1 is a very convenient way to visualize the decision model and methodology. Decision nodes (square blocks) are sequential and are related to a time line, as shown in Figure 1. Other nodes within the tree represent random events (circles) and terminal nodes (triangles) represent end consequences. Branches between decision nodes and random event nodes represent alternative selections or decisions. Branches between random event nodes and terminal nodes represent the states of nature that are uncontrollable (Ossenbruggen, 1984). These would include, for example, the state of nature that a contaminant plume reached a monitoring well. Every decision or alternative leads to a consequence that has a certain probability of occurring. Sometimes the probability of occurrence is known but usually is uncertain and may be determined using models. This is where stochastic modeling assists in determining

probabilities. This DAM framework systematically assists the decision maker in determining the best alternative based on a cost and risk minimization strategy under conditions of uncertainty. The present worth values of capital cost and future monetary value of loss to property and human life are used as the measures of the consequence (Ossenbruggen, 1984). The consequence will depend upon the alternative chosen and the actual state of nature.

Figure 1. Decision tree used to select alternatives under uncertain conditions.

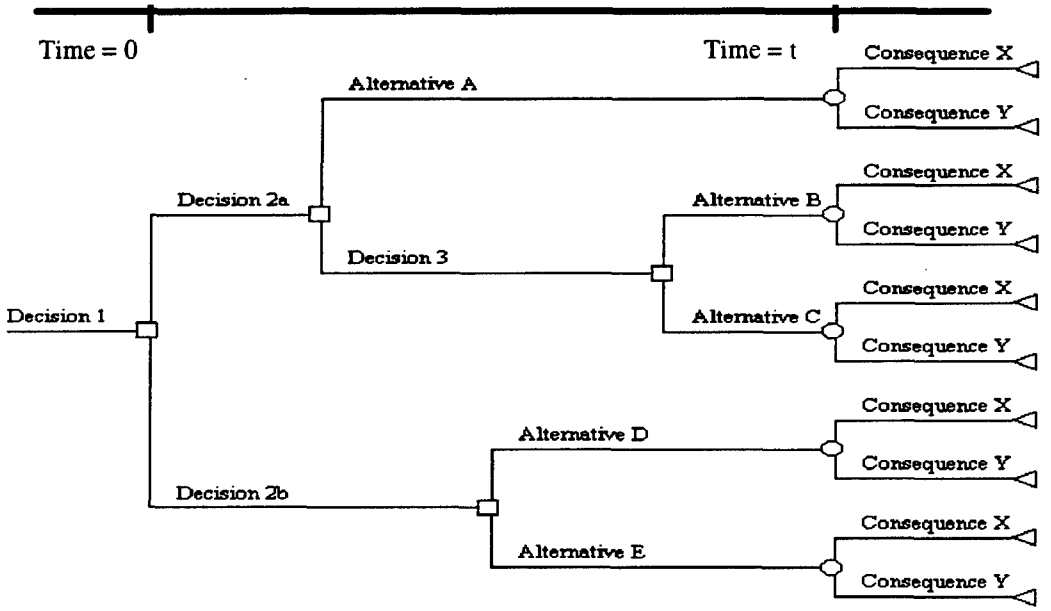

The fundamental goal of this thesis was to develop a decision-oriented methodology within a framework that was conducive to various situations at the tactical, operational and strategic levels of decision making. These levels of decision making were considered synonymous to the levels of war as defined in the U.S. Army Field Manual 100-5, Operations, June 1993. In this way, an existing planning structure already familiar to military planners could be applied to an alternative approach. Activities at the strategic level establish policy, requirements, objectives, develop plans and provide resources to

achieve objectives at the strategic level (FM 100-5, 1993). This is equivalent to strategic environmental policy making that encompasses social, political and economic issues. An example would be the passing of the National Environmental Policy Act (NEPA) by Congress, where environmental strategic policy was made by developing requirements, objectives and authority to achieve objectives within the act. At the tactical level, operations are planned and executed to accomplish more specific objectives that are assigned from the operational level (FM 100-5, 1993). Similarly, tactics is on-the-ground problem solving that is usually rapid and dynamic in nature (FM 100-5, 1993). At this level, the decision maker has been provided guidance and resources but must utilize the resources to their fullest potential. An example in environmental remediation would be the directing of remedial actions through movement of equipment and personnel to achieve the remedial objective.

The operational level is the link between strategy and tactics where major operations are planned, conducted and sustained to accomplish strategic objectives within an area of operations (FM 100-1, 1994). Operational decision making involves enforcement of environmental policy, direction and allocation of resources, issuance of guidance concerning strategic policy and setting priorities. Using the NEPA example, the Environmental Protection Agency (EPA) exercises operational control through promulgation and enforcement of NEPA regulations. Additionally the EPA provides guidance regarding the regulations and the intentions of the act. These types of actions are considered operational because they link strategic policy to tactical actions.

Users of Methodology

The structure of the DAM presented in this thesis is suitable for both private and governmental users at various decision making levels. Flexibility is a key feature of this methodology in that it can be applied at the three decision making levels previously discussed. To illustrate the decision analysis methodology, it was applied to a tactical problem involving groundwater contamination from a federal site. The problem is considered tactical because the decisions involve what remediation actions should be taken within regulatory and budgetary constraints.

Development of Methodology Structure

Military Decision Process

The military decision process is a method developed and used by military leaders to solve problems. This problem-solving method forms the basic foundation from which DAM was developed. The problem solving process, as taught by the U.S. Army's Command and Staff College (CSC) located at Fort Leavenworth, Kansas, has six steps, which are illustrated in Figure 2. Defining the problem, the first step, is critical. Without an accurate definition of the problem, solution is practically impossible. Care must be taken to insure a correct definition, or all subsequent steps will be of no value to the real problem. Gathering facts and information, step 2, is important to making a decision based on judgment rather than intuition. Included in this step is data collection, analysis and evaluation, which provide the decision maker with the facts. Information gathered within this step facilitates estimating the situation, developing courses of action (COA)

and evaluation criteria. An integral part of this step involves making feasible assumptions when facts are not available. Assumptions are made to aid the process, not to assume the problem away. Determining COAs, step 3, is susceptible to subjective thinking depending on the type of process used. Once the situation is known then COAs capable of solving the problem are developed. The next step involves developing and applying screening criteria to each COA. Screening criteria include constraints such as regulatory, time, budget, contaminant levels, plume migration, etc. It is important not to evaluate the COAs within this step. It is in the subsequent step that the various COAs are evaluated and weighed against each other with respect to evaluation criteria. Once the best COA is determined the final step involves implementing the COA. This problem-solving approach is also a hypothetical approach to solving environmental problems. It will be shown subsequently how it relates to DAM.

Figure 2. Military decision making process flow chart.

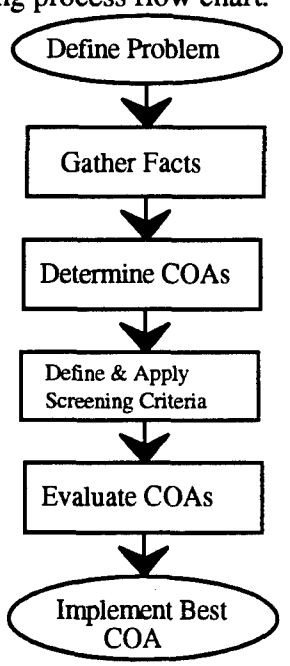

Even though the U.S. Army Training and Doctrine Command formally teaches this process, there are differences of opinion among experts outside the military community relative to definition and order of the steps in Figure 2. Baird (1978) states that the following are critical steps in the decision making process: Definition of the problem, listing of options, definition of criteria, analysis of the options and choice of a course of action. This differs from the steps itemized in Figure 2 in that no fact gathering step is included. Differences primarily occur in definition of events and their order of occurrence. As is seen between Baird's steps and Figure 2, his critical steps are in concert with the CSCs fundamental steps to problem solving.

Military Decision Process Adapted for DAM

For any contaminated site, successful decision analysis of the site is dependent on evaluation of numerous factors involving some degree of uncertainty. Probability-based methods such as Monte Carlo simulation, stochastic modeling and statistics are used to quantify the uncertainty but the output sometimes is not compatible with decision analysis (Freeze et al., 1990). A link between uncertainty and decision analysis was necessary. Two steps were added to the military decision process in this thesis to establish the link between them. These additional steps link technical and uncertainty analysis to an economics-based decision framework. Because the resource involved is typically money, it is logical to base the decision on economics. A discussion of processes involving quantifying risk monetarily is included in Chapter III. Figure 3, however, shows how these steps integrate into the decision making process. Notice that the fundamental structure of Figure 2 remains unchanged.

During the fact gathering step, factual information may be sparse or nonexistent in some cases. In the absence of factual information, assumptions must be made to continue the process. Associated with assumptions is uncertainty, and quantifying that uncertainty is the reason for processing any factual information and conducting an uncertainty analysis. In a problem involving groundwater contamination for which data from only a few monitoring wells is available, contaminant plume size and location is uncertain except at the well locations. The information processing step can utilize geostatistic methods to provide some probable distribution of the plume. After the information is processed and screening criteria are defined, the next step is quantifying the uncertainty associated with off-site transport of a chemical. This defines the uncertainties associated with estimating the chemical concentrations and their arrival times at pre-defined points of compliance. This, in turn, establishes a range of statistically defined times when remediation will be most effective. In this step, Monte Carlo simulations along with statistical probability methods are utilized to quantify the uncertainty. It is important to define screening criteria prior to the uncertainty analysis because of the association of clean-up objectives, compliance requirements and technology capabilities to screening criteria. During the uncertainty analysis there may be occasions when screening criteria tolerances or definitions will affect the analysis.

The information processing step within Figure 3 involves statistical analysis of data to determine the distribution and/or definition of model parameters and boundary conditions. These values are then utilized in the uncertainty analysis step as input to models. Uncertainty analysis conducts stochastic modeling to determine the distribution of outcomes for a given situation.

Figure 3. Decision making process adapted to incorporate technical and uncertainty analysis.

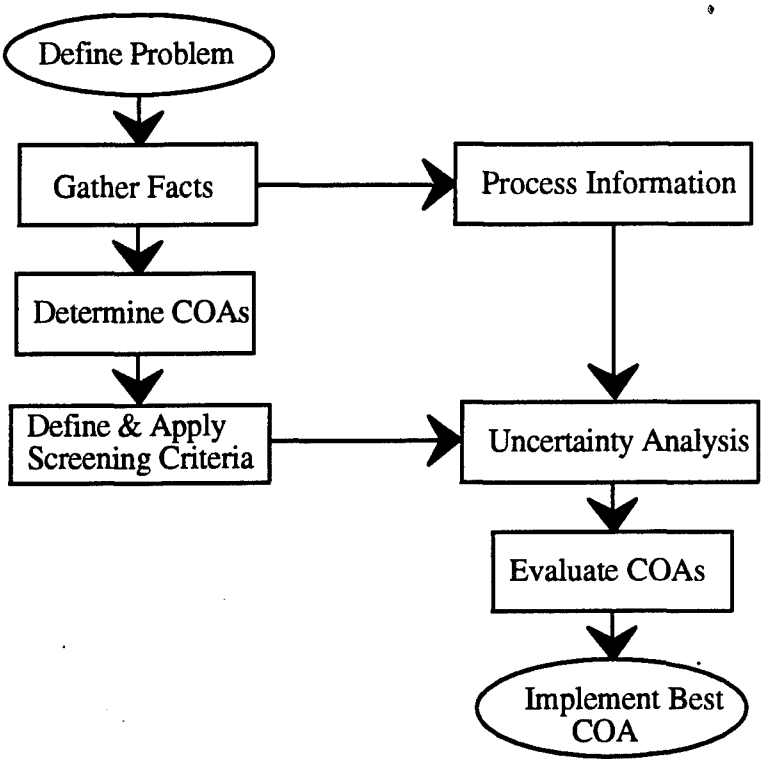

Integrating Stochastic Models into DAM

Recent work by Freeze, Gorelick, Massmann and others (Freeze et al., 1990 and 1992; Gorelick et al., 1984; Massmann et al., 1991) has been instrumental in linking uncertainty analysis to decision making and optimization. Their methods have primarily dealt with specific tactical level problems such as placement of monitoring wells. This approach in some cases is too specific; therefore a method more flexible is needed.

Freeze and coworkers (1990), introduced a decision analysis framework that linked hydrogeologic technical and uncertainty analysis to an economic framework that could be used in decision analysis. Their work primarily involved applying the framework to engineering applications involving groundwater. Critical elements of this framework

were integrated into Figure 3. Even though their framework was developed for hydrogeological problems, it had other applications. The information processing step utilized their technique of modeling uncertainty for stochastic simulation in the subsequent step. In this step simulation models can be utilized to quantify the uncertainty for use in a decision model.

Figure 4 illustrates the decision analysis methodology presented in this thesis. The flow and structure did not change from Figure 3 but the information process and uncertainty analysis steps were renamed to condition uncertainty model and simulation model, respectively. The title changes describe the actions conducted within these steps. Condition uncertainty, not to be confused with the geostatistic operation called conditional simulation, processes the data with certain models or statistics to develop simulation model parameters or boundary conditions. The additional processing provides a better understanding of the situation and uncertainty pertaining to environmental conditions such as hydrologic boundaries, geologic boundaries and hydrogeologic boundaries. This step is flexible to various models dependent upon the situation and the users needs and capabilities.

Figure 4. Decision analysis methodology framework presented in this thesis.

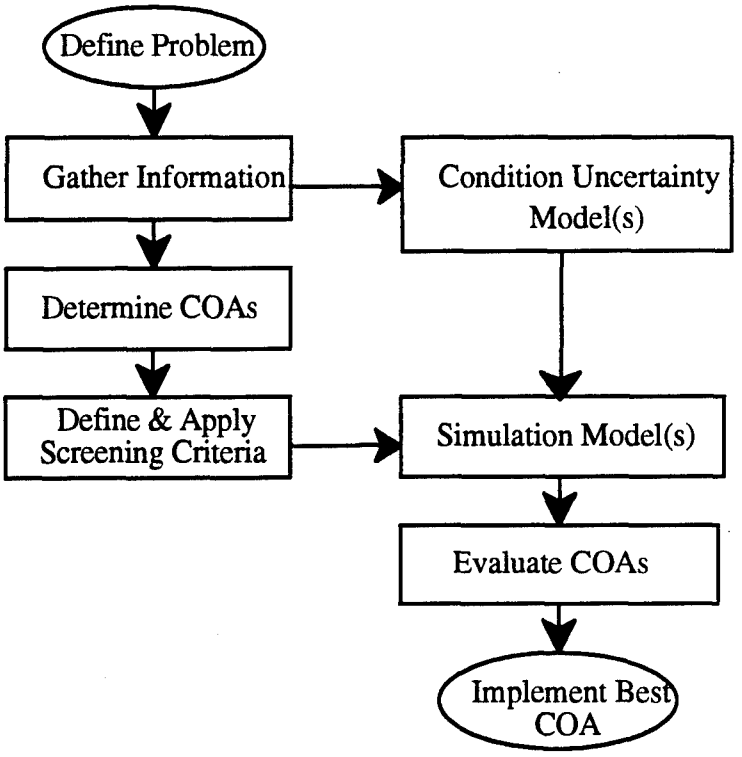

Once the condition uncertainty step is completed, along with the "define and apply screening criteria" step, simulation model(s) can be utilized to define or quantify the uncertainty of a problem into terms usable for the decision maker. Stochastic modeling techniques can be used to develop probability distributions to address the problems uncertainty. For example, transport modeling can be used to determine the probability that a contaminant will reach a specified point. The probability distributions can then be linked to a decision model that optimizes cost and risk used in the decision tree format from Figure 1. That is, the transport modeling probabilities are utilized in the decision tree analysis as probabilities for the consequences. Decision tree analysis was the tool used for the "evaluation of the course of actions" (COAs) step of Figure 4.

CHAPTER II

EXAMPLE PROBLEM INTRODUCTION

Decision Analysis Methodology Applied to an Example Problem

Problem Situation and Site Location

Presentation of the methodology was applied to a tactical problem using a military installation data set. The site is a U.S. Army-owned munitions plant known as Longhorn Army Ammunition Plant (LHAAP) located in Harrison County, Texas near the Louisiana border (see Figure 5). The U.S. Army Corps of Engineer Tulsa District was charged with managing the project, in which a remediation phase was initiated in 1995 after years of site characterization (Cliff Murry, 1995).

The complex, which had been secured from trespass by unauthorized individuals, is contractor-operated to load, assemble and pack pyrotechnics, illumination/signal ammunition and solid rocket propellant motors (Green et al., 1990). Since the early 1950's this industrial complex (see Figure 6) has disposed of solid and liquid explosives, pyrotechnics and combustible solvent wastes by open burning, incineration, evaporation and burial (Green et al., 1990). A large portion of the wastes were disposed of in area called "Burning Ground 3" and the now closed unlined evaporation pond (UEP), see inset to Figure 6 (USACE, 1993).

Figure 5. Location of example problem used in thesis (ArcUSA, 1992).

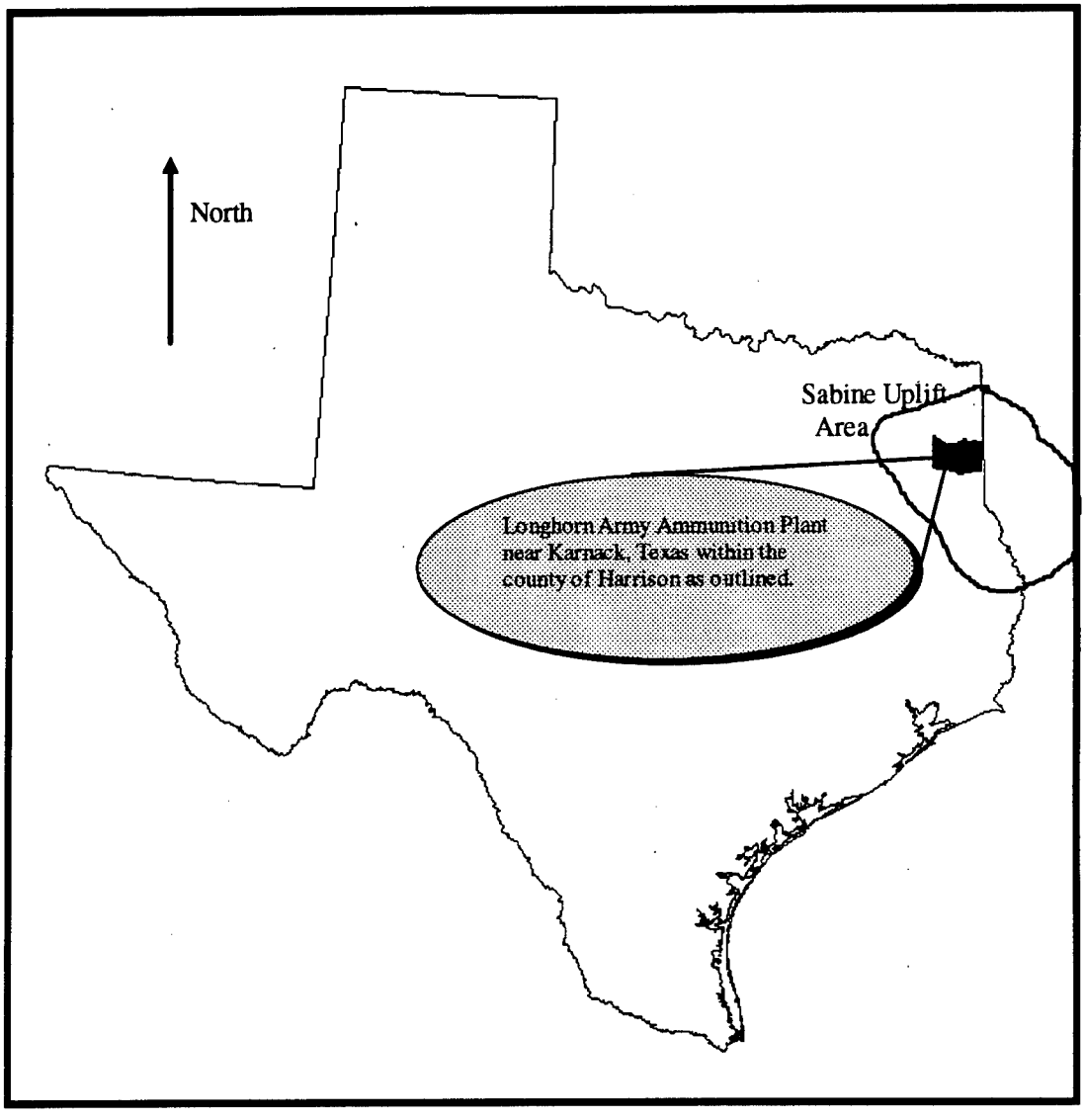

Figure 6. Longhorn Army Ammunition Plant site location with respect to Caddo Lake and Karnack, Texas (MAPEXPERT, 1993).

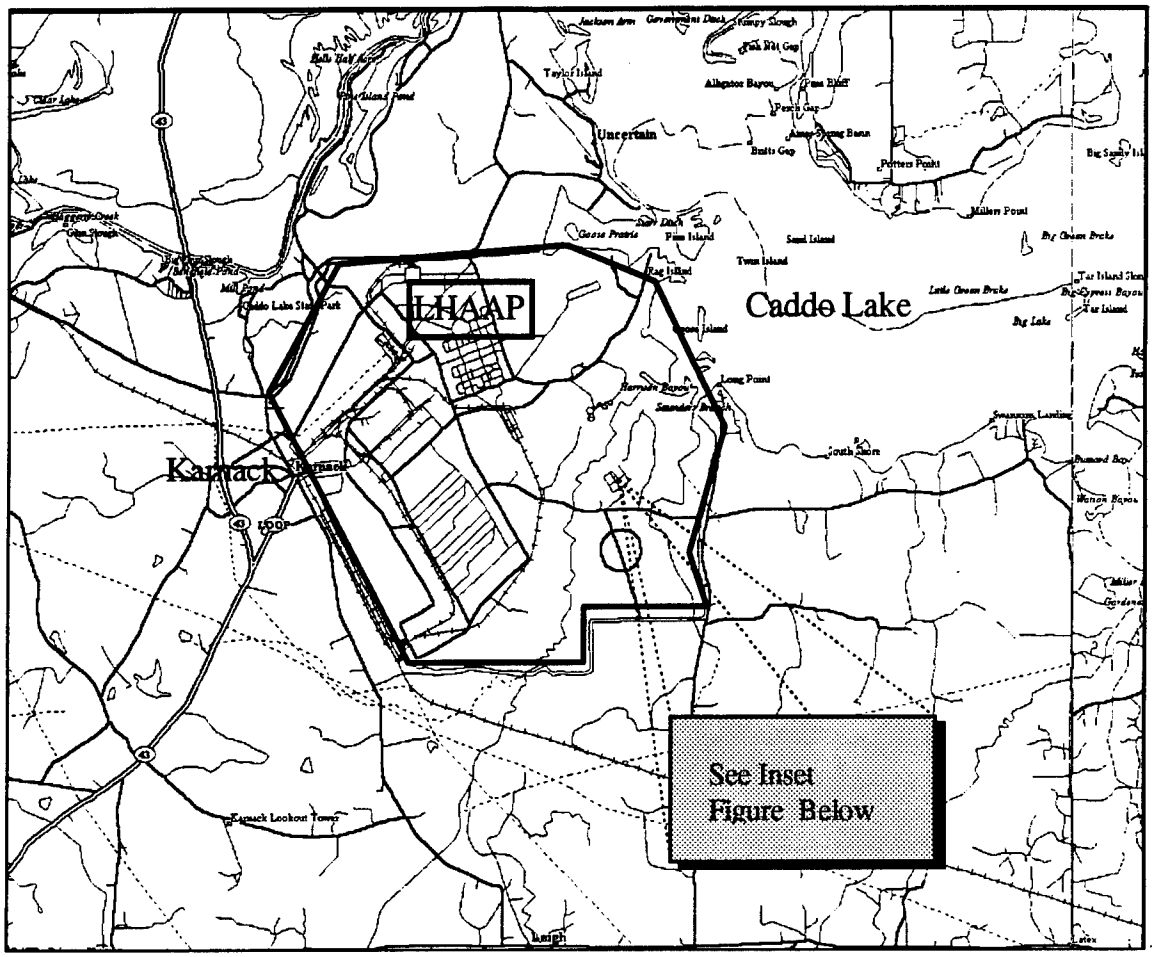

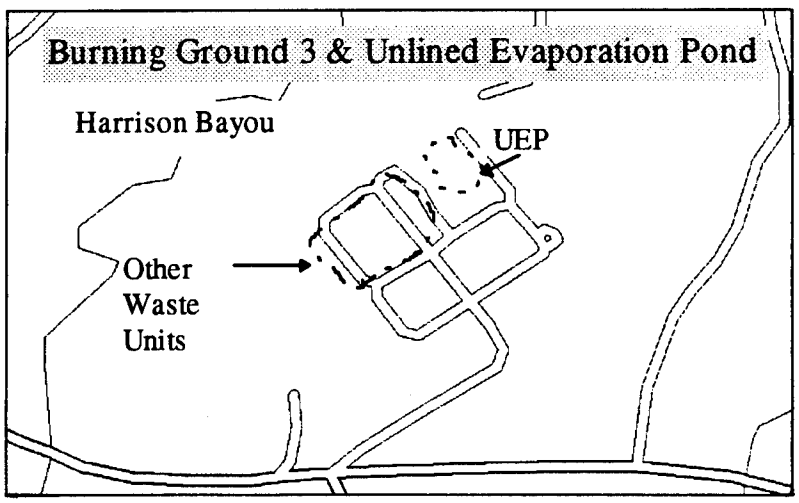

Site Hydrogeology

LHAAP is in the middle of the East Texas timber belt, characterized by sandy rolling forested topography (Green et al., 1990). Geological formations beneath the site are the Wilcox and Midway groups (Cushing et al., 1964). The Wilcox formation in Harrison County is characterized as a depositional facies of tributary channel deposits from the Tertiary age (Fisher et al., 1969). It is typical for these types of deposits to consist of about 40% channel deposits (sand) and 60% overbank deposits (silt and clay) (Fisher et al., 1969). Due to the depositional environment, the Wilcox Aquifer is made up of interbedded sand, silt and clay (see Figure 7). The beds are lenticular, with lenses of clay, silt and sand pinching out or grading into one another over short distances (Green et al., 1990). Some clay lenses are extensive enough to cause confining conditions locally (Hosman et al., 1991). There is considerable vertical resistance to groundwater flow because of the interbedded clay and overall low permeability of about 65 gpd per ft^2 (Hosman et al., 1968). The aquifer varies in depth from 90 to 150 feet with the Midway group acting as a lower boundary unit. Aquifer depth variance is due to the slight Northwest dipping of the Wilcox and Midway groups caused by the Sabine uplift. The uplift (see Figure 5) is a geologic structural feature that has pushed Upper Cretaceous beds to within 700 feet of the surface (Matson, 1916). In areas adjacent to the uplift the same beds are 5000 to 6000 feet from the surface (Matson, 1916). The regional groundwater gradient is about .0015 to the northeast (Hosman et al., 1991) but is affected locally by mounding of the water table beneath the burning ground and UEP. The mounding causes a radial gradient outward from the site for a short distance

(USACE, 1993). This mounding was attributed to the increased levels of infiltration due to activities at the site which removed topsoil and vegetation. The remaining land surface was highly porous, allowing increased infiltration to recharge the Wilcox aquifer, thus carrying the contaminants.

Figure 7. Typical stratigraphic cross section of the Wilcox and Midway groups with detail of interbedded silts clays and sand (not to scale).

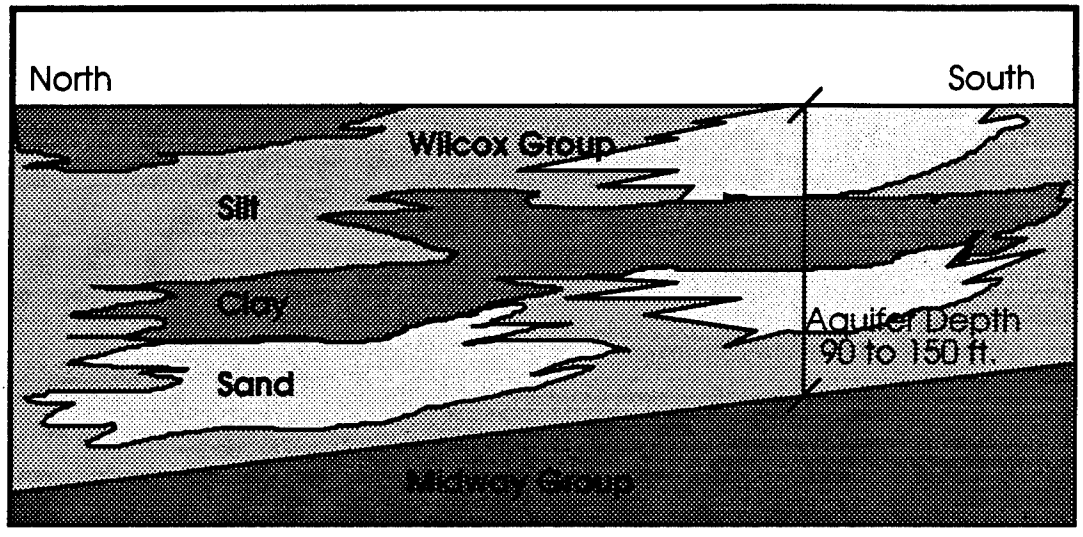

Site Contamination

The disposal site incorporates several waste units within a 300 m by 150 m rectangular area (see inset to Figure 6). All of the units have received a variety of waste, depending on the type of ammunition production at the time of disposal. The waste units include past demolition burn and burial pits, burn pans, a heavy propellant pit, 18 various burn pits, burn cages, liquid waste sump, an unlined evaporation pond and an air curtain destroyer (USACE, 1993). A summary listing in Table 1 categorizes the known pollutants into specific heavy metals, volatile organic compounds and explosives.

Table 1. Most significant contaminants detected at the burning ground (USACE, 1993).

- Heavy Metals
  - Barium
  - Chromium
  - Lead
  - Zinc
- Volatile Organic Compounds
  - Trichloroethylene
  - Methylene Chloride
  - Vinyl Chloride
  - Acetone
- Explosives
  - HMX
  - RDX
  - 1,3,5-TNB

For simplicity, only one contaminant was used to test the decision analysis methodology developed during this effort. The criteria used in choosing one of the above listed contaminants were as follows: A human health and environment (HH&E) threat, as defined by the EPA (EPA, 1987), found in large quantities and a reasonable amount of monitoring data available. Trichloroethylene (TCE) was chosen for this analysis because it not only met all the criteria, but also because it is a very common contaminant throughout the country (Sawyer et al., 1994). This allowed some transfer of the developed methodology to other locations or applications. TCE was used as an industrial solvent for many years on the site. It is a dense non-aqueous phase liquid (DNAPL) exhibiting the physical characteristics listed in Table 2. These characteristics are conducive to the contaminant's potential for migration through the unsaturated into and through the saturated zones.

Table 2. Physical characteristics for Trichloroethylene.

Physical Characteristic	Value	Source
Solubility	1100 mg/l (25° C)	Verschueren, 1983
Specific Gravity	1.46	Weast, 1980
Density	1.33 g/ml	Weast, 1980
Adsorbability (K_{oc})	122.84 (ug/gOC)/(ug/ml)	Sawyer et al., 1994
Henrys Constant	450 (atm-m^3 water)/(m^3 air)	Sullivan, 1984

Contaminants from the burning ground have been under continual monitoring since 1976 using a variety of sampling methods including groundwater monitoring and soil borings (USACE, 1993). Currently (August, 1995) there are 44 groundwater monitoring wells that are relatively shallow compared to the total thickness of the aquifer. These are presented in Figure 8, together with depth frequencies for the sampled wells. The most frequent well depth occurs between 20-39 feet, with twenty monitoring wells within that range. From well log data, aquifer thickness varies from 90 to 150 feet (USACE, 1993),

therefore a majority of the collected data represents the shallower portions of the aquifer.

Figure 8. Bar diagram showing monitoring well depth range and number of wells within each range (USACE, 1993).

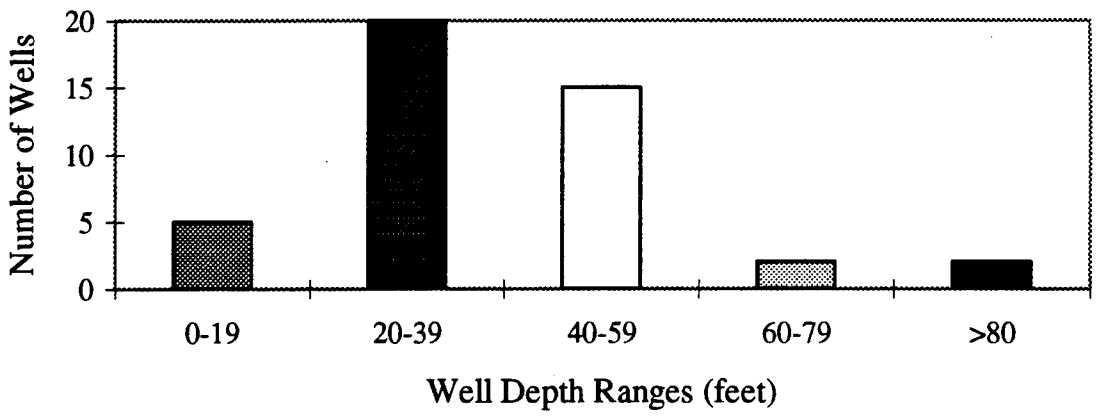

This analysis was therefore limited to the upper portion of the aquifer. This was consistent with the monitoring and remediation objectives of the U.S. Army Corps of Engineers (USACE, 1993). Figure 9 presents the locations of these monitoring wells on the site. As site characterization evolved, so did the installation of the monitoring wells. Monitoring well installation occurred in four phases from 1980 through 1989, where 22 wells were initially completed in early 1980, followed by 18 wells in June and July of 1982, 10 wells between 1984 and 1986, and 24 wells between 1987 and 1989 (USACE, 1993). The sum of these wells does not agree with current active monitoring well numbers because many of the older wells were closed. In addition to groundwater monitoring, soil borings were taken and tested for the various contaminants. A total of 20 borings were completed and analyzed for volatile organic compounds and heavy metals (USACE, 1993). Figure 10 shows the locations of the bore holes utilized in this monitoring program.

Figure 9. Locations of monitoring wells for groundwater sampling (USACE, 1993).

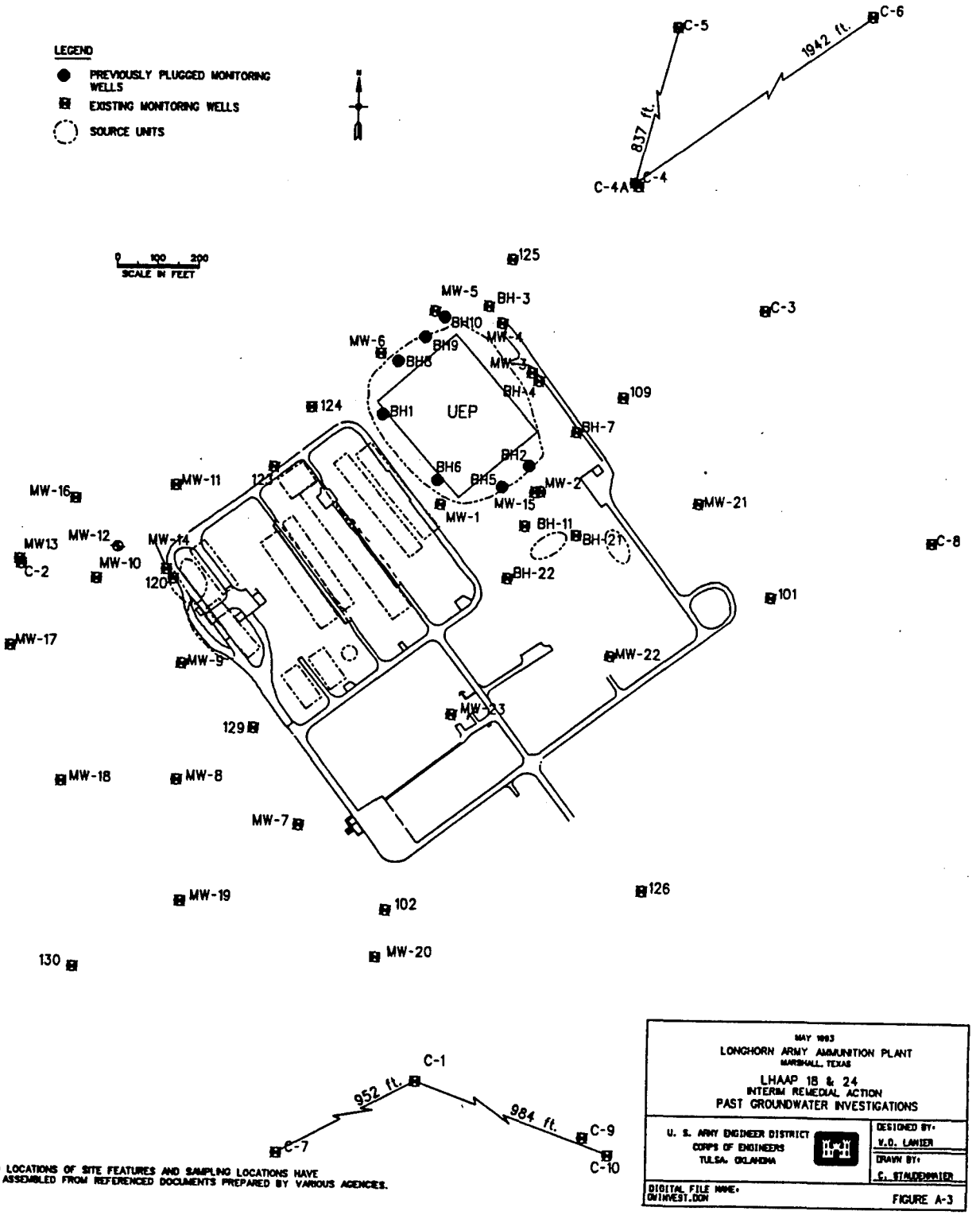

Figure 10. Locations of soil borings along with existing monitoring wells (USACE, 1993).

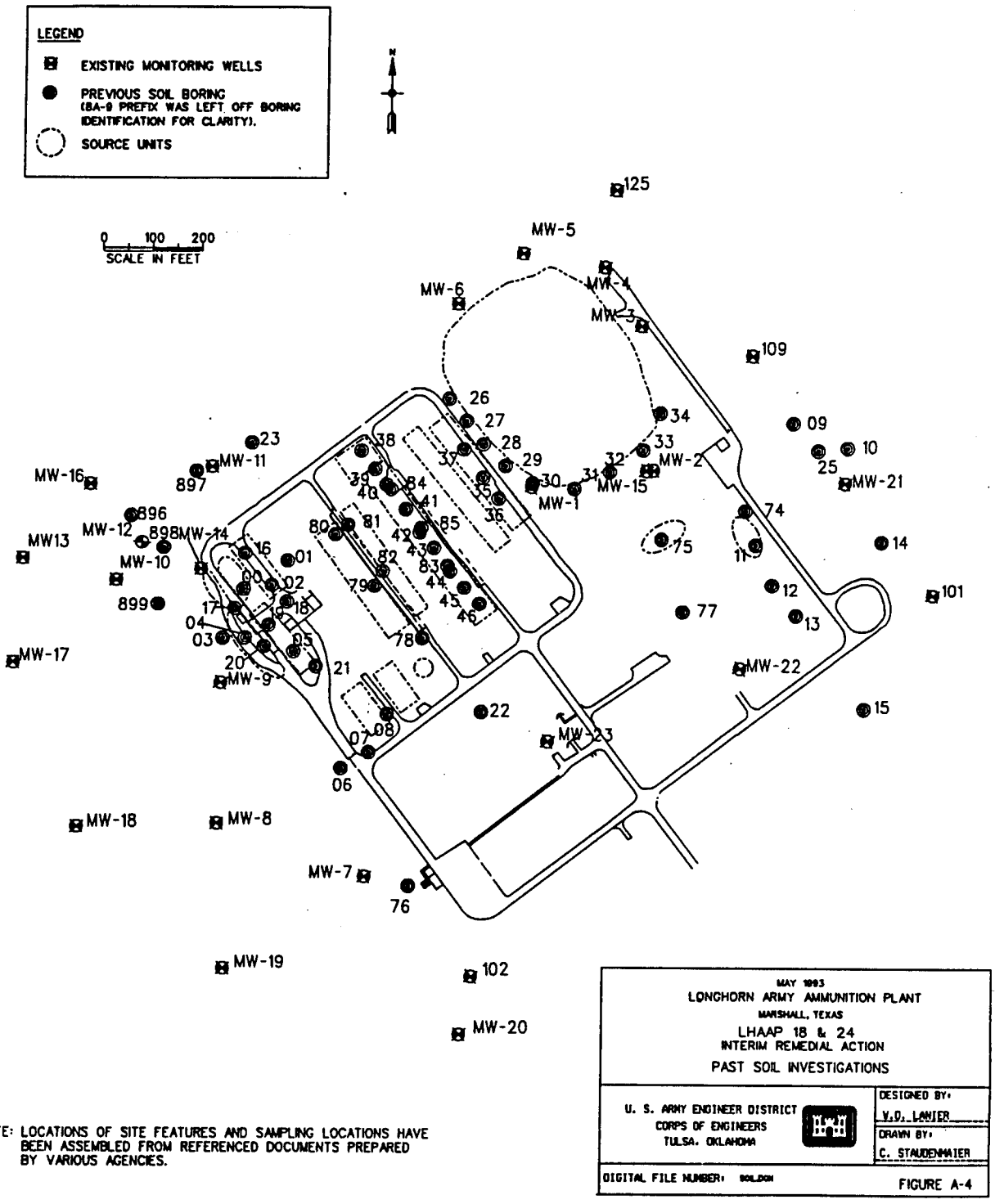

NOTE: LOCATIONS OF SITE FEATURES AND SAMPLING LOCATIONS HAVE BEEN ASSEMBLED FROM REFERENCED DOCUMENTS PREPARED BY VARIOUS AGENCIES.

Monitoring data show that there was a significant amount of TCE contaminating the soil and groundwater on site. Figure 11, prepared from these data, shows the strength and migration of TCE over the years for a few selected wells. Monitoring wells C-1, MW-16 and MW-17 were located down-gradient from the original waste units and showed a progressive increase in TCE concentrations over the time of monitoring. Monitoring well MW-1 was located adjacent to the evaporation pond and showed a significant amount of TCE contamination. Free-phase testing in this well yielded TCE concentrations of 30,000 to 50,000 ug/l. This was expected given the flow characteristics of TCE and the proximity of the well to the waste unit (reference Figure 9).

Figure 11. Variation of strength and migration of TCE within the burning ground for select monitoring wells.

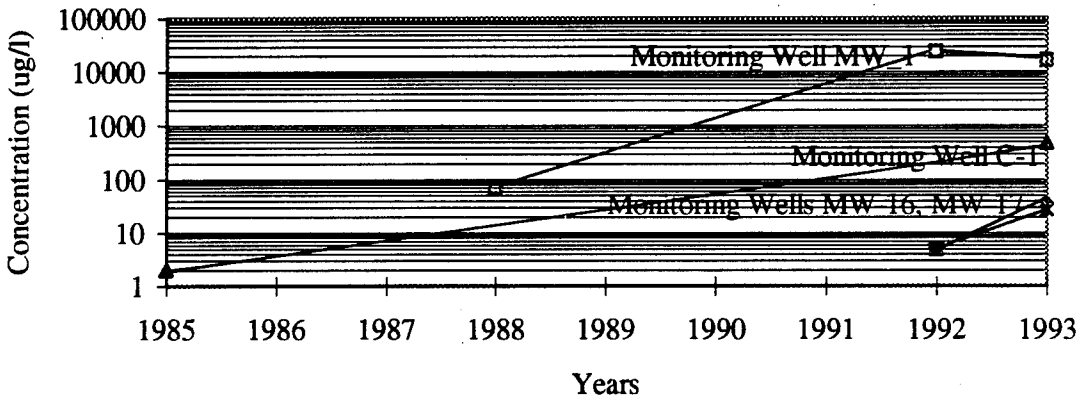

The UEP (unlined evaporation pond) is of particular importance since it was the primary means for disposal of liquid wastes since 1955 (Green et al., 1990). Prior to that time, various trenches and burn pits were used to dispose of the liquid industrial wastes. The UEP was closed in 1985 with the removal of the remaining liquid and sludge. It was then capped to prevent water infiltration (Green et al., 1990). As part of the clean

closure procedure, samples were collected from the floating material in the pond, the sediment layer on the pond's bottom, and the soil layer beneath the pond and tested for inorganic and organic compounds (Green et al., 1990). Of the three layers tested, only the aqueous layer had consistent detection of TCE (Green et al., 1990). Even though tests were conducted for volatile organic compounds (VOC) during closing procedures of the UEP, they were not used as parameters for clean closure of the UEP (USACE, 1993). A significant VOC plume within the saturated zone exists under the site, as shown in Figure 12. This figure shows the U.S. Army Corps of Engineers' estimated isoconcentration contours using November, 1992 monitoring well data. Even though clean closure (contaminant source removed) methods were used, the presence of VOCs after closure was significant enough to suggest continued loading into the saturated zone from wastes located in the vadose zone which were disposed years before. Surface soil testing for VOCs was conducted during the cleanup but none within the vadose zone directly under the UEP (USACE, 1993). Groundwater monitoring data since 1985 showed the contaminant plume continued to increase within the saturated zone (see Figure 11). It can be assumed that contaminated soils in both the vadose and saturated zones beneath the site continued to act as a source of contamination to the groundwater.

Figure 12. TCE isoconcentration contours and groundwater elevation contours using November, 1992 monitoring well data.

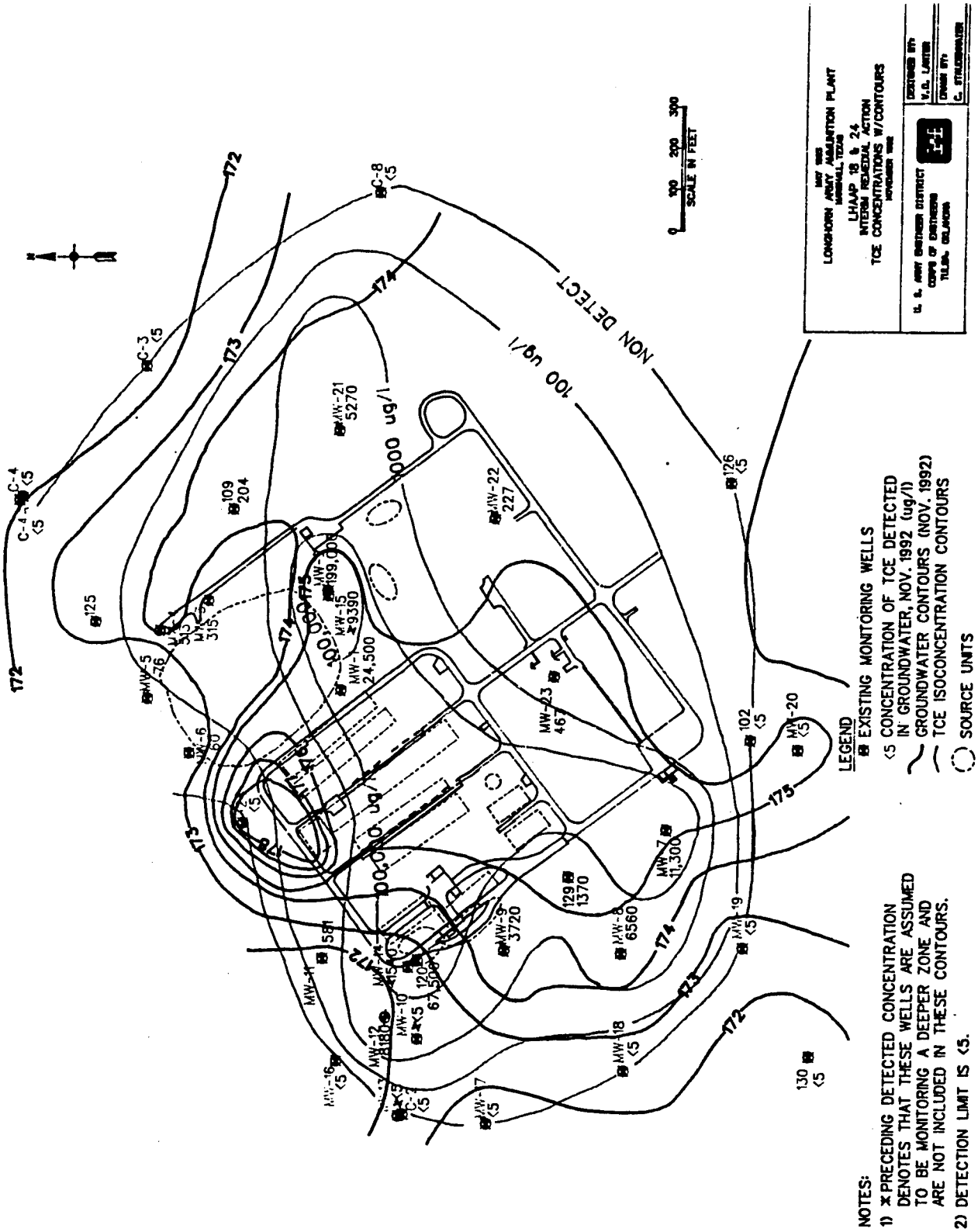

Contamination Risk

Three features must be present for a contaminant to pose a threat to HH&E: source of contamination, receptor for contamination and a pathway from the source to the receptor (EPA, 1987).

Even though the capacity of the Wilcox aquifer is small to moderate, its potential use as a domestic water source is high for rural home sites (Hosman et al., 1991). In addition, the industrial complex is bounded to the northeast by Caddo Lake, which serves as a drinking water source to the local communities of approximately 50,000 people (Golden et al., 1994). Therefore, the potential for drinking water contamination from the site exists. With the regional ground water gradient generally oriented northward, Harrison Bayou would be the primary location to intercept a contaminant plume migrating with the regional groundwater gradient from the site (Figure 6). For this effort, therefore, the immediate receptor path was taken to travel through Harrison Bayou.

Identifying the receptor path was important in determining the plane of compliance (POC), identifying alternative actions and potential receptors. The POC established for this problem existed along an interface between the groundwater and surface waters with the Harrison Bayou. Figure 13 shows the approximate alignment of the POC.

Figure 13. Location of the POC with respect to the source, Harrison Bayou and the potential receptors (MAPEXPERT, 1993).

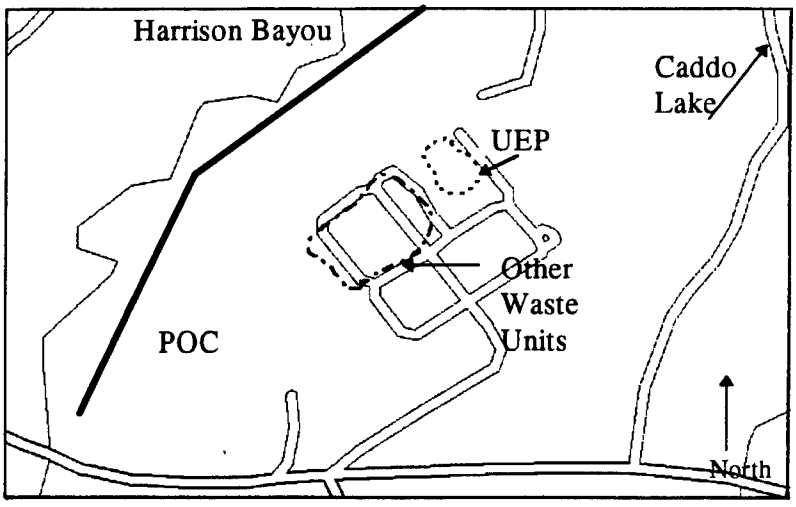

Decision Model Constraints

Based on the given data, TCE is present in significant amounts and has the physical capability to migrate through a potentially usable aquifer. The amount of TCE detected in the groundwater exceeds the national drinking water standard of 5 ug/l. TCE is an EPA listed contaminant known to have non-carcinogenic effects on humans (Sawyer et al., 1994). Therefore, a risk to HH&E does exist under these circumstances. As manager of such a facility the questions to be asked are: Do I remediate, when should remediation start and what type of remediation technique should I use? Chapter one outlined the importance of developing decision criteria and a model. The constraints important to this specific problem are technical more than they are social or political. Even though social or political issues are not addressed in this example problem, they can be addressed within the methodology. This can be done through development of criteria catering to those issues.

The following are the criteria used in the Long Horn Army Ammunition Plant problem.

- Limit of contaminant migration.

  Defined as the furthest point the contaminant can migrate off the site. An imaginary boundary called the plane of compliance (POC) was used to mark this point. It was set as the swampy interface with Harrison Bayou just North of the burning grounds (see Figure 13). Any contamination migrating beyond the POC with a strength greater than or equal to the set maximum contaminant level (MCL) was considered failure.

- Maximum contaminant level.

  Defined as the maximum allowable concentration of contaminant in groundwater. Measured in micrograms of contaminant per liter of water, the MCL used will be that which is set by the EPA for drinking water of 5 ug/l for TCE (Sawyer, et. al., 1994).

An objective function was used to calculate the cost of each consequence in a decision tree similar to Figure 1. The least costly consequence inherently includes the optimum alternatives within the decision tree. Being a cost minimization decision model, the objective function's goal is to minimize the cost of remediation and minimize risk (probability of failure). Failure for this problem was defined as TCE in a concentration equal to or greater than the MCL migrating to the POC. Equation (1) presents the objective function developed for this problem. The first part of the objective function is a typical present-worth model that was used to evaluate each alternative in present dollars. The remedial cost function (C(t)) and the failure cost function (R(t)) are the core for this equation. Costs of additional testing and monitoring groundwater were also factored into

the objective function. The probability function is the quantification of the problem's uncertainty, which represents the probability a certain state of nature will exist.

$$\text{Minimize } \$ = [[(1/(1+i)^t) * (C(t) + R(t) + T(t))] + M(t)] * P(sn_x) \quad (1)$$

where	$	=	cost in dollars
	i	=	index rate for money
	t	=	time unit from 0 to T
	C(t)	=	remedial action cost function
	R(t)	=	risk failure cost function
	T(t)	=	additional testing cost function
	M(t)	=	monitoring well cost function
	$P(sn_x)$	=	probability for a given state of nature

The remedial cost function is the estimated capital and operation costs for each of the consequences involving remediation actions. This cost variable is a function of time; therefore a uniform series model was used to calculate a present worth for operational costs, as shown below.

$$C(t) = RACAP + RAOM[(1+i)^t-1]/[i(1+i)^t] \quad (2)$$

where	RACAP	=	capital cost for remedial action
	RAOM	=	operation and maintenance cost for remedial action

Uncertainty for this function involves the size and location of the contaminant plume. Since remedial cost are typically proportional to the plume volume, remedial cost estimates inherit the uncertainties associated with defining the plume. A geostatistical approach called conditional simulation was used to determine the size of the plume and its concentration distribution. The method utilized proven geostatistical software to define the spatial statistics of the monitoring data. These spatial statistics were then run through a kriging and conditional simulation algorithm using Monte Carlo techniques. A statistical analysis was then conducted to determine the upper boundary of the 95%

confidence interval (UB 95 CI) for the plume's two-dimensional size, location and concentration distribution. The UB 95 CI plume size and concentration distribution were used to determine the various remediation alternatives and to calculate their cost.

The failure cost function puts a monetary value on failure; therefore it is associated with minimizing costs for each alternative. Failure, previously defined as TCE migration greater than 5 ug/l across the POC, can result in substantial costs due to litigation, new domestic water source development, etc. Because this variable is a function of time, the present cost of a uniform series is applied to any recurring costs associated with failure.

$$R(t) = FCAP + FOM[(1+i)^t-1]/[i(1+i)^t] \quad (3)$$

where FCAP = capital cost for failure
FOM = operation and maintenance cost for failure

In this particular decision model a decision sequence was added, called "Additional Testing". This concept utilizes Bayes' theorem to provide a refined probability for a given state of nature. The Bayesian concept will be discussed in depth later, but as utilized in this problem, the potential monitoring data obtained from installing additional groundwater monitoring wells were used to calculate a revised probability of TCE migrating to the POC. Both capital and operational costs were incurred for installing monitoring wells. Again the variable was a function of time, so a uniform series model was used to calculate a present worth for T(t) operational costs as shown below.

$$T(t) = TCAP + TOM[(1+i)^t-1]/[i(1+i)^t] \quad (4)$$

where TCAP = capital cost for testing
TOM = operation and maintenance cost for testing

The monitoring well cost function was the operation costs for monitoring existing wells and associated laboratory analysis. This function had no capital costs because the monitoring wells already existed. The cost variable was a function of time. Therefore a uniform series model was used to calculate a present worth for operational costs as shown below.

$$M(t) = MOM[(1+i)^t-1]/[i(1+i)^t] \quad (5)$$

where MOM = operation and maintenance cost for monitoring groundwater in existing wells

A majority of the problem's uncertainty analysis was associated with the probability function. For the given contamination problem, three states of nature were used based on the concentration of TCE within the groundwater reaching the POC. States of nature were defined as: (1) no detectable amount of TCE reached POC, (2) less than 5 ug/l TCE reached POC and (3) $\geq$ 5 ug/l TCE reached POC. Given these three random events without any other information, the probability of one being the true state of nature was 1/3. In reality the three states of nature do not have the same probability of occurrence. Therefore an uncertainty analysis was conducted to better define the probabilities for the states of nature.

A stochastic approach was used to determine the probabilities of these states of nature. An analytical groundwater model using Monte Carlo simulation techniques developed a probability versus TCE concentration plot for various time periods. Probabilities for the states of nature were taken from these plots and used in the decision tree analysis.

Capital, operational and maintenance costs for all functions were determined using the EPA's Cost of Remediation Alternatives (CORA) software. This expert system provides the user with remediation alternatives and their associated costs. Developing "cost for failure" value also utilized the CORA software by determining cost for providing alternative drinking water sources.

The Bayesian or probability updating concept used in the model was based on Bayes Theorem, which was derived from the definition of the probability of an intersection and the use of the definition of conditional probability (Ossenbruggen, 1984). The objective of this concept was to improve the probabilities for the states of nature through additional testing. The prior probability was defined as the probability that the true state of nature is the event S_i, or $P[S_i]$ (Ossenbruggen, 1984). Revised probability is equal to the conditional probability where the true state of nature is the event S_i given the outcome of a test is Z_j or $P[S_i/Z_j]$ (Ossenbruggen, 1984). Definition of the probability of an intersection and the use of conditional probability definition yields (Ossenbruggen, 1984):

$$P[S_i \cap Z_j] = P[Z_j \cap S_i] \quad (6)$$

or

$$P[S_i \mid Z_j]\, P[Z_j] = P[Z_j \mid S_i]\, P[S_i] \quad (7)$$

Rearranging the equation, the posterior probability is obtained.

$$P[S_i \mid Z_j] = P[Z_j \mid S_i]\, P[S_i] / P[Z_j] \quad (8)$$

From equation (8) it can be seen that the revised probability is a function of the prior probability (Ossenbruggen, 1984). The sample likelihood $P[Z_j \mid S_i]$ is the probability that

the test event Z_j occurs given the true conditional state of nature S_i (Ossenbruggen, 1984).

In this project the Bayesian or updating model was applied to uncertainties associated with monitoring data adequately delineating between the three states of nature previously described. That is, there are sampling, processing and analytical errors associated with each monitoring data point. These errors may result in either false positive or false negative samples being reported. A false positive is defined as a sample where the reported TCE concentration was greater than the 5 ug/l when, in fact, it was less than this concentration. A false negative similarly defines a cleaner state of nature than is warranted by the actual aquifer contaminant levels.

The Bayesian analysis used in this effort was applied only to possible analytic error, as they are the only ones reported (Medina et al., 1989). The technique employed, however, can be readily extended to sampling and processing as data become available.

At this point, the example problem has been introduced. Referring to the decision making process in Figure 4, the "define problem" and "gather information" steps have been completed. The decision maker now must develop courses of action, process the data (condition uncertainty modeling) and performing simulations to develop probabilities for the possible states of nature that will be used in the decision tree analysis. Chapter three discusses the methods used within each of these steps as they were applied to the example problem.

Chapter III

METHODOLOGY

Determination of Contaminant Concentration

Contaminant Flux to Groundwater Analysis

Purpose and Objective: Contaminant movement to the POC involved two separate transport components: contaminant loading into the aquifer from the vadose zone and transport through the aquifer. Stochastic analysis of the contaminant loading established the probability and associated uncertainties necessary for modeling contaminant transport through the saturated zone. The objective of this section was to identify the methods used to determine the initial flux of TCE into the underlying aquifer using known TCE soil concentrations measured within the vadose zone. This flux value will be used as the release rate (pulse loading) parameter necessary in the saturated zone transport model.

Method Developed and Applied. Past studies have shown that advective transport of a compound past a stationary point exhibits a concentration variation with time as represented in Figure 14 (Fetter, 1980).

Figure 14. Concentration versus time under advective transport conditions.

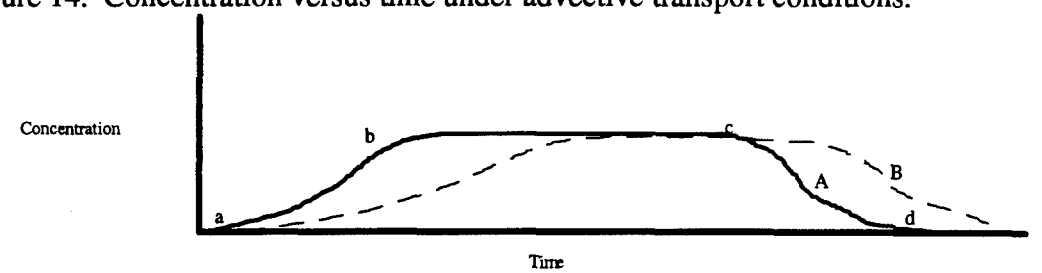

Curve shapes in Figure 14 are a function of the contaminant properties and hydrogeologic conditions in which the contaminant travels. An increase in concentration, as seen between points a and b of curve A, represent the plume arrival to a stationary monitoring point. Flattening of the curve, as shown between points b and c, shows plume strength at its maximum indicated continuous loading from the source. When the curve starts to subside, as shown between points c and d, this could be an indication that continuous loading has ceased, given that the plume has not changed directions or undergone significant decay. Curves A and B represent two separate compounds with such different transport properties, such as adsorption and/or ion exchange (retardation), within the same hydrogeologic environment.

This theoretical transport behavior was applied to this research by changing the concentration to a mass loading. Utilizing a plot similar to Figure 14, a mass loading versus time plot was developed utilizing classical transport theory. Contaminant soil concentrations and soil properties had previously been measured in 1988 from the bore holes shown in Figure 10 (USACE, 1993). These data were used to develop a mass loading curve similar to Figure 14. Since the source, having been removed in 1985, was no longer loading TCE into the unsaturated zone, the mass loading to groundwater should lie somewhere between points c and d of Figure 14 and could be approximated by advective-dispersive modeling. Modeling contaminant transport was conducted in two phases. The first phase traced mass loading from the time the units were opened (1950) until present and had as its objective the development of the shape of the mass loading curve with respect to time. Since contaminant soil concentrations were not available

prior to 1988, an initial soil level was selected which was considered to be representative. The subsequent modeling runs proved that the mass loading shape was not dependent on the soil concentration of the contaminant. Phase two used the contaminant soil concentration data from 1988 to determined where the mass loadings for 1988 and subsequent years were located on the curve. From this point on the curve, maximum mass loading was extrapolated to determine a maximum mass loading into the aquifer.

Tool Utilized. The Jury unsaturated zone model incorporated in the American Petroleum Institute's Decision Support System for Exposure and Risk Assessment (APIDSS) software was used to estimate the contaminant flux into the aquifer (APIDSS, 1994 and Jury et al., 1983). The Jury model is a screening-level tool that can be used to estimate the contaminant mass loading to a water table aquifer (APIDSS, 1994). It is based on the analytical solution to the differential mass balance equation and initial conditions presented below (APIDSS, 1994):

Differential mass balance equation:

$$(\partial C_T/\partial t) + \mu C_T = D_E (\partial^2 C_T/\partial z^2) - V_E (\partial C_T/\partial z) \qquad (9)$$

where

C_T	=	total soil concentration as defined by eq. (11) (mg of contaminant/cm^3 of wet soil)
t	=	time (day)
μ	=	first order decay rate constant (1/day)
D_E	=	effective diffusion coefficient estimated by eq. (14) (cm^2/d)
z	=	depth measured positive downwards from the soil surface (cm)
V_E	=	effective contaminant velocity estimated by eq. (15) (cm/d)

The initial condition is:

$$C_T(0 < z < L, t=0) = C_o \qquad (10a)$$

$$C_T(z \geq L, t=0) = 0 \qquad (10b)$$

Equations (10a) and (10b) imply that initially the contaminant is uniformly incorporated to a depth L. In equation (9), the total soil concentration is assumed to be distributed between the solid, aqueous and the vapor phases and is estimated using:

$$C_T = \rho_b C_s + \theta_w C_l + \theta_a C_g \quad (11)$$

where

ρ_b = the bulk density of soil (g of dry soil/cm^3 of wet soil)
C_s = the adsorbed phase concentration (g of contaminant/g of dry soil)
θ_w = the volumetric water content (cm^3 of water/cm^3 of wet soil)
C_l = the dissolved phase concentration (g contaminant/cm^3 solution)
θ_a = the air porosity (cm^3 gas in soil/cm^3 wet soil)
C_g = the dissolved phase concentration (g contaminant/cm^3 gas in soil)

The three individual phase concentrations C_s, C_l and C_g are related by partition coefficients as follows:

$$C_s = K_d C_l \quad (12)$$

and

$$C_g = H C_l \quad (13)$$

where

K_d = the chemical-specific soil-water partition coefficient [(mg/g of dry soil)/(g/cm^3 of solution)]
= $K_{oc} f_{oc}$
H = the dimensionless form of the Henry's constant [(mg/l of vapor)/(mg/l of solution)]

The effective diffusion coefficient in equation (9) is estimated by:

$$D_E = [(\theta_a^{10/3} D_g^a H + \theta_w^{10/3} D_l^w)/\theta^2]/[\rho_b f_{oc} K_{oc} + \theta_w + \theta_a H] \quad (14)$$

where

D_g^a = the chemical specific gaseous diffusion coefficient in air (cm^2/day)
D_l^w = the chemical specific liquid diffusion coefficient in water (cm^2/day)
θ = the total soil porosity (cm^3 voids/cm^3 wet soil)
θ_w = the volumetric water content (cm^3 of water/cm^3 of wet soil)

θ_a = the air porosity (cm^3 gas in soil/cm^3 wet soil)
f_{oc} = fraction of organic carbon in soil (mg of organic carbon/mg of soil)

The effective contaminant velocity in soil in equation (9) is estimated by:

$$V_E = J_w / [\rho_b f_{oc} K_{oc} + \theta_w + \theta_a H_E] \quad (15)$$

where
J_w = the volumetric soil-water flux, i.e., percolation rate when J_w is positive, (cm/day)

The variable H_E is defined as:

$$H_E = h (\rho_b K_d + \theta_w + \theta_a H)^{-1} \quad (16)$$

where
h = boundary layer transfer coefficient (cm/day) estimated as:

$$h = D_g^a/d \quad (17)$$

where
d = the stagnant air boundary layer thickness (cm)

Concentrations estimated at the water table are used to compute the contaminant flux to the water table using:

$$M_{wt} = VC_lA + D(\Delta C / \Delta Z)A \quad (18)$$

where
M_{wt} = annual mass loading to water table (mg/yr)
V = infiltration rate (m/yr)
A = area of the source (m^2)
C_l = liquid phase concentration at the water table (mg/m^3)
D = hydrodynamic dispersion coefficient (m^2/yr)
$\Delta C/\Delta Z$ = concentration gradient at the water table ($mg/m^3/m$)

Tool Assumptions. Assumptions associated with the model are as follows (APIDSS, 1994):

- The soil column is assumed to be homogenous and isotropic without any variations with depth.
- The infiltration rate is assumed to be uniform and steady.

- The contaminant is initially incorporated uniformly from the top of the soil column to a depth 'L' cm below the surface. Note that the model can analyze a contaminant incorporated in a thickness 'D' cm buried below a clean layer of soil using the principle of superposition.
- Contaminant decay is assumed to follow a first order function.
- The partitioning of contaminant concentrations between the three phases, i.e., solid phase, dissolved aqueous phase and the vapor phase is assumed to be linear. Compositional equilibrium among phases is assumed at all locations at all times.
- The effective diffusion of contaminant in the vapor and liquid phase within the soil is based on the following relationships:

$$D_g = D_g^a \theta_a^{10/3}/\theta_t^2 \quad (19)$$

and $$D_l = D_l^w \theta_w^{10/3}/\theta_t^2 \quad (20)$$

where

D_g^a = the chemical specific gaseous diffusion coefficient in air (cm^2/day)

D_l^w = the chemical specific liquid diffusion coefficient in water (cm^2/day)

θ_a = the air porosity (cm^3 gas in soil/cm^3 wet soil)

θ_w = the volumetric water content (cm^3 of water/cm^3 of wet soil)

θ_t = the total soil porosity (cm^3 voids/cm^3 wet soil)

Modeling Analysis. As mentioned, modeling the flux of TCE into the groundwater was conducted in two phases. The first phase determined the shape of the mass loading curve given the soil properties within the burning ground. During the next phase, the maximum mass loading value was calculated using data from the 1988 sampling set. Since there was no longer a contaminant source, the assumption was made that the measured 1988 mass loading point occurred somewhere along curve A between points c and d (see Figure 14). Once the curve was developed, the maximum mass loading value was extrapolated along this curve. Figure 15 illustrates conceptual first and second phase modeling curves developed by the Jury transport model. First phase

modeling developed the shape of curve A in Figure 15 with respect to the actual time line. The second phase developed the darkened portion of curve A, between points c and d. This phase did determine mass loading over time. The maximum mass loading, point c, was then extrapolated from phase two modeling values and phase one curve shape.

Figure 15. Modeling phase one idealized plot.

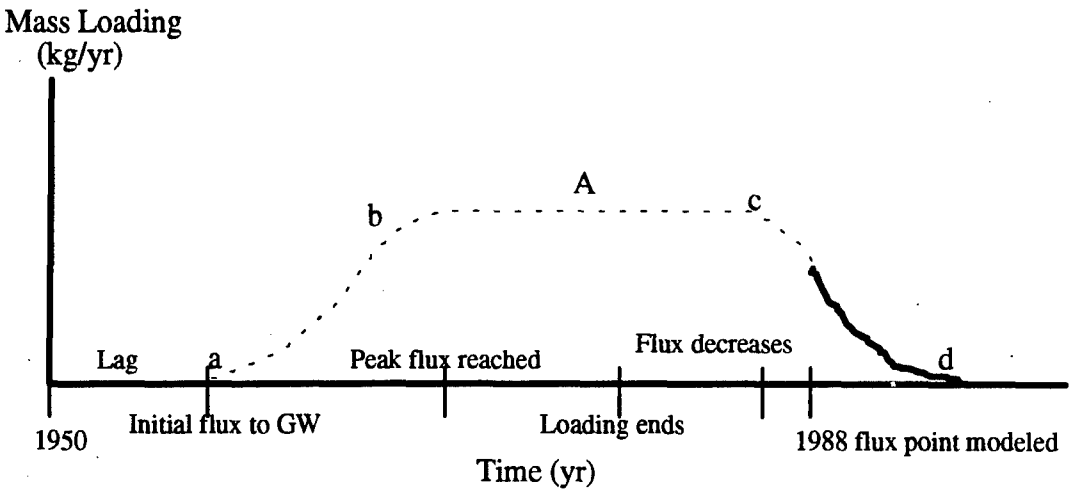

Phase One Modeling. It is known that contaminant dumping started about 1950 and continued into the mid 1980's, with the UEP closing in 1985 (Green et al, 1990). Therefore, a modeling period of 50 years was used to determine the mass loading curve shape. The following assumptions were made with respect to both modeling phases:

- Phase one thickness of contaminant incorporation was one meter. This was based on the information from the data summary report on depths of the UEP and disposal trenches (USACE, 1993).
- For modeling purposes, the depth of the unsaturated zone was considered uniform over the entire site. This figure was derived using simple statistics of the depth to water table data from 44 groundwater wells.
- It is assumed that by 1988 the entire unsaturated zone thickness was contaminated under the source. Therefore, phase two thickness of contaminant incorporation was 5.74 m, equal to the unsaturated zone depth.

- Since the majority of the waste was disposed into trenches and the UEP, it was valid to assume there was no cover over these units (USACE, 1993).
- Fifteen different waste units were located within an area 159 m by 305 m. Since the waste units occupied more than 50% of this area, the area was modeled as one unit.
- A simple statistical analysis of the soil concentration data from 1988 provided a mean and upper boundary of the 95% confidence interval (UB 95 CI) to be used as the contaminant concentration in the soil.

Table 3 lists the parameter definition and values used in phase one modeling. Two parameters, simulation time and incorporation thickness, have two values. These correspond to the two modeling phases having different values with respect to these parameters. Two values shown under the soil concentration parameter corresponded to the mean and UB 95 CI as discussed in the assumptions.

Table 3. Data used in Jury model to determine contaminant loading into the aquifer.

Parameter Definition	Units	Value	Source
Model Control Parameters			
simulation time	years	[1]50 and [2]20	USACE, 1993
simulation type	-	deterministic	N/A
Media Specific Parameters			
volumetric water content	-	0.26	USACE, 1993
effective porosity	-	0.4	USACE, 1993
dry weight soil bulk density	g/cm^3	1.6	USACE, 1993
thickness of incorporation	m	[1]1 and [2]5.74	USACE, 1993
thickness of soil cover	m	0.0	USACE, 1993
depth of unsaturated zone	m	5.74	USACE, 1993
fraction of organic carbon	-	0.01	Golden et al., 1994
boundary layer thickness	cm	0.5	Jury et al., 1990
infiltration	cm/yr	43	Golden et al., 1994
X-dimension of the source	m	305	USACE, 1993
Y-dimension of the source	m	159	USACE, 1993
Chemical Specific Parameters			
total concentration in soil	mg/kg	[3]23.0 & 45.6	USACE, 1993
diffusion coefficient in air	cm^2/s	$1.0x10^{-3}$	APIDSS, 1994
diffusion coefficient in water	cm^2/s	$1.0x10^{-6}$	APIDSS, 1994
Henry's law constant	-	$37.7x10^{-2}$	Howard et al., 1990
K_{oc}[4]	(ug/gOC)/(ug/ml)	122.84	Sawyer et al., 1994
solubility	mg/l	1100	Verschueren, 1983
decay rate constant	day^{-1}	$2.13x10^{-3}$	Callahan, 1979

1. Phase one modeling parameter value.
2. Phase two modeling parameter value.
3. Mean and upper boundary of the 95% confidence interval of measured soil concentration.
4. The organic carbon partition coefficient is estimated from the partition coefficient (K_{ow}) using the relationship $K_{oc}=.63(K_{ow})$ (Karickhoff et al., 1979).

Phase one modeling produced the mass loading to groundwater curve shown in Figure 16. Since the model did not allow continuous loading of the vadose zone from a source, the curve peaked out and then declined. This peak was taken to be equivalent to point b in the idealized curve shown in Figure 15, but with simulated loadings of actual conditions. Under constant source loading, maximum mass loading would be maintained until source loading stopped, having a mass loading versus time plot similar to Figure 15. From the modeling analysis, peak mass loading was achieved at year 24 or calendar year 1974. Year 0 corresponded to calendar year 1950, when contaminant disposal started. Maximum loading was maintained for a period of 11 years, from 1974 to 1985. In 1985 the UEP was closed, with removal of all solids and liquids (Green et al., 1990). This period was used to construct the b-c equivalent segment of Figure 15 with the simulated mass loading data. As mentioned, the shape of the curve in Figure 16 was a function of the soil and chemical transport properties, not of the contaminant soil concentrations.

Figure 16. Mass loading to groundwater curve shape for phase one Jury modeling without continuous loading.

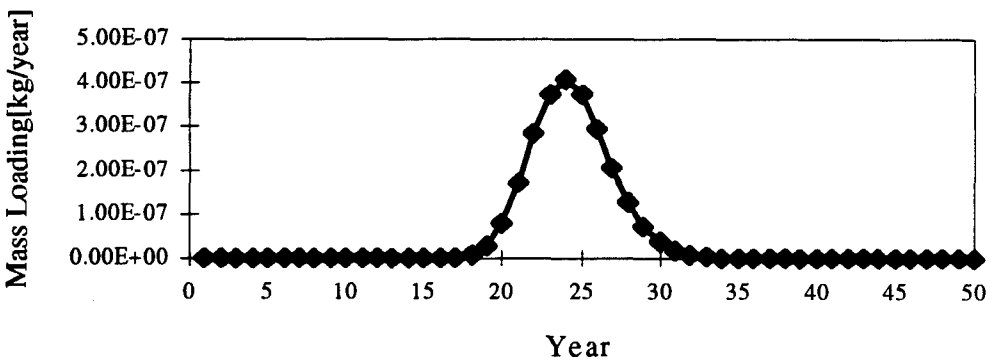

A curve similar to Figure 16 was later used to determine the pulse load (yearly loading into the aquifer) by determining the area under the curve.

Phase Two Modeling. This phase used measured 1988 data to determine mass loading. Once the shape of the mass loading curve was determined, values for mass loading were needed to determine the flux to the water table aquifer required for transport modeling. The soil concentration data were from 1988 soil analyses that were conducted on bore holes within the source area. Two values, a mean and UB 95 CI, were used in a stochastic approach to determine mass loading into the aquifer. Figures 17 and 18 present plots of the mass loading calculated during phase two. Year 0 in these figures corresponds to 1988. Notice that the shape of each curve was relatively the same but the magnitudes of mass loading differed. Mass loading for 1988 was 175 kg/yr and 347 kg/yr for the mean and UB 95 CI respectively. Each curve had a similar shape, as expected, under similar soil and chemical transport properties.

Figure 17. Mean mass loading to groundwater curve for phase two Jury modeling.

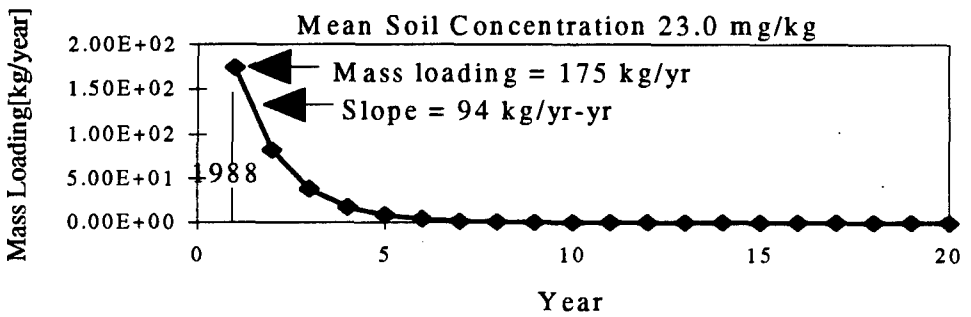

The slope for each curve varied due to the variance in mass loading. Back extrapolation of the slope simulated for the period 1988/89 was completed to the 1985-88 period to

complete the curve from closure through recession (i.e. the c-d limb of Figure 15). The extrapolation assumed the slope was constant through years 1985-89. Another assumption was that the peak mass loading rate presented in Figure 16 corresponded to point c of Figure 15 and was considered the maximum mass loading rate.

Figure 18. Upper 95% confidence level mass loading to groundwater curve for phase two Jury modeling.

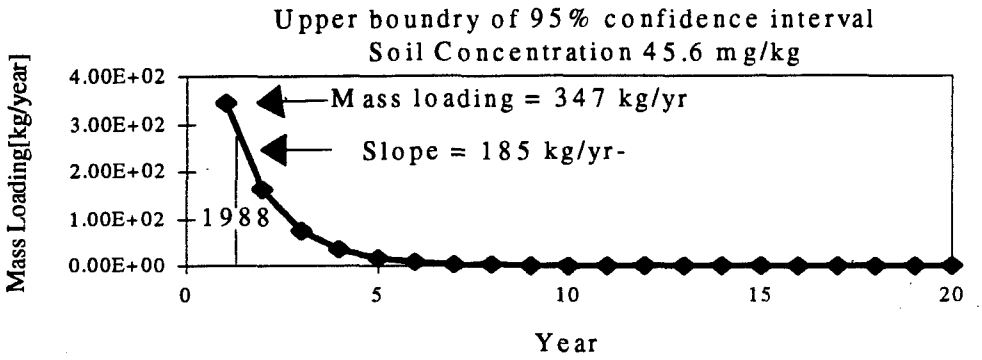

Comparing the various figures developed, the starting point in Figures 17 and 18 corresponded to a point midway on the recession limb of Figure 16. Figure 19 combines these figures into one for comparison and for calculation of total loading of TCE. The figure shows continuous loading into the aquifer starting in 1967, increasing through 1973 and then decreasing from 1985 to 1997.

The area under the curve in Figure 19 represents the total mass of TCE that was loaded into the aquifer at the mean and higher flux rates. Multiplying the mass loading (kg/yr) by the number of years yielded the mass of TCE in kilograms. Calculation was done for both curves. Each area was divided into three geometric shapes, a rectangle and two triangles on both sides of the rectangle. Total loading values calculated for the UB 95 CI and mean curves were 18,942 kg and 7998 kg, respectively. The total load values

were divided by 30 years to derive uniform pulse loadings of 631 kg/yr and 267 kg/yr for the UB 95 CI and mean curves respectively.

Figure 19. Mass loading of TCE to groundwater at the burning grounds using Jury model.

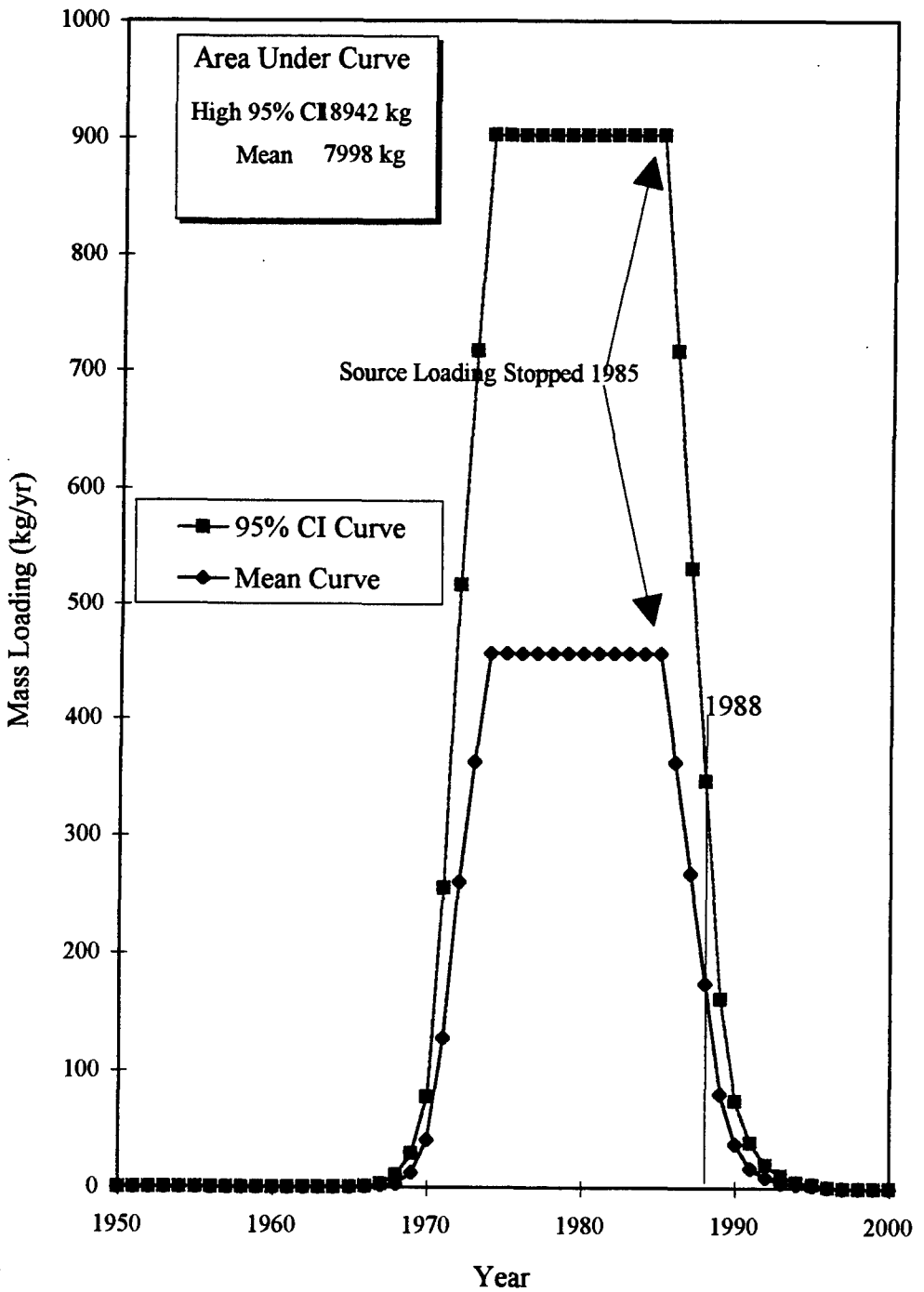

Contaminated Groundwater Transport Analysis

Purpose and Objective. This was the second contaminant transport activity to be analyzed. The previous analysis provided a contaminant source term for this modeling effort. This analysis will quantify a probability of TCE reaching the plane of compliance (POC) over a specified period of time, subject to predetermined constraints. The objective was to determine the probability of the plume reaching the POC at a specified concentration.

Method Used. A two-dimensional analytical model was used in Monte Carlo fashion to develop numerous possible scenarios. The scenarios were statistically analyzed and a cumulative probability density plot developed.

Numerous concentration break-through curves similar to Figure 20 were simulated to show the time and concentration relationship of TCE at the POC. Each of the three example simulations in the Figure 20 plot illustrates the TCE concentration at the POC over time.

Figure 20. Typical contaminant break-through curve simulated at the POC well.

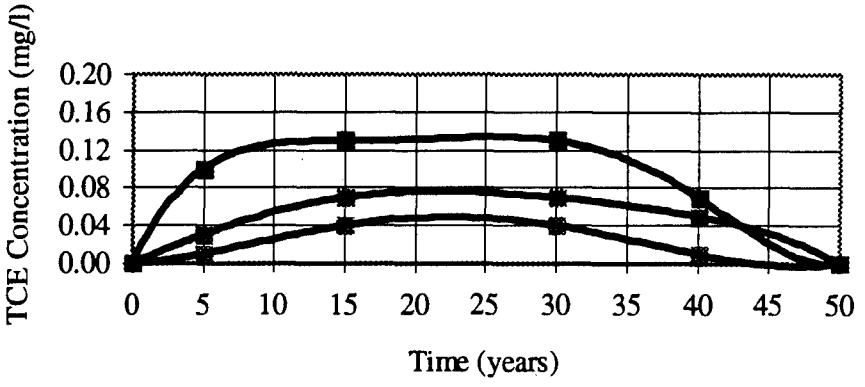

The simulations were statistically analyzed to develop a probability distribution plot for TCE concentrations for various time periods. Figure 21 illustrates an example of a probability plot for two time periods. For example, the first curve represents the probability of a concentration of X mg/l reaching the POC within a specified time period of Y years. The second curve represents the probability a concentration X mg/l reaches the POC within a specified time period of (Y+Z) years.

Figure 21. Probability plot of TCE concentration reaching POC for different time periods.

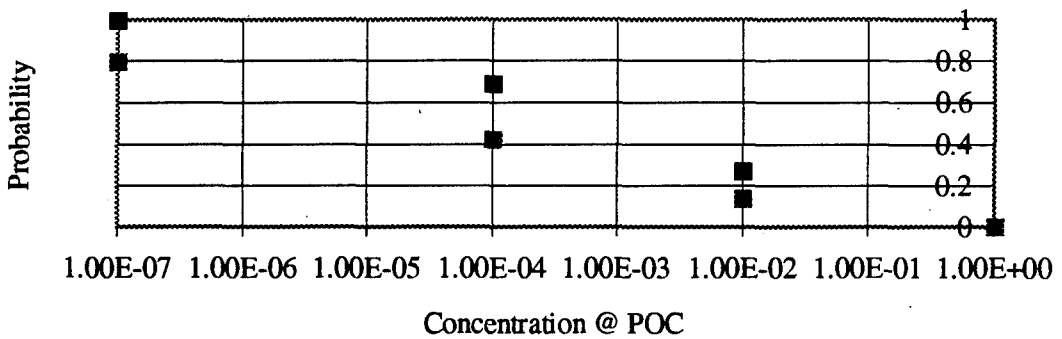

The probabilities developed were utilized within the decision analysis method to assign probabilities for the previously described states of nature. Uncertainty of contaminant transport is quantified as a probability that can be integrated into the decision analysis.

Tool Utilized. The publicly available code, Analytical Transport: One, Two and Three Dimensional (AT123D) incorporated in the APIDSS software package was utilized for this analysis. The code was developed by G.T. Yeh in 1981 at the Oak Ridge National Laboratory, Oak Ridge, Tennessee. AT123D provides flexibility to the user with the following features (Yeh, 1981 and APIDSS, 1994):

- Sources may be simulated as instantaneous releases or as time-varying load rates into the groundwater system. Time-varying loading is further subdivided into continuous and finite duration releases.
- The saturated zone may be infinite or finite in the lateral and vertical directions.
- Has the ability to simulate a variety of contaminant source geometry's oriented in different ways along the x, y and z directions. Sources can include point, line, area or volume sources.
- For our purposes, the model can be used to estimate concentrations as a function of time at any location specified by x, y and z coordinates.

AT123D uses Green's function to solve the advection-dispersion equation for the conditions listed below, and a separate solution is used for each type of source and boundary condition (APIDSS, 1994):

- Groundwater flow is assumed to be one-dimensional, steady and uniform in the down-gradient direction.
- AT123D simulates: Three-dimensional dispersion, one-dimensional uniform advection, linear and reversible equilibrium adsorption and lumped first-order decay for both chemical and biodegradation.
- Saturated zone is assumed to be homogenous and isotropic in terms of its physical properties.

Pertinent equations governing the transport and distribution of soluble contaminant are (Yeh, 1981):

$$\overbrace{\frac{\partial n_e C}{\partial t}}^{a} = \overbrace{\nabla (n_e D \nabla C)}^{b} - \overbrace{\nabla (C \mathbf{q})}^{c} + \overbrace{M}^{d} - \overbrace{(K n_e C)}^{e} - \overbrace{(\lambda n_e C)}^{f} - \overbrace{\frac{\partial(\rho_b C_s)}{\partial t} + (\lambda \rho_b C_s)}^{g} \quad (21)$$

where

$\mathbf{q}$	=	Darcy velocity vector (L/T)
D	=	hydraulic dispersion coefficient tensor (L^2/T)
C	=	dissolved concentration of the solute (M/L^3)
C_s	=	absorbed concentration in the solid (M/M)
ρ_b	=	bulk density of the media (M/L^3)
M	=	rate of release of source ($M/(L^3*T)$)
n_e	=	effective porosity (L^o)
λ	=	radioactive decay constant (1/T) (set to zero in APIDSS)
K	=	degradation rate (1/T)

Term (a) in equation (21) is the time rate of change of waste solute mass per unit volume of the aquifer water; term (b), the combined effect of hydraulic dispersion and molecular diffusion; term (c), the effects of advective transport; term (d), the contribution of waste source; term (e), the effects of first order chemical and biological degradation; term (f), the effects of radioactive decay which is set to zero by APIDSS; and term (g), the effects of reversible ion exchange or sorption (Yeh, 1981). The solution of equation (21) for a complex groundwater system is extremely difficult, therefore it is usually simplified (Yeh, 1981).

The fundamental advective-dispersion solute transport equation in three-dimension found in all basic hydrogeology texts (Freeze and Cherry, 1979) can be simplified to equation (22) if the following assumptions are made:

- Groundwater characteristics are considered uniform. Because the transport of TCE is primarily through highly conductive channel sand deposits within the Wilcox aquifer, modeling the transport within a finite aquifer (channel sand deposits) which can be assumed homogeneous.
- Sorption is in a state of instantaneous linear isothermal equilibrium (Yeh, 1981).

$$\partial C/\partial t = \nabla (K \nabla C) - \nabla (\mathbf{U} C) - [(K/R_d) + \lambda]C + M/(n_e R_d) \qquad (22)$$

where

R_d = retardation factor = $1 + \rho_b(K_d/n_e)$
K = retarded dispersion tensor = D/R_d
$\mathbf{U}$ = retarded seepage velocity = $(\mathbf{q}/n_e)^2/R_d$
K_d = distribution coefficient

Subject to the conditions that no contaminant can flow across the impervious boundaries, flow through open boundaries are located at infinity and that it is a finite duration release, solution of equation (22) is reduced to the following (Yeh, 1981):

$$C(x,y,z,t) = \int_0^T [M/(n_e R_d)]\, F_{ijk}(x,y,z,t;\tau)\, d\tau \qquad (23)$$

where

F_{ijk}	=	integral of Green's function over the source space (Yeh, 1981)
M	=	instantaneous release of total mass
T	=	duration of waste release

Tool Assumptions. Assumptions associated with the model are as follows (APIDSS, 1994):

- The saturated zone was assumed to be homogenous, isotropic and of uniform geometry.
- The water table was assumed to be steady without any fluctuations.
- The flow direction was uniform, one-dimensional and steady state.
- Contaminant decay was assumed to follow a lumped, first order decay rate.
- Contaminant adsorption was considered to follow linear adsorption.
- Concentrations in the liquid and solid phase of the aquifer assumed to be in equilibrium at all times.
- The AT123D model simulated the dissolved phase contaminants only and was not applicable to simulate the transport of free products.
- APIDSS employed an approximate method to estimate average well concentrations. Concentrations are estimated by AT123D at a user-specified number of equally-spaced vertical intervals across the well screen; these were then arithmetically averaged to compute the well concentration.

Modeling Analysis. Within this analysis several assumptions were made that were inherent to using AT123D, as previously discussed. In addition to these, other assumptions were made with regard to actual site conditions and defining parameters. Their discussion is included with the discussion of parameter sources in the following paragraphs.

Table 4 provides the parameter values and their sources used in the AT123D modeling analysis. Parameters listed in Table 4 that have their reference source highlighted with an asterisk are discussed in detail in the following paragraphs. These

extended discussions were necessary for the reader to fully understand how the parameter value was derived and the assumptions made with respect to the parameter. The following include the highlighted parameter sources:

⇒ Aquifer geometry

The aquifer was determined to be finite after thorough analysis of the site's geology and modeling the underlying aquifer as infinite and finite. Chapter Two discussed the complex depositional environment characterizing the area aquifer. The Wilcox aquifer in this area was characterized by channels of sand (remnants of previous river channels) interbedded with silt and clay deposits. Well drilling logs and geologic cross-sections provided in the data summary report confirmed the presence of sandy channel deposits. The channel sands were generally oriented Northeast to the Southwest but have substantial meandering at right angles to their orientation. Hydraulic conductivity tests performed within the various soil types also showed that the channel sands were significantly more conducive to contaminant transport than the silt and clay. Local and regional groundwater gradients had a Northern orientation (Hosman et al., 1968 and USACE, 1993). Monitoring well data for well C-6 had a TCE concentration of 139 ug/l in 1993 and less than 5 ug/l in 1992. This monitoring well was 2400 feet Northeast of the UEP. Additionally, some monitoring wells between C-6 and the UEP never had TCE detected. From the cross-section data, wells without contamination may not be hydraulically connected to the channel sand deposit C-6 is screened. Cross-sections were developed from the drilling logs to determine the channel sand deposit dimensions as given in Table 4.

⇒ Hydraulic conductivity

Hydraulic conductivity had a significant variance within the channel sand deposits, with ranges from 47 m/yr to 3045 m/yr. Hydraulic conductivity was measured in-situ using the slug test. These values were found in the data summary report for a large number of wells and bore holes (USACE, 1993). Their statistical distribution was log-normally distributed, and a Monte Carlo approach was used in a stochastic analysis utilizing the statistical distribution.

⇒ Receptor well geometry

Chapter Two discussed, in detail, the plane of compliance (POC) and its significance to the problem. AT123D modeled contaminant migration to a receptor that was defined as a point and not a plane. It was established the POC would likely be North of the site in Harrison Bayou. Along this POC a point was chosen for its location with respect to the interface of ground water with surface water. This interface was assumed to occur just South of Harrison Bayou in a low swampy area. Since the groundwater interfaces with surface water, the screening level (Z-dimension) for the receptor point was

chosen from ground level to five meters below the surface. It was assumed that any TCE migrating within this zone was captured by surface water draining into the lake.

⇒ Source geometry

Source geometry in the X and Y directions was discussed previously in this chapter. The Z-dimension parameter was set to zero because the contaminant flux was across a plane rather than from a volume. Pulse duration was set to 36 years representing TCE dumping from 1950 to 1985. The release rate was determined by the two phase soil mass loading rate analyses previously discussed and was considered to have uniform distribution between the mean and higher boundary of the 95% confidence interval.

A typical method used to determine the maximum precision of the Monte Carlo analysis involves plotting the mean concentration at the receptor point against the number of simulations. For a given number of simulations, a mean POC concentration was calculated given the concentrations from each of the simulations. As the number of simulations increased, the mean concentrations oscillated around a maximum precision value. Figure 22 shows the Monte Carlo maximum precision plot used to determine that 300 simulations insured a proper representation of all possible outcomes.

Figure 22. Monte Carlo maximum precision plot.

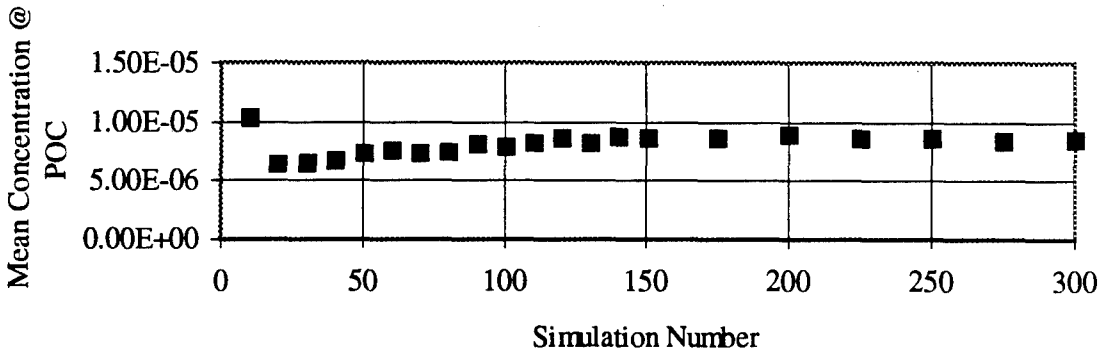

Table 4. Parameter values used in the AT123D contaminant transport model.

Parameter Definition	Units	Value	Source
Model Control Parameters			
infinite aquifer laterally	-	no	Hosman et al., 1968*
infinite aquifer depth	-	no	Hosman et al., 1968*
type of source	-	pulse	USACE, 1993
simulation time	years	50	USACE, 1993
simulation type	-	Monte Carlo	N/A
Media Specific Parameters			
hydraulic conductivity	m/yr	log-normal[1]	USACE, 1993*
effective porosity	-	0.4	USACE, 1993
hydraulic gradient	-	0.00369	USACE, 1993
longitudinal dispersivity	m	100	Yeh, 1981
transverse dispersivity	m	10	Yeh, 1981
vertical dispersivity	m	1	Yeh, 1981
dry weight soil bulk density	g/cm^3	1.58	USACE, 1993
fraction of organic carbon	-	0.01	Golden et al., 1994
thickness of the aquifer	m	5	USACE, 1993
width of the aquifer	m	106	USACE, 1993
Receptor Well Geometry			
X-coordinate of well	m	366	*
Y-coordinate of well	m	96	*
Z-coordinate top of screen	m	0	*
Z-coordinate bottom of screen	m	5	*
Source Geometry			
X-dimension of the source	m	305	USACE, 1993
Y-dimension of the source	m	159	USACE, 1993
Z-dimension of the source	m	0	*
time duration of pulse	yr	36	USACE, 1993
Chemical Specific Parameters			
release rate for pulse period	kg/yr	uniform[2]	Jury model analysis
K_{oc}	(ug/gOC)/(ug/ml)	122.84	Sawyer et al., 1994
degradation rate constant	day^{-1}	2.13×10^{-3}	Callahan, 1979
molecular diffusion coefficient	cm^2/s	1.0×10^{-6}	APIDSS, 1994

1. Hydraulic conductivity is log-normally distributed with following statistical values: Mean, 187.44; Standard Deviation, 633.514; Minimum, 47.535; Maximum, 3045.
2. Chemical release rate has uniform distribution between the minimum value (267 kg/yr) and maximum value (631 kg/yr), as modeled using Jury.

* Discussion of parameter values and sources given in previous two pages.

As a check to assure that the contaminant transport simulations were producing reasonable output, a calibration analysis was conducted. During this analysis, all model parameters were held constant except for the receptor well geometry. The new receptor well chosen was an actual monitoring well on site. Monitoring well 109 was chosen for its hydrologic connection with the UEP (see Figure 10) and its extensive monitoring history. Geologic cross-sections showed a channel sand deposit connecting MW 109 with the UEP (USACE, 1993). This provided the best possible homogeneous situation in which to conduct the simulations. Additionally, MW 109 had a monitoring record that spans 11 years (1982-93) (USACE, 1993). Initially in 1982, there was no TCE contamination detected (USACE, 1993). In subsequent years the detected amounts have fluctuated between 29 and 10,000 ug/l (USACE, 1993). The results from this check will be presented in the next chapter of this thesis.

Contaminant Plume Uncertainty

Geostatistics Definition

Geostatistics (Clark, 1979; Journel and Huijbregts, 1978; Matheron, 1971) is defined as a set of statistical procedures for describing the correlation of spatially distributed random variables and for performing interpolation and areal estimation for these variables (Cooper and Istok, 1988). This technique evolved from the empirical methods developed and applied to ore bodies in South Africa by D. G. Krige during the 1950's (Cressie, 1991). In recent years, geostatistical methods have been used in a variety of problems involving hydrogeology (ASCE Task Committee, 1990 and Cooper

and Istok, 1988). It is a potentially powerful tool for the analysis of contaminant concentration data from contaminant plumes in groundwater (Cooper and Istok, 1988). The principle reason is that estimation techniques, based on the theory of regionalized variable, can be used to obtain the best and unbiased estimates of contaminant concentrations at unmeasured points in the plume, based on a limited number of groundwater samples (Cooper and Istok, 1988). The term "best" is in the sense that the estimation error is minimized (Cooper and Istok, 1988). Geostatistical methods are useful for site assessment and monitoring situations where data are collected on a spatial network of sampling locations, and are particularly suited to cases where contour maps of pollutant concentration or other variables are desired (Englund and Sparks, 1991).

Geostatistics Objective

The objective in this analysis was to use some of the geostatistical techniques available to develop an isoconcentration map of the TCE plume. Even though there were forty sampling points within the burning grounds, there was still some level of uncertainty with respect to the plume's dimensions and concentration contours. The output from this analysis was important to the decision analysis because the plume characteristics were used to identify various alternative remedial actions and their attendant costs for the subsequent decision model.

Method Developed and Applied

The flow chart illustrated in Figure 23 represents the geostatistical methods used in this analysis. Following data collection from the sample sites, Variance Analysis was conducted to determine the variance (spatial statistics) between all the sampling points. An experimental variogram was developed to describe the pattern of spatial correlation displayed by the data (Cooper and Istok, 1988). After the experimental variogram was developed, a variogram model was chosen for interpretation of the spatial correlation structure of the data set (Englund and Sparks, 1991). The computation, interpretation and modeling of variograms is the "heart" of a geostatistical study (Englund and Sparks, 1991). This analysis controls interpolation during the conditional simulation step as well as the ultimate quality of the results by kriging and/or conditional simulation (Englund and Sparks, 1991). Time spent within this step should be greater than any one step within the flow chart.

Figure 23. Flow chart graphically depicting the geostatistical methods used in this thesis.

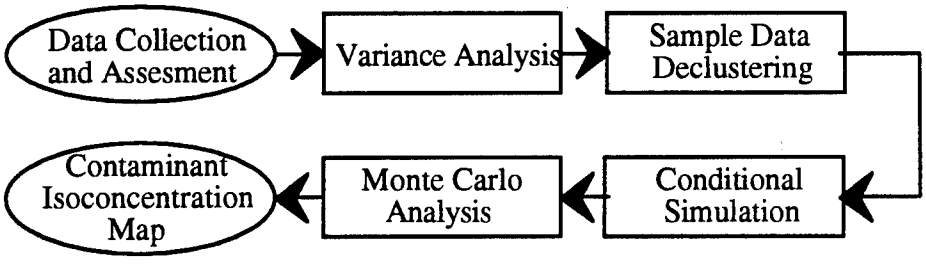

The Sample Data Declustering step was used for this particular data set because many of the sample points were spatially clustered. Clustering of wells within the plume is common for groundwater contamination problems because the objective is to locate and define the plume. Therefore, the collected data may be skewed and not a true

representation of the entire area encompassing the sample points. To obtain a representative distribution, one approach is to assign declustering weights, whereby values in areas with more data receive less weight than those in sparsely sampled areas (Deutsch and Journel, 1992).

Conditional simulation is a method utilized to estimate the concentration of the contaminant at unsampled locations. This method is a technique of the Monte Carlo type for generating multiple random realizations of two- or three-dimensional fields of a regionalized variable (Delhomme, 1979). A simulation is considered conditioned when it honors the observed values of the regionalized variable (Hohn, 1988). Thus, a conditional simulation can be defined as a surface which has the same variability as the studied phenomenon and passes through the observed points maintaining their values (Delhomme, 1978). With numerous simulations, each considered possible versions of reality, an analysis can be conducted on the statistical distribution of the contaminant concentrations (Delhomme, 1979). This analysis results in an isoconcentration map for the TCE plume and a measure of statistical variance around each point that can be used within the decision model.

Data Assessment

The objective of this step was to become familiar with and statistically analyze the data set (Englund and Sparks, 1991). This step was required because geostatistics requires that the regionalized variable (ReV) be normally distributed (Cooper and Istok, 1988). A combination of statistics and graphical displays are used to look at the range

and shape of the distribution, to look for outliers which may be erroneous or unrepresentative, to look at the spatial coverage of the data and to look for spatial patterns in the data (Englund and Sparks, 1991). In many cases a transformation is used to improve the fit of the ReV to a normal distribution (Cooper and Istok, 1988).

The tool used in this step was Geostatistical Environmental Assessment Software (Geo-EAS) version 1.2.1 (Englund and Sparks, 1991). Refer to Appendix A for a discussion of Geo-EAS and methods applied in data assessment.

Data Spatial Variance Analysis

Purpose and Objective. As previously mentioned, this step is probably the most important. A majority of time in the geostatistical analysis was spent developing the variogram model that best fit the experimental variogram. There are two objectives within this step: (1) developing the experimental variogram from the sampling set and (2) fitting a variogram model to the experimental variogram. The purpose of the model was to approximate the "true variogram" that is later used during the conditional simulation step (Englund and Sparks, 1991).

Methods Applied. Cooper and Istok (1988) discuss the methodology for calculating the experimental variogram and fitting a model to the variogram. Two moments of Z(x) (with Z(x) representing the random function of contaminant densities) are required for a linear geostatistical analysis. The first-order moment is the mean of Z(x) and the second-order moment includes:

variance: $$\mathrm{Var}[Z(x)] = E\{[Z(x) - m]^2\} = C(0) \quad (24)$$

covariance: $C(\mathbf{h}) = E\{[Z(x + \mathbf{h})]\,[Z(x)]\} - m^2$ (25)

variogram: $2\gamma(\mathbf{h}) = E\{[Z(x + \mathbf{h}) - Z(x)]^2\} = C(0) - C(\mathbf{h})$ (26)

where

m = $E[Z(x)]$ = mean or expected value (27)

$\mathbf{h}$ = $x_i - x_{i+1}$ (vector) (28)

$\gamma(\mathbf{h})$ = variogram in the form used most often

The semivariogram is the principal tool used in geostatistics because it can be applied with less restrictive assumptions than the variance or covariance (Cooper and Istok, 1988). The semivariogram defined in equation (26) represents the true semivariogram of the ReV. Since there are a limited number of sampling points not covering the entire area of interest, it is only possible to estimate the true structure (Cooper and Istok, 1988). This estimate is called the experimental semivariogram (Cooper and Istok, 1988):

$$\gamma^*(\mathbf{h}) = [2N(\mathbf{h})]^{-1} \sum_{i=1}^{N(\mathbf{h})} [z(x_{i+\mathbf{h}}) - z(x_i)]^2 \quad (29)$$

where

$N(\mathbf{h})$ = the number of sample pairs separated by the vector $\mathbf{h}$.

Rules to follow for estimating the true semivariogram from a set of sample values are (Journel and Huijbregts, 1978):

$N(\mathbf{h}) >$ 30 to 50 sampling points (30)

$|\mathbf{h}| < L/2$ (31)

where

$|\mathbf{h}|$ = magnitude of the separation vector $\mathbf{h}$

L = longest dimension of the contaminant plume

After the experimental variogram is developed, fitting that variogram to a model follows. The most commonly used models are linear, spherical, exponential and gaussian (Cooper and Istok, 1988).

Preliminary comparisons of the variogram model with the experimental model are made by eye (Cooper and Istok, 1988). Fitting utilizes knowledge of the physical properties of the contaminant, the plume, aquifer and groundwater flow patterns (Cooper and Istok, 1988). A variogram may be unidirectional. Therefore, different variograms can exist in different directions exhibiting anisotropies (Hohn, 1988). The type of model was obvious from the experimental variogram calculated during this analysis. Appendix A discusses the techniques and Geo-EAS tools utilized in developing the variogram model to ensure a best fit of the model to the experimental variogram.

Sample Data Declustering

The purpose of groundwater monitoring wells is to detect contamination. Therefore, the data collected can have an inherent bias due to the placement of the wells and not represent the true data set. This is especially true for the burning ground example problem where the purpose of placing monitoring wells was to locate and define the groundwater contamination plume. Figure 10 shows the location of the monitoring well with respect to the waste units and the clustering of the wells within the TCE plume as shown in Figure 12. For this particular problem the data were treated as if it were spatially clustered. The purpose of this step is to obtain a representative data sample without the clustering bias. An approach taken was to assign declustering weights to sample points, whereby values in areas with more data receive less weight than those in sparsely sampled areas (Deutsch and Journel, 1992). Appendix A discusses the techniques and tools utilized in assigning declustering weights to sampling points.

Conditional Simulation

Purpose and Objective. Conditional simulation (CS) uses the variogram model and sample data to generate two-dimensional realizations of the regionalized variable (log-normal TCE concentration). Each realization is a possibility of reality but is not necessarily reality. When (n) number of realizations are generated, they can be statistically analyzed to determine the distribution around a statistical mean. The mean, at a simulated point, will show the value estimated by kriging and its corresponding estimation variance (Delhomme, 1978). The objective is to develop an isoconcentration map of the plume within some designated confidence interval.

Methods Applied. Kriging (Delhomme, 1978) is one of the original methods of interpolating a regionalized variable. The method is considered an exact interpolator, providing at every simulated point the best possible linear estimate (Delhomme, 1978). Kriged output is smoother, less detailed than the true values, and a true (versus a spatially weighted) error is unknown (Delhomme, 1978). Conditional simulation provides a solution to kriging by providing more detail and the ability to approximate (estimate) the true error (Delhomme, 1979). The following equation depicts the differences between kriging and CS (Delhomme, 1979):

true value	=	kriging estimate		true error	(32)
$z(x)$	=	$z^*(x)$	+	$[z(x) - z^*(x)]$	

Kriging cannot calculate the true error because the algorithm does not have a value for $z(x)$ as shown in the kriging error definition. Conditional simulation estimates the error by using the underlying spatial structure of the variable of concern to simulate an

estimation error. That is, the CS method uses the modeled validated variogram as the indicator of spatial variation for the simulated variables.

Traditionally, CS is divided into two steps: (1) generation of nonconditional simulations (NCS) and (2) conditioning (Delhomme, 1979). Nonconditional simulations vary from conditioned in the fact NCS does not honor observed values.

- Step 1 (Delhomme, 1978): Simulation of the error for equation (32) is performed using NCS methods such as "turning bands" (Matheron, 1973) that simulates a realization s(x) of a random function S(x) having the same spatial variation as z(x). Kriging can be performed on s(x) using the true data locations. As the variogram is the same, the kriging estimate $s^*(x)$ at point x are computed with the same kriging weights as for $z^*(x)$. The term s(x) is now defined as:

  $$s(x) = s^*(x) + [s(x) - s^*(x)] \quad (33)$$

  and can be substituted into equation (32):

  $$[z(x) - z^*(x)] = [s(x) - s^*(x)]$$

- Step 2 (Delhomme, 1978): Each of the NCS obtained in the first step are conditioned to the sample values. From the actual sample values, kriging has yielded an estimate $z^*(x)$ at any point x. If x is not a sample point, the true value z(x) is not available, and the kriging error $[z(x) - z^*(x)]$ remains unknown. But the first step determined the kriging error as shown in equations (32) and (33). Therefore the CS $z_s(x)$ is defined as:

  $$z_s(x) = z^*(x) + [s(x) - s^*(x)] \quad (34)$$

Tool Utilized. The sequential gaussian simulation program (SGSIM) was utilized for the conditional simulation step (Deutsch and Journel, 1992). This newer algorithm, available from Geostatistical Software Library (GSLIB) by Deutsch and Journel (1992), streamlined the simulation by producing direct conditioned estimates without the intermediate unconditioned step. Sequential simulation conditioning is extended to include all data available within a neighborhood of the simulated variable, including the original data and all previously simulated values (Deutsch and Journel, 1992).

Using SGSIM, each variable was simulated sequentially according to its normal conditional cumulative distribution function (ccdf) fully characterized through a simple kriging system (Deutsch and Journel, 1992). The conditioning data consist of all original data and all previously simulated values found within a neighborhood of the location being simulated (Deutsch and Journel, 1992).

Using the SGSIM program, the conditional simulation of a continuous variable $z(\mathbf{u})$ modeled by a Gaussian-related stationary random function $Z(\mathbf{u})$ proceeds as follows (Deutsch and Journel, 1992):

- Using the cumulative distribution function (cdf) $F_Z(z)$, performs the normal score transform of z-data into y-data with a standard normal cumulative distribution function.
- Defines a random path that visits each node of the grid (not necessarily regular) once. At each node $\mathbf{u}$, retains a specified number of neighboring conditioning data including both original y-data and previously simulated grid node y-values.
- Uses simple kriging with the normal score variogram model to determine the parameters (mean and variance) of the ccdf of the random function $Y(\mathbf{u})$ at location $\mathbf{u}$.
- Draws a simulated value $y^{(l)}(\mathbf{u})$ from the ccdf.
- Adds the simulated value $y^{(l)}(\mathbf{u})$ to the data set.
- Proceeds to the next node, and loop until all nodes are simulated.
- Back transforms the simulated normal values $\{ y^{(l)}(\mathbf{u}), \mathbf{u} \in A \}$ into simulated values for the original variable $\{ z^{(l)}(\mathbf{u}) = \varphi^{-1}(y^{(l)}(\mathbf{u})), \mathbf{u} \in A \}$.
- For multiple realizations $\{ z^{(l)}(\mathbf{u}), \mathbf{u} \in A \}$, $l = 1,...,L$, the previous algorithm is repeated L times with either one of the following options: Uses the same random path to visit nodes or a different random path for each realization.

Monte Carlo Analysis

Purpose and Objective. Each of the numerous simulations represents a possible realization of the true TCE concentrations within the groundwater aquifer. A statistical analysis was conducted on the numerous simulations to determine the isoconcentration map of the TCE plume within certain confidence intervals. Three product outcomes include: a mean isoconcentration map, an upper boundary of the 95% confidence interval map and a upper boundary of the 90% confidence interval map.

Tool Utilized and Methods Applied. The contaminated site was represented on a grid network of 75 feet square, 3750 feet East-West boundary and 4500 feet North-South boundary. Each grid intersection was represented by a node for which a value $z^{(l)}(\mathbf{u})$ was simulated. A statistical analysis was calculated for each of the node locations to estimate the cumulative probability distribution. If $z(\mathbf{u})$ represents the true concentration value at any node, then (Dean et al., 1989):

$$z(\mathbf{u}) = g(\mathbf{X}) \quad (35)$$

where

g = function representing the conditional simulation
$\mathbf{X}$ = vector of all simulation inputs

Since the components of $\mathbf{X}$ contain the cumulative distribution function (cdf) $F_z(z)$ the goal of Monte Carlo analysis is to calculate the cdf $F_{z(u)}(z_s(\mathbf{u}))$ given the probabilistic characterization of $\mathbf{X}$ (Dean et al., 1989). $F_{z(u)}(z_s(\mathbf{u}))$ is defined as (Dean et al., 1989):

$$F_{z(u)}(z_s(\mathbf{u})) = \text{Probability}(z(\mathbf{u}) \leq z_s(\mathbf{u})) \quad (36)$$

where

$z_s(\mathbf{u})$ = is the CS output

Given a set of deterministic values for each of the input parameters, X_1, X_2, ..., X_n, SGSIM computes the output simulation value as (Dean et al., 1989):

$$z(\mathbf{u}) = g(X_1, X_2, ..., X_n) \quad (37)$$

Application of the Monte Carlo simulation procedure requires that at least one of the input variables, X_n, be uncertain and the uncertainty is represented by a cumulative probability distribution (Dean et al., 1989). The simulation is then conducted numerous times to generate a series of $z_s(\mathbf{u})$ values for each of the nodes within the two-dimensional grid simulated. The simulated outputs are then statistically analyzed to yield the cumulative probability distribution of the simulated output (Dean et al., 1989). The steps involved in the application of the Monte Carlo technique was (Dean et al., 1989):

1. Select the appropriate cumulative probability distribution function for describing uncertainty in the input variable(s).
2. Select a random number from the distribution and use this as input to the model.
3. Run the model using the random number taken from the input distribution to calculate the output.
4. Repeat steps 2 and 3 for a number (n) times.
5. Determine the cumulative probability distribution function of the output step 3.
6. Analyze the output distribution and utilize the statistics (i.e. mean and UB 95 CI).

A subsequent grid with the statistical values of the simulated values was developed on a spreadsheet and plotted.

To ensure adequate representation of the random field *A* and that all possible realizations were simulated, a Monte Carlo maximum precision plot was developed using

the same procedures defined previously in the groundwater contaminant transport section.

Cost Analysis

Purpose and Objective

A primary goal of this decision analysis was to ensure that cost estimates did not influence the decision process. That is, decisions alternatives should not show a sensitivity to cost estimates. Cost estimates were developed by Cost of Remedial Action (CORA), a program developed by CH2M Hill under contract to the U.S. EPA's Office of Solid Waste and Emergency Response (CH2M Hill, 1990). The model was commissioned to assist EPA in compiling a list of, and developing cost estimates for site management options at Superfund sites (CH2M Hill, 1990). Using a model such as CORA provided an objective means to estimate costs for the various alternatives within the decision model.

Tool Utilized

The CORA model is comprised of two subsystems: the expert system and the cost system (CH2M Hill, 1990). Both were used in this analysis. The expert system provided a number of potential remedial action scenarios for the site in question (CH2M Hill, 1990). The remedial action scenarios were then used to develop the alternatives within the decision model. Output from the system comes in the form of a list of cost modules that were accessed through CORA's cost system.

The cost system consisted of the cost module building blocks and a book keeping system for storing and retrieving data (CH2M Hill, 1990). The cost module blocks utilized to develop estimates of capital and operational costs for the following objective function variables: cost of remedial action, cost of failure, cost of additional testing, and cost of monitoring groundwater wells. For any specific consequence, there may be costs associated with all or some of the listed variables.

Cost estimates were made for the following actions using CORA:

- Remedial Action Cost (capital and operational)
  - Groundwater Extraction (module 206)
  - In-Situ Bioremediation (module 304)
  - Discharge to Surface Water (module 406)
  - Air Stripping Treatment (module 307)
  - Granular Activated Carbon Treatment (module 309)
  - Site Preparation (no module number)

- Failure Cost (capital and operational)
  - Surface Water Diversion (module 105)
  - Site Access Restrictions (module 504)
  - Municipal Water Supply (module 502)

- Additional Testing (capital and operational)
  - Groundwater Monitoring Well Construction (module 503)
  - Groundwater Monitoring (module 503)

- Existing Groundwater Monitoring (operational) (module 503)

Methodology Applied

Groundwater Extraction. Utilizing the isoconcentration map (Figure 40) to estimate the length of an extraction well barrier line, a line of 15 wells with overlapping depression cones was chosen as needed to remove the contaminant in the ten year remediation time period. The pumping rate was estimated as 500 gpm (Hosman et al.,

1968) while the other parameters used for this module were based on site characteristics and climatalogical data for the area of study. These parameters as well as those for the other cost modules are presented in Tables 7-17. Parameters involving protection above grade and during drilling were not employed in this analysis.

In-situ Bioremediation. Similar assumptions as were made for groundwater extraction were also applied in this module. The isoconcentration map for the UB 95 CI (Figure 40) was used for determining the area of contamination and the initial contaminant concentration by calculating the mean concentration over the entire plume. Bioremediation-specific parameters were taken from the suggested CORA parameters when a value was unknown for the site such as efficiency of hydrogen peroxide and oxygen demand. The remediation period was held constant at 10 years for both bioremediation and the groundwater extraction alternative.

Discharge to Surface Water. Due to the sites remote location and no accessibility to a permitted waste water treatment plant, the assumption was made that the extracted groundwater would be treated and released into the local drainage feature. Costs associated with treating and discharging the extracted groundwater were developed. This module considered only the cost associated with discharge. Two types of treatment were compared for the treated groundwater.

Granular Activated Carbon Treatment. This treatment was the first considered for treatment of the extracted groundwater. This treatment and air stripping were considered to illustrate the methodology's flexibility to changing decision criteria. If there are future changes in regulatory requirements, the decision analysis has the flexibility to

adjust to other alternatives. Two assumptions were made, that the water flow was 2000 gpm and the total organic carbon was 10000 ug/l based on the initial concentration calculations made from the isoconcentration map. As with any granular activated carbon system, the largest expense incurred was due to the high cost of activated carbon. CORA estimated the amount of activated carbon required and used this estimation for developing operational costs.

Air Stripping Treatment. The second of the two water treatment operations incorporated into the groundwater extraction alternative cost was air stripping. Input parameters such as flow of water, chemical constants and concentration were used by CORA to develop an air stripping tower design that would meet the specified effluent concentration. The resulting tower design was used by CORA to estimate the costs for construction and operation of the system. The cost estimate made for this treatment operation was based on the assumption that the vapors would not be secondarily treated.

Failure Costs. Developing costs for failure was difficult to determine, as these had the potential to influence the subsequent decision model through the calculation of the expected monetary value. The approach taken was that any TCE concentration ≥ 5 ug/l reaching the POC would be considered failure, and costs associated with this failure were then calculated. An assumption of the analysis was that remedial action was considered 100% effective and no failure costs would be incurred. Three cost modules: runoff diversion, site security and municipal water replacement were used to estimate the failure costs. Their calculation was critical to the analysis. The costs that included runoff diversion involve the diversion of contaminated surface runoff from the surrounding

drainage features. In addition, if contamination reached Harrison Bayou, some excavation of contaminated soil was necessary. The second category of costs were site access restrictions for areas contaminated beyond the boundaries of the ammunition plant. Security would be required for protection of the remediation equipment as well as securing the contaminated site from unwarranted access by the general public. The third failure cost included supplying municipal water to those affected by contaminated groundwater. The approach employed determined the costs of municipal water supply for a number of residential and commercial connections to the distribution system.

Decision Model

Purpose and Objective

The decision model's purpose is to provide the decision maker with a way of concisely visualizing the problem and a means to evaluate decisions/alternatives within the model. The objective is to assist the decision maker in the decision process to solve a problem or set of problems. The example problem involved TCE contamination of the groundwater that could potentially reach a source of drinking water for the surrounding communities. Problem definition was to choose the best alternative that minimized both the cost of remediation and environmental risk.

Methodology Discussion

As discussed in Chapter I, the methodology was an adaptation of the military decision making process. The decision model utilized the decision tree analysis approach

as discussed by Ossenbruggen (1984) and Chechile (1991). A description of decision tree analysis follows (Chechile, 1991):

> "A decision tree is a visual portrayal of the entire structure of a decision problem. It shows alternative courses of action; it shows all the possible outcomes that could result along with their associated probability values; it shows the sequence of decisions that could result; and it shows the resulting consequence cost for each outcome."

Tool Utilized

The Decision Analysis software by TreeAge (DATA) was used to implement the decision tree analysis (DATA, 1994). DATA is capable of performing the analysis quickly and has other options including the ability to evaluate intermediate points within the tree, conduct Monte Carlo simulations and conduct sensitivity analysis on variables.

Methodology Applied

Decision Framework Scoping. Developing the decision tree framework starts with visualizing the problem and developing a logical flow diagram of the decisions that must be made. This process is tedious and usually requires changes or adjustments to the tree. Using a program such as DATA was helpful with its ability to edit large trees quickly. Figure 24 is the basic decision tree developed after visualizing the example problem. This decision tree only shows the decisions or alternatives within the tree and does not include the chance node branches.

Given the example problem discussed in Chapter II, the decision maker was faced with the possible decision to "take action" or "postpone action". Postponement could be for budgetary reasons, better site assessment or others. If "take action" was chosen, then subsequent decisions involving additional testing and remedial action follow in the decision tree. The same questions involving remedial action follow the postponement decision. An assumption inherent to the postponement decision is that additional testing requirements are incorporated into this decision.

Assumptions made with regard to decision tree variables and the analysis include:

- The time required to remediate the site was 10 years for all remedial action alternatives.
- If remediating action was taken, the monitoring period was 13 years. Ten years is during the remediation phase and three years for post closure monitoring.
- If remediation action is delayed, the monitoring period was equal to the delay time plus the 13 years. The delay was set as 10 years, therefore monitoring was equal to 23 years.
- If no action was taken, then the monitoring period was set as 50 years. This is equal to the time the unit was in operation and must be monitored for that period of time after closure.
- Failure costs would be incurred for a period of 50 years. This takes into account the biodegradation and dispersion of the contaminant to levels below the MCL.
- Calculation of present worth value of future payments used a discount rate of 7%.
- The additional monitoring wells installed provided early warning to contaminant reaching the POC. Therefore the cost of failure was assumed to be zero.
- Remediation was assumed 100% effective and cost of failure is zero.
- All recurring costs are on a yearly basis.

Figure 24. Decision tree in skeletal form, depicting decision nodes within the tree.

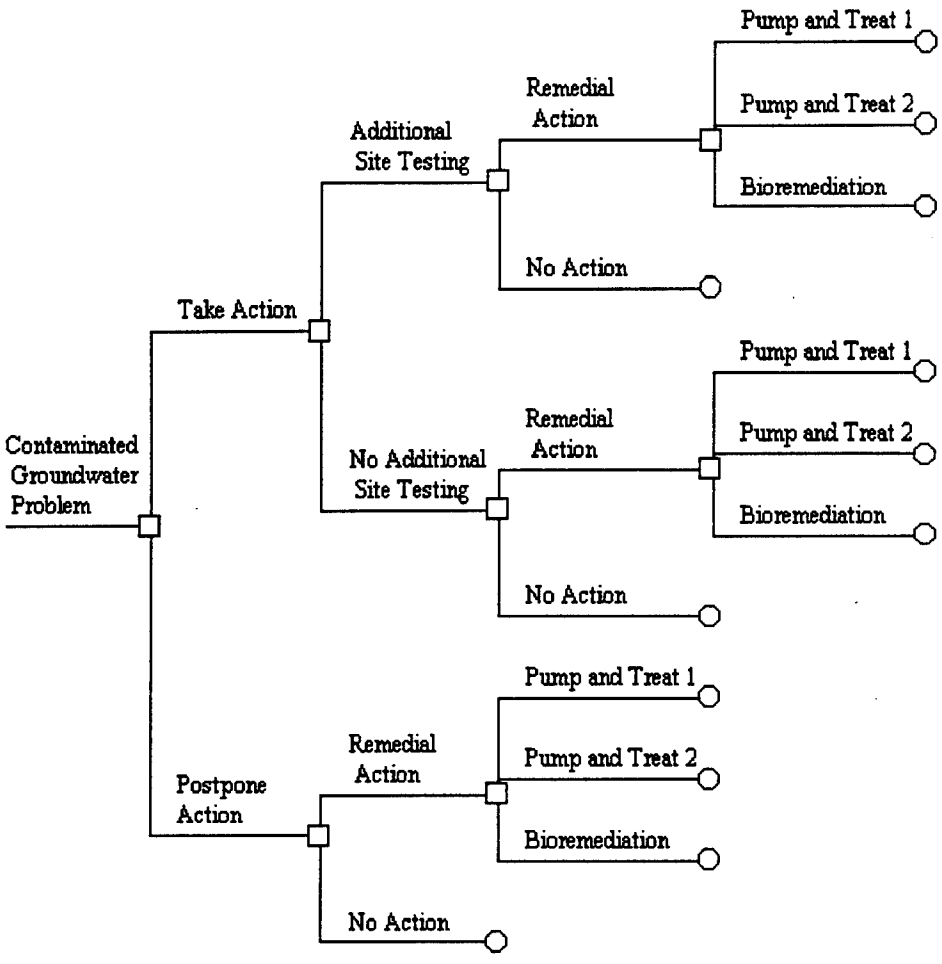

Uncertainty Integration. The uncertainty of the problem is depicted by chance nodes within the decision tree. The result of a chance node is the true state of nature of a given situation. Figures 24 and 25 show where a majority of the chance nodes were located at the ends of the remedial and no action alternatives in the developing decision tree. Another type of decision node will be introduced in a later section that discusses prior and posterior probabilities resulting from additional testing.

Figure 25. Integrating chance nodes and states of nature within the decision tree.

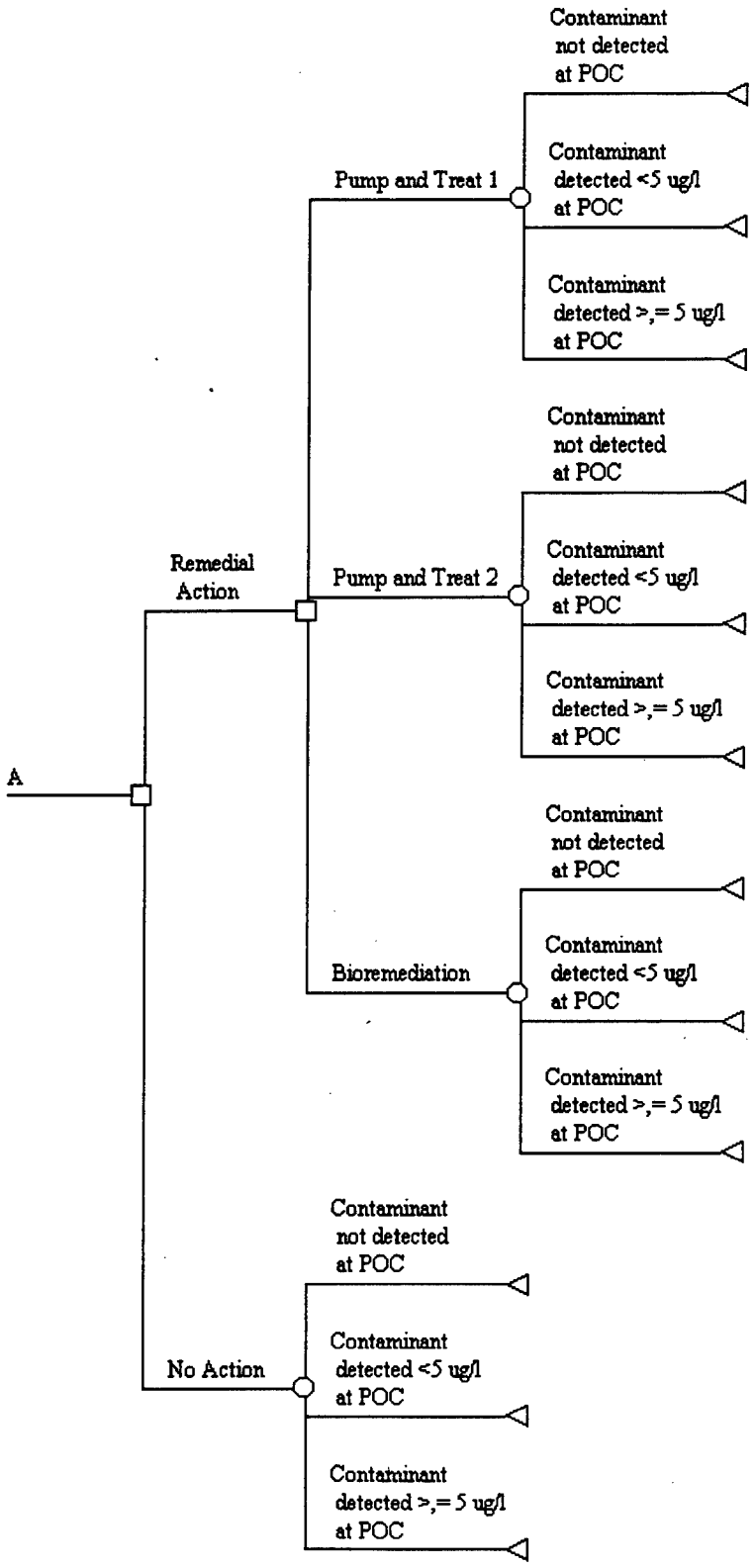

Branching out from the chance nodes are three states of nature; no detectable TCE at the POC, < 5 ug/l of TCE detected at the POC and > 5 ug/l of TCE detected at the POC as shown in Figure 25. Probabilities are assigned to each state of nature resulting from the transport analysis conducted using APIDSS. Since there were no further decisions beyond the states of nature, DATA identified these nodes as terminal and prompts the user for the objective function. In this example problem the objective function is the cost that was defined in equation (1) in Chapter II. Figure 25 represents a sub-tree that is incorporated into any of the decisions in Figure 24 that precede remedial action and no-action decisions.

Prior and Posterior Probabilities. From the contaminant transport analysis, probabilities were established for the states of nature because the true state of nature was unknown. Probabilities were dependent upon the methods and data used for their calculation. In the example, there was uncertainty involved with transport parameters and the monitoring data. This uncertainty was carried onto the probabilities. A method of improving or updating probabilities involved the use of Bayes Theorem, which states that revised probability is proportional to the sample likelihood times the prior probability (Press, 1989). Sample likelihood is the same as conditional probability or the probability that test event Z_j occurs given the true state of nature (Ossenbruggen, 1984). Therefore, the revised probability can be illustrated with the following equation (Ossenbruggen, 1984):

$$P[S_i/Z_j] = \frac{P[Z_j/S_i] * P[S_i]}{P[Z_j]} \quad (38)$$

where

$P[Z_j/S_i]$ = conditional probability

$$P[Z_j] = \sum P[Z_j/S_i] * P[S_i] \quad (39)$$

$P[S_i]$ = probability for state of nature i

Utilizing the Bayes Theorem equation, revised probabilities were determined given the additional information/data that could be gained from newly constructed monitoring wells. This test was considered an imperfect test due to the possibility of error during laboratory analysis of TCE concentrations (Standard Methods, 1989). Conditional probability was calculated about the MCL of 5 ug/l for TCE using the following equations (Standard Methods, 1989):

$$\text{Expected measured bias} = .92C - .1 \qquad (40)$$

$$\text{Overall precision standard deviation} = .32\sqrt{X} - .57 \qquad (41)$$

where

$\underline{C}$ = true concentration of TCE
X = expected measured bias

Three states of nature were established for the example problem, each having two probabilities associated. Probabilities for states of nature defined for current conditions will not be the same for future times. The states of nature are defined as:

1. S_1: no detectable contamination at the POC.
2. S_2: less than 5 ug/l of contamination detected at the POC.
3. S_3: greater than or equal to 5 ug/l of contamination detected at the POC.

Three experimental outcomes were established and defined as:

1. Z_1: no detection of TCE during analysis, minimum detection limit is .12 ug/l (Standard Methods, 1989).
2. Z_2: less than 5 ug/l of contamination detected during analysis.
3. Z_3: greater than or equal to 5 ug/l of contamination detected during analysis.

Conditional probabilities are summarized in the following table using equations (40) and (41) for their calculation. The table is configured with states of nature S_n in columns and

the experimental outcomes Z_n in rows. Conditional probability, $P[Z_j/S_i]$, is the sum of the probabilities of an experimental outcome given a S_n divided by the probability of the state of nature. For example, the conditional probability for a test yielding < 5 ug/l of TCE given that the true state of nature is no detectable amount of TCE present will be .4286 or 43%. That is, referring to the table, the $P[Z_2/S_1] = .4286$ and is found at the intersection of the Z_2 row and the S_1 column.

Table 5. Conditional probability values used in the development of the revised probabilities for the decision tree analysis.

$P[Z_j/S_i]$	S_1	S_2	S_3
Z_1	.5714	0	0
Z_2	.4286	.5714	.4286
Z_3	0	.4286	.5714

Bayesian analysis was incorporated into the decision tree analysis to determine if additional testing would enhance the available data and provide a revised state of nature with less uncertainty. The decision to conduct additional site testing was located at two places within the decision tree (see Figure 24). It was assumed that any postponement of action would require the decision maker to perform additional testing. Therefore, in the Postpone Action decision branch, additional site testing was incorporated without any decision. The structure of the additional site testing sub-branch is illustrated in Figure 26.

Utilizing Bayes Theorem into the decision analysis provided the analysis with a revised probability for the states of nature but also a means to evaluate the worth of additional data. Decision tree analysis took into account the cost of procuring the additional data and provided the analysis with the results that additional testing would yield in the form of revised probabilities.

Figure 26. Additional Site Testing sub-branch incorporated into the overall decision tree.

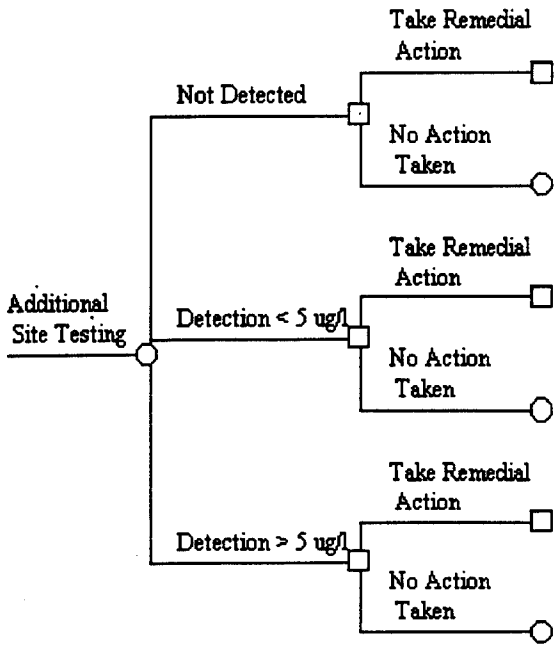

Objective Function Variable Sensitivity Analysis. The sensitivity analysis was conducted using an option available in DATA (1995). Two types of sensitivity plots were utilized to show the sensitivity of the respective variable to changes in the expected monetary value (EMV) and the resultant cost. The tornado diagram illustrated in Figure 27 gets its name from the shape exhibited by the boxes within the plot. This type of plot illustrates several variables with their respective sensitivity shown by the block width. For example, the block for monitoring operational costs illustrates that the variable is sensitive from an EMV of $1.0 million to $9.0 million. That is, if the EMV within this range was to increase for the optimal alternative then a change in the optimal alternative would occur. The dotted vertical line represents the EMV for the optimal alternative calculated during the analysis.

Figure 27. Typical tornado diagram illustrating sensitivity for numerous objective function variables.

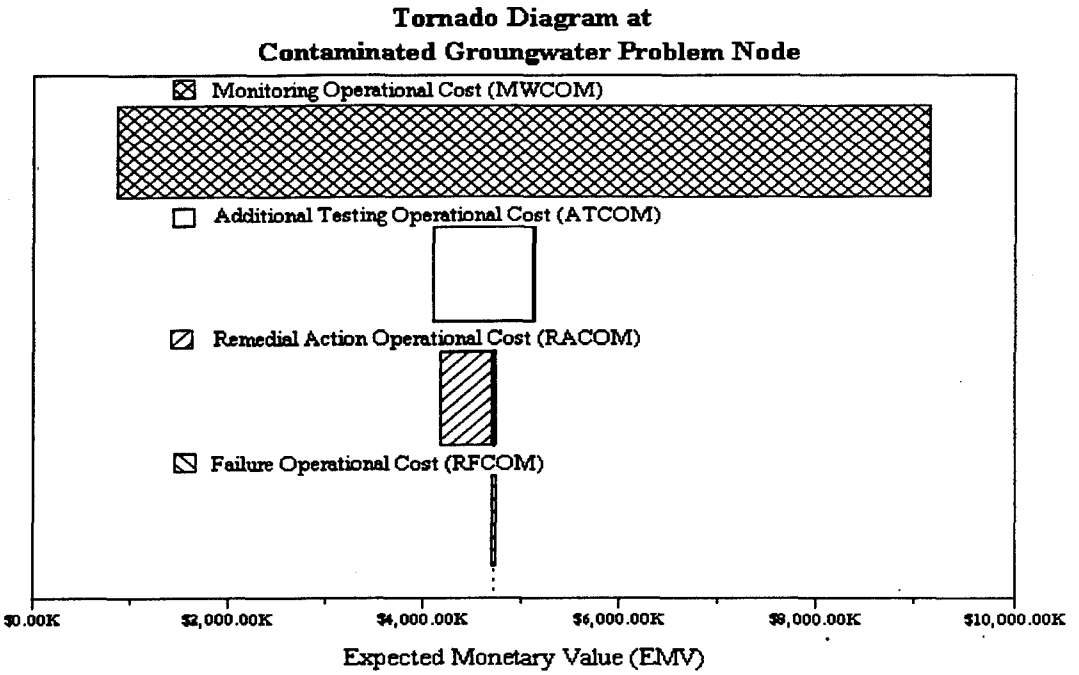

The dark vertical lines within the sensitivity boxes for the variables of additional testing operation costs (ATCOM), and remedial action operation costs (RACOM) illustrated that a threshold value existed for the variable. This threshold value is better presented in Figure 28, as shown by the intersection of the two decision alternatives to take action and postpone action. Cost for ATCOM above the threshold value of $76,000 results in the optimum alternative of postpone action and if below that threshold the optimum alternative changes to immediate remedial action.

The utility of the tornado diagram is apparent when there were numerous variables within the objective function. Instead of looking at each variable separately, the tornado diagram can be used to illustrate the sensitivity of numerous variables. Variables exhibiting sensitivity in the diagram can then be evaluated further utilizing the sensitivity

plot shown in Figure 28. When a variable was suspect, then a plot similar to Figure 28 was utilized to further determine the threshold point at which the optimal decision alternative could change.

Figure 28. Sensitivity analysis plot of an individual objective function variable cost versus EMV.

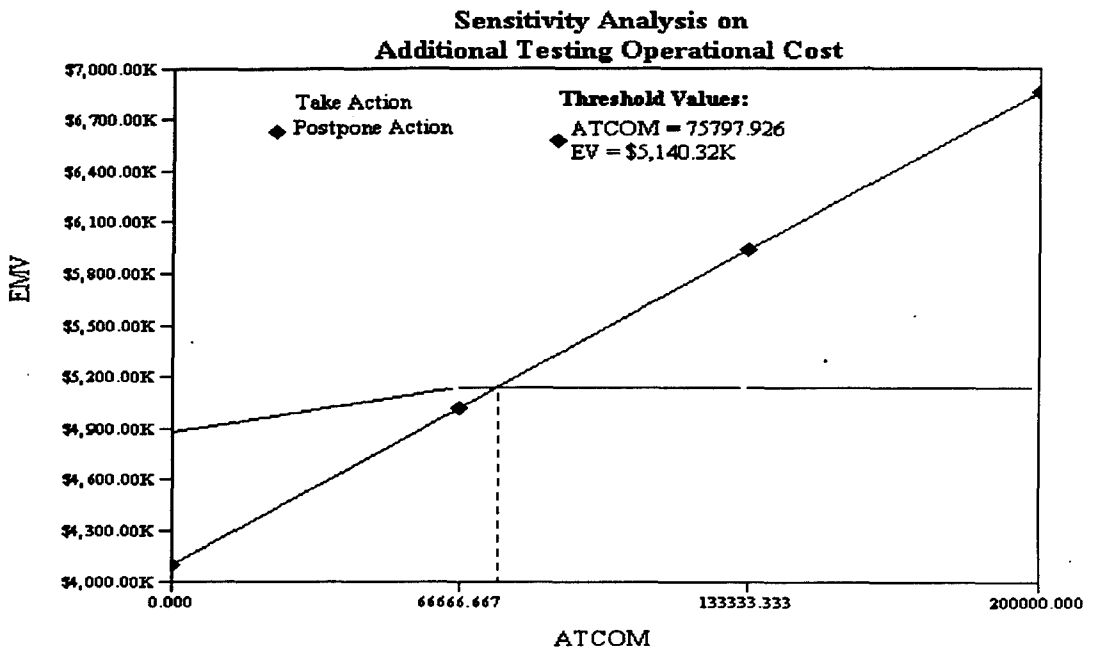

Chapter IV

RESULTS

Contaminated Groundwater Transport Analysis Results

Purpose and Method

This analysis used a two-dimensional analytical model in Monte Carlo fashion to determine the probability of TCE reaching the plane of compliance (POC) at a specified concentration. The probability was taken from a probability distribution function developed from this analysis. Results of this analysis were categorized into four groups: contaminant break through curves of alternative transport scenarios, Monte Carlo maximum precision analysis, model calibration to monitoring well data development of probabilities of TCE reaching the POC. These results are used along with the decision model's objective function to calculate the expected monetary value within a decision tree analysis.

Monte Carlo Maximum Precision Determination

Maximum precision of the Monte Carlo analysis was found to occur between 275 and 300 simulations, where the mean concentration at the POC was plotted with an increasing number of simulations, as shown in Figure 29. Mean concentrations from 1 through 100 simulations showed much variation before tapering toward a relatively constant precision point. This point occurred at about 250 simulations, with a mean

concentration of .0015 mg/l (1.5 ug/l). The 300 simulations used in this analysis were beyond the minimum required simulations for maximum precision. Simulations numbers beyond 300 theoretically had no effect on the stochastic analysis. That is, a maximum precision level was reached at approximately 250 simulations. The effects of variation in hydraulic conductivity inputs were reduced to the lowest possible levels given the distribution of the variable and the transport model employed.

Figure 29. Maximum precision plot for Monte Carlo analysis.

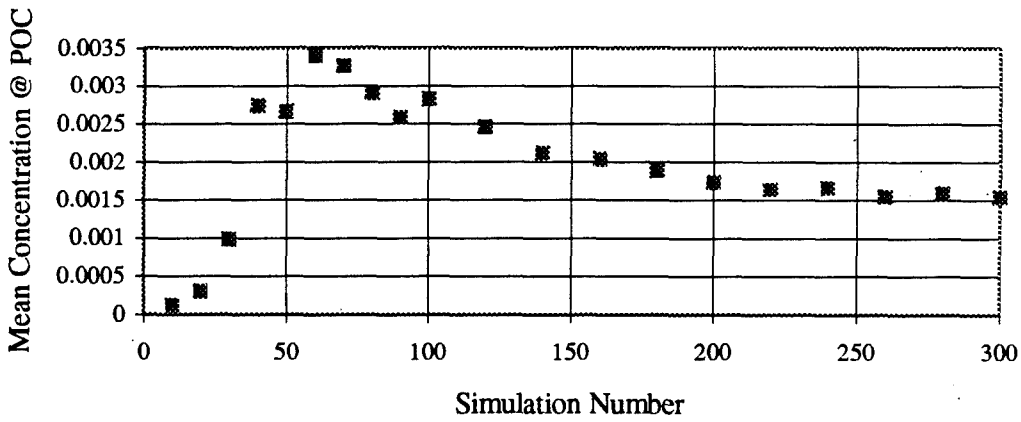

Modeling Calibration to Monitoring Data

The transport model calibration analysis results are illustrated in Table 6, which compares the measured data from monitoring well (MW) 109 for years 1982-1993 to the modeled concentrations resulting from the pertinent transport simulations. The comparisons show that TCE concentrations measured in MW 109 were within the modeled concentration range. Years 1986-1992 exhibited higher measured concentrations (0.11 to 0.204) then were predicted by the model (0.00 to 0.10) but were

within the same order of magnitude. Results of this analysis illustrated some reliability in the model configurations and parameters used in transport simulations.

Table 6. Comparison of monitoring data to modeling data for MW 109.

Year Measured/Simulated	Measured Data (mg/l)	Modeling Data (range in mg/l)
NOV 82/year 32	not detected	0 - .09
APR 83/year 33	.029	0 - .09
SEP 84/year 34	<.05	0 - .09
SEP 86/year 36	.11	0 - .09
SEP 87/year 37	.16	0 - .09
SEP 88/year 38	.19	0 - .10
NOV 92/year 42	.204	0 - .02
NOV 93/year 43	.094	0 - .01

Monte Carlo Simulations

Figure 30 illustrates the breakthrough curves for contaminant concentration at the POC for 300 simulations over a simulation period of 50 years. The concentrations at the POC varied from zero to over .07 mg/l (70 ug/l), with a majority of the simulations showing contaminant concentrations within the 0-.01 mg/l zone. The simulated time period for the TCE concentrations to peak at the POC ranged between five and ten years. Dissipation of the concentrations from their peak to zero, at the end of the simulation period, had a simulated time between five and fifteen years.

Figure 30. AT123D modeling results for contaminant transport to the POC.

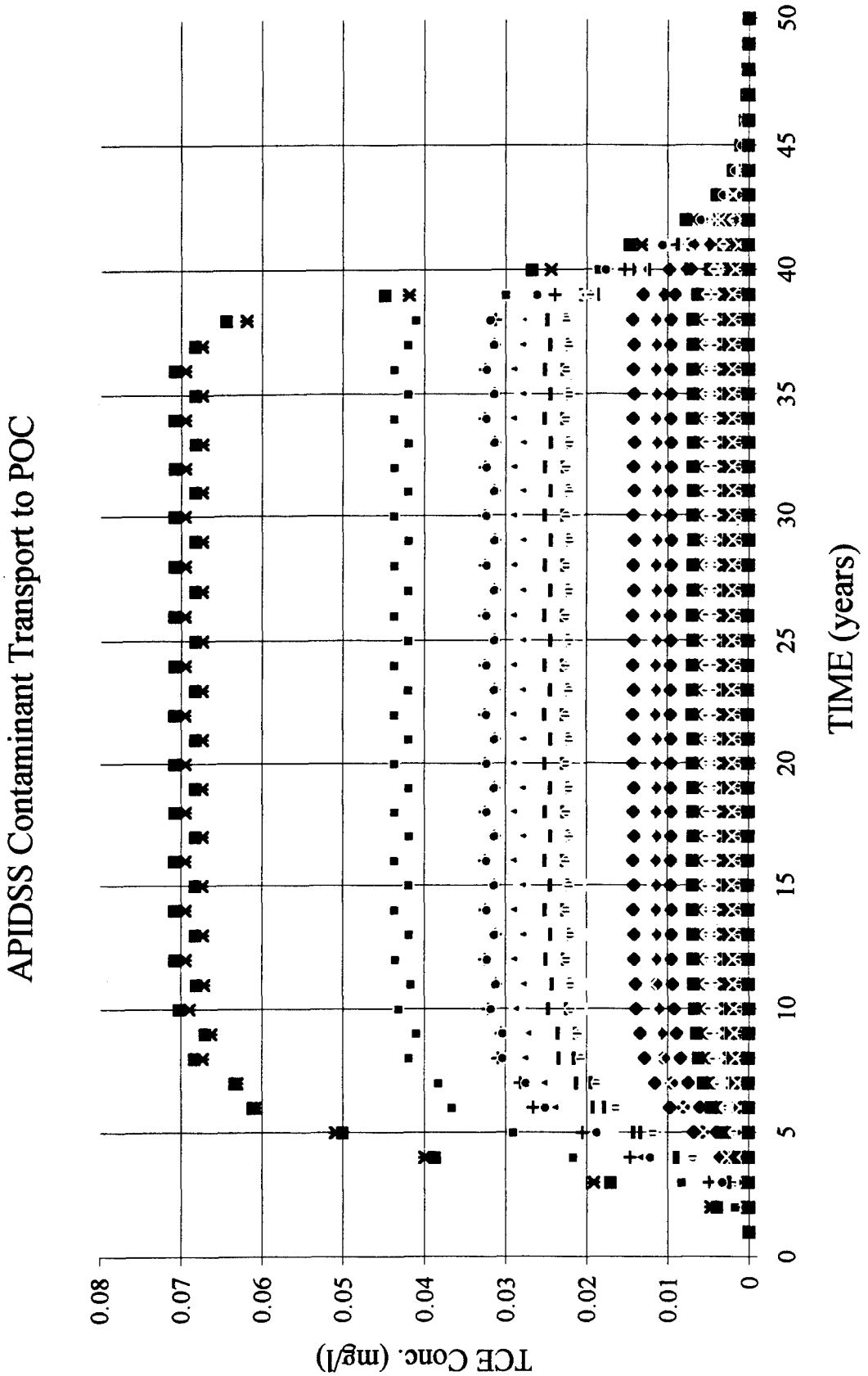

Contaminant Transport Probabilities

The probability distributions for TCE concentrations at the POC are shown in Figure 31. The Monte Carlo simulations presented in Figure 30 were statistically analyzed to develop these probability distributions for TCE concentrations expected at five separate time periods within the simulation period. The probabilities were developed by calculating the statistical distribution of the simulated TCE concentrations at the POC that ranged from $1.0x10^{-6}$-1000 ug/l. In Figure 31, each of the five curves illustrated the probability distribution of contamination at the POC within a specific time period. Curve A represents the probability distribution of the simulated TCE concentrations at the POC within the entire 50 year simulation period. Curve B shows the probability distribution of simulated concentrations at the POC for simulation years 1-10 while curve C addresses simulation years 11-20. Curves B and C show a significant difference in probability distribution. The probability for .001 mg/l (1 ug/l) of TCE to migrate to the POC is about 19% in the first 10 years as opposed to 2% in the following ten years, as represented by curve C. After 20 years of transport time, the probability is almost zero, as shown by curves D and E. Probability curves B and C were important when analyzing the decision option to postpone any remedial actions.

Figure 31. Contaminant transport probability for concentrations at the POC.

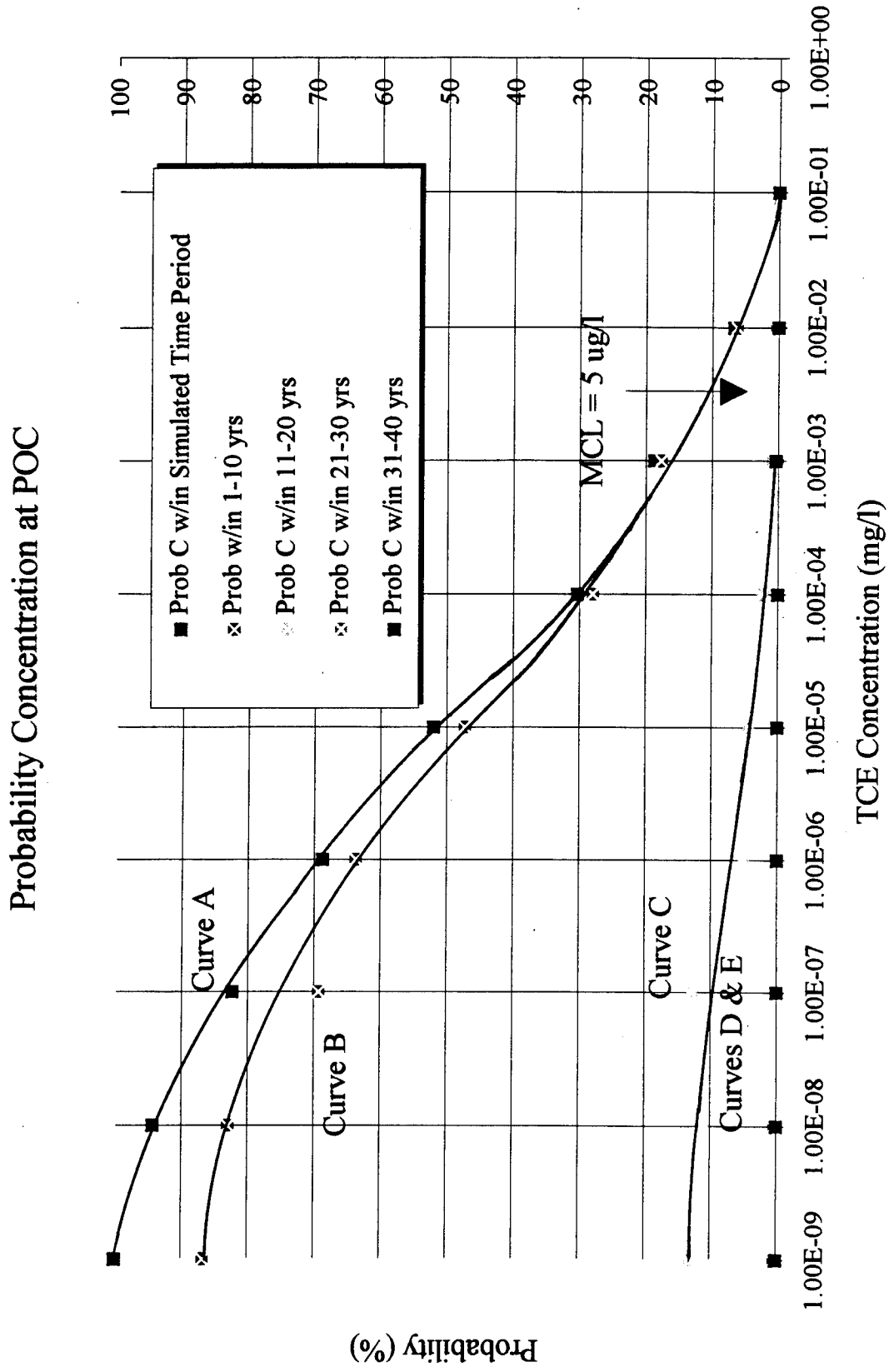

Objective

The objective was to use geostatistical techniques to develop an isoconcentration map that delineated the TCE plume. The output from this effort was important to the decision analysis because select plume characteristics were used as constraints for alternative actions within the decision model. That is, the question to be asked is, would uncertainties in defining the contaminant plume produce an alternative optimum remediation design? Presentation of the results in this analysis followed the chronology previously shown in Figure 23 and repeated here in Figure 32 for clarity, where the initial step was to collect data and determine the spatial statistics or variance analysis. Subsequently, the data were conditionally simulated in Monte Carlo fashion to develop the contaminant isoconcentration map. Additional discussion for each follows.

Figure 32. Flow chart graphically depicting the geostatistical methods used in this thesis.

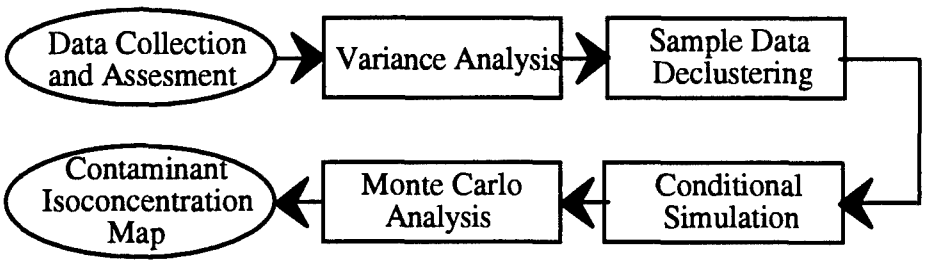

Data Assessment

Thirty-seven sampling points were used out of a possible 44 monitoring wells sampled by the Corps of Engineers. Four monitoring wells were not used because they

were not tested in 1993, the target year. Another three wells were not used in the analysis because small scale geologic structures near the well locations caused anomalous data values.

From Chapter III, it was noted that the geostatistical variable must have a normal distribution before kriging or conditional simulation. Figures 33 and 34 display the histograms for the TCE concentration and the log-normal transformed concentration distributions. Figure 33 shows that the measured concentrations were heavily skewed toward low TCE concentrations. Figure 34 shows that log-normal transformation of the TCE concentrations had a nearer normal distribution that could be used in further geostatistical analysis. A more detailed statistical discussion is given in Appendix A illustrating the log-normal transformation having a near normal distribution. The log-normal transformed TCE concentrations were used in the geostatistical analysis due to the near normal distribution exhibited.

Figure 33. Histogram plot of 1993 monitoring data concentrations ug/l, not transformed.

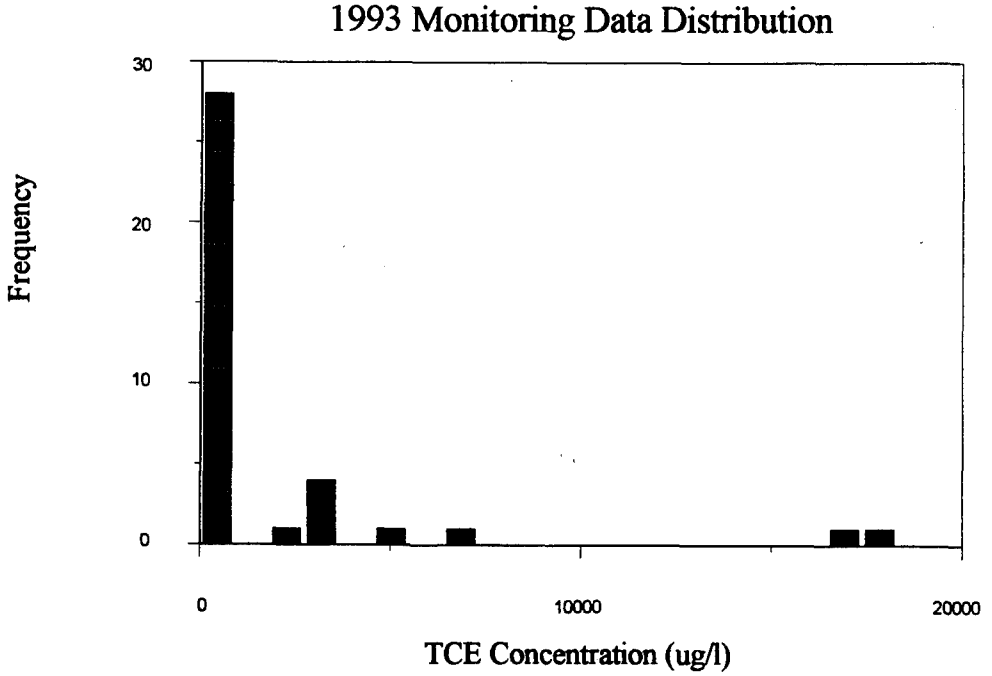

Figure 34. Histogram plot of 1993 monitoring data concentrations transformed into log-normal ug/l.

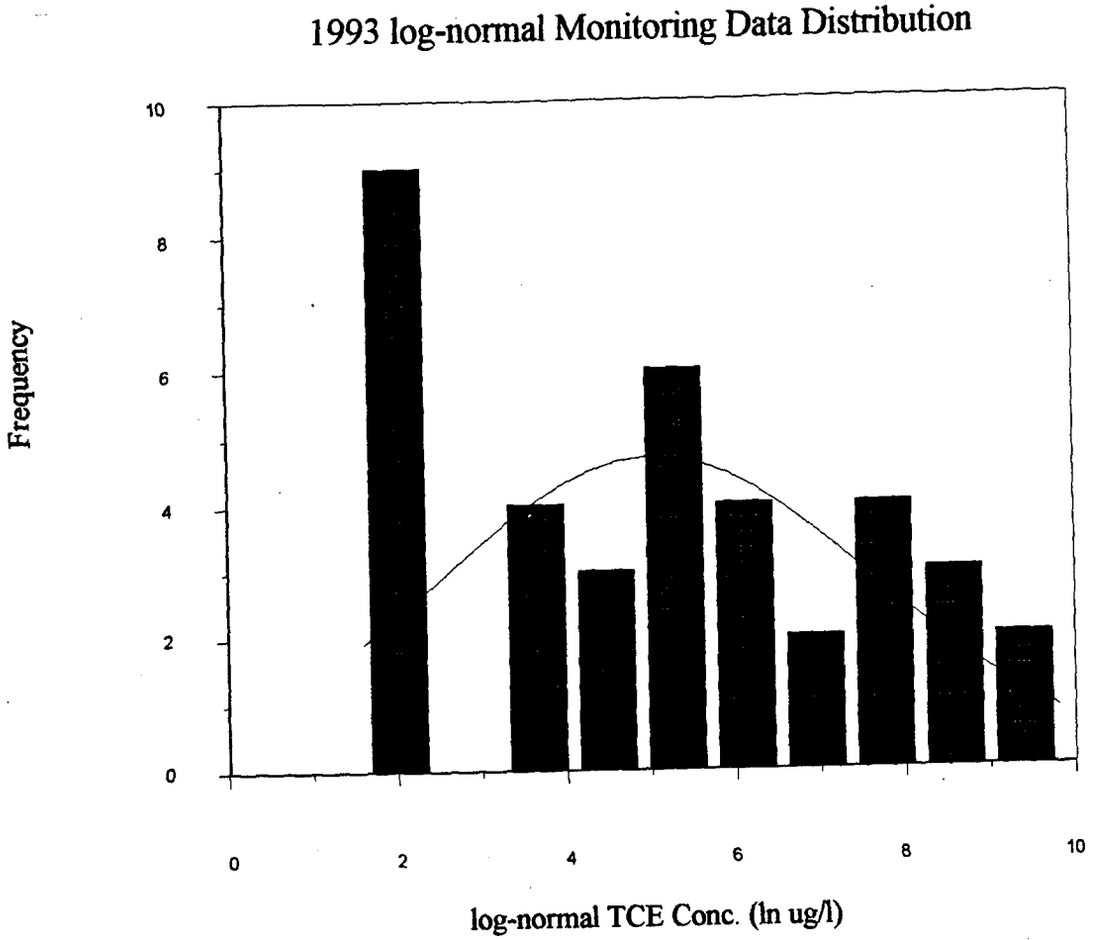

Data Spatial Variance Analysis

The spatial variance analysis had two objectives: develop the experimental variogram that was representative of the true variogram and fit a model to the experimental variogram. The resulting experimental and model variograms are illustrated in Figure 35 with the vertical axis representing the variance of the variable (log- normal TCE concentration in groundwater) and the horizontal axis representing separation distance in feet.

The variogram showed a variance ceiling of about 7.5 beyond the range of 400 feet. Between the origin and 400 feet the structure was not well defined. The lack of structure near the origin was apparently due to the complexity of the geology and the sparse sampling data, thus hindering the capability to detect small concentration variations within the incremental lag spacing of 290 feet. Another incremental lag spacing of 200 feet was used to assist in defining the structure near the origin. Figure 36 illustrates the new variogram that had two points versus one between the origin and 400 feet on the x-axis. Reducing the incremental lag spacing caused the variance at further points to have greater scatter in Figure 36 than exhibited in Figure 35. This highlighted the importance of conducting several iterations of variogram development. Both of these experimental variograms were utilized to develop the model variogram. Figure 35 assisted in determining the variogram sill with its relatively good structure beyond 400 feet. Figure 36 was important to verify the lower end structure with additional variance points less than 400 feet. These lower end points assisted in defining the model variogram shape and verification of a nugget effect.

Figure 35. Experimental and model variogram for log-normal sample data with a maximum lag of 1200 feet and an incremental lag spacing of 290 feet.

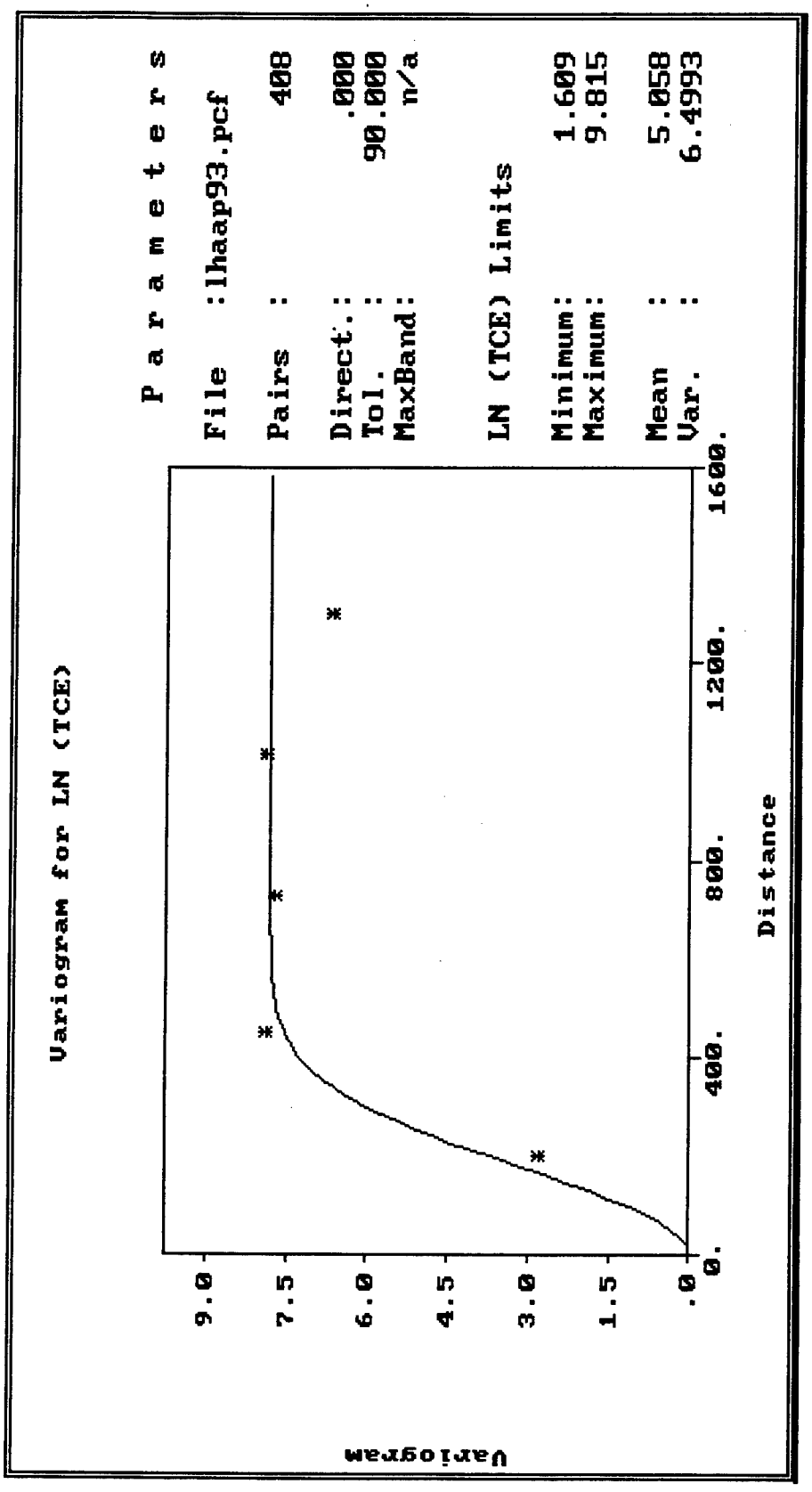

Figure 36. Experimental and model variogram for log-normal sample data with a maximum lag of 1200 feet and an incremental lag spacing of 200 feet.

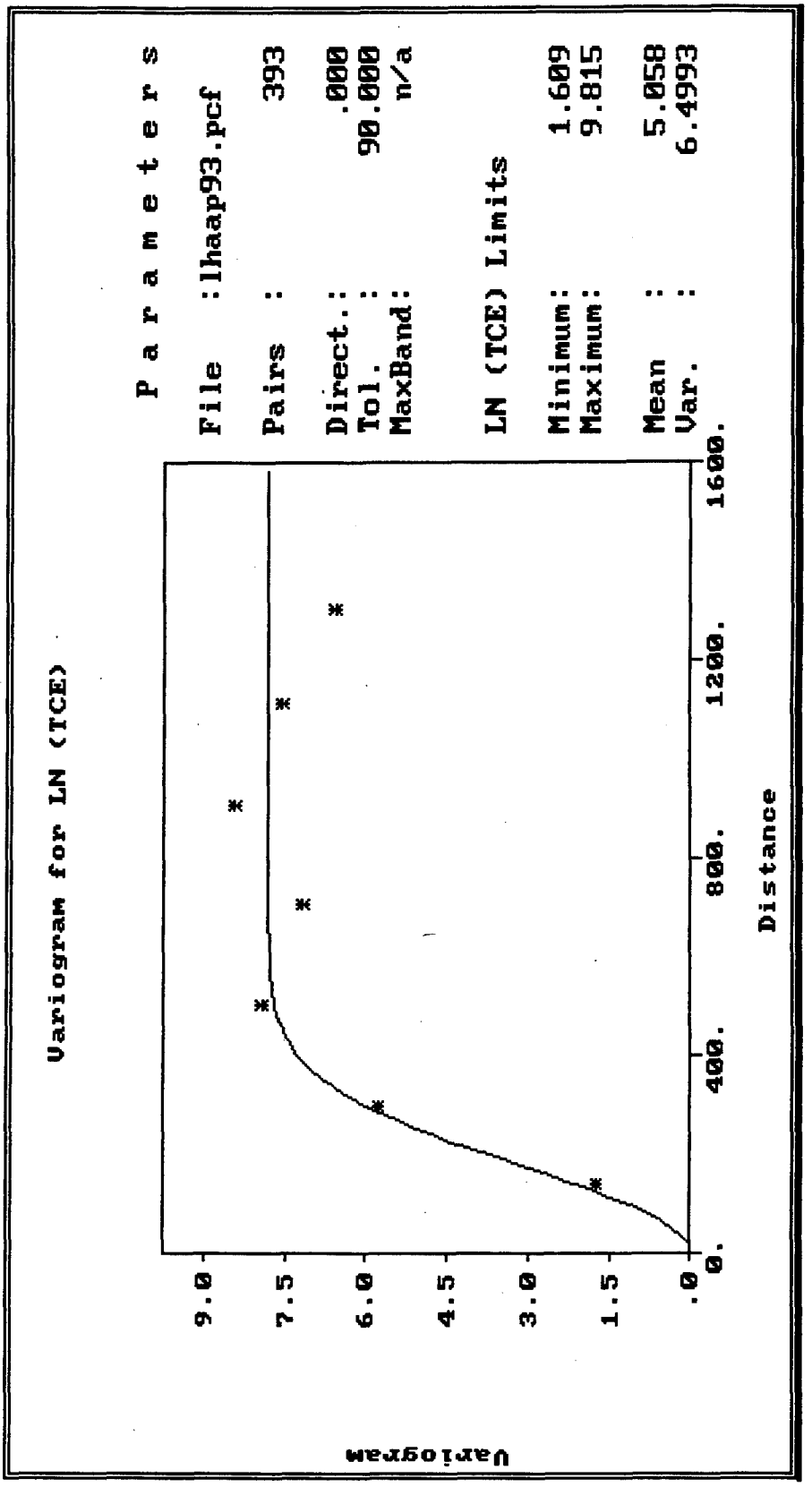

The variogram figures illustrate a gaussian model fitted to the experimental variograms. The model variogram was characterized by a sill value of 7.8, a nugget of 0.0 and a range of 425 feet. This model variogram fit the experimental variogram very closely and was representative of the true variogram (see Figures 35 and 36).

An assumption made in the variogram analysis was that the underlying structure was isotropic and that no anisotropic structures occurred within the aquifer. That is, the complexity and randomness of the depositional structures within the aquifer precluded modeling the random anisotropic structures and was beyond the presentation of the methodology in this thesis. Therefore the experimental variograms developed were considered omni-directional as illustrated in Figures 35 and 36 by the direction and tolerance parameters set at 0.0 and 90° respectively. Additional discussion of the data spatial variance analysis is provided in Appendix A, where the detailed discussion summarizes the variogram cross-validation analysis that was used to evaluate the model variogram development. Also included in Appendix A is the sample data declustering discussion which, while an important preliminary step to conditional simulation, is not as relevant to the overall decision analysis.

Conditional Simulation

Kriging Versus Conditional Simulation. Conditional simulation utilized Monte Carlo techniques in a stochastic analysis that produced numerous two-dimensional realizations of the contaminant plume. Each simulation was a possible realization of the true TCE plume distribution. Figure 37 illustrates the output from one conditional

simulation realization. Each realization contained simulated data as well as the true or measured values at the sampling points. Figure 37 and subsequent simulation figures were plotted on a grid network that was 3750 feet along the east axis and 4500 feet along the north axis, with each grid 75 foot square. Comparing one conditional simulation realization with a kriged realization (see Figure 38) produced noticeable differences between the two simulation methods. The smoothing effect inherent to Kriging (Deutsch and Journel, 1992) between known data points was very noticeable when compared to the conditional simulation figure. The smoothing effect that Kriging created is one of the fundamental differences between it and conditional simulation. The detail exhibited with the conditionally simulated plume was much more defined, with greater variation over shorter distance than with the kriged example. This greater detail, together with the opportunity to develop two-dimensional, spatially correlated statistical distributions of the TCE plume strongly supported the use of conditional simulation over the more typically applied contouring or Kriging approaches.

Figure 37. Isoconcentration map of one conditional simulation realization. TCE values in the legend are log-normal transformed values.

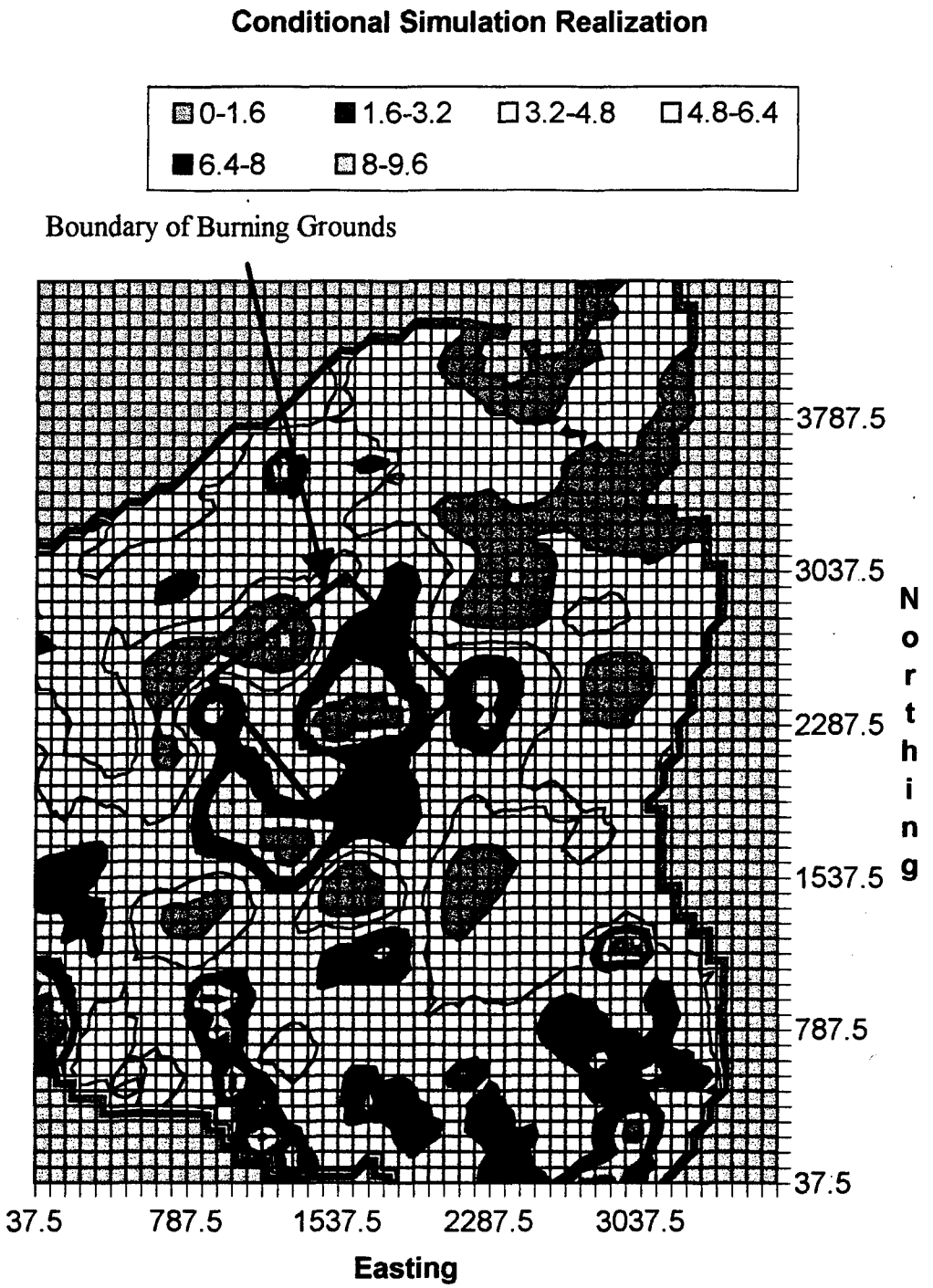

Figure 38. Isoconcentration map of the Kriged estimates. TCE values in the legend are log-normal transformed values.

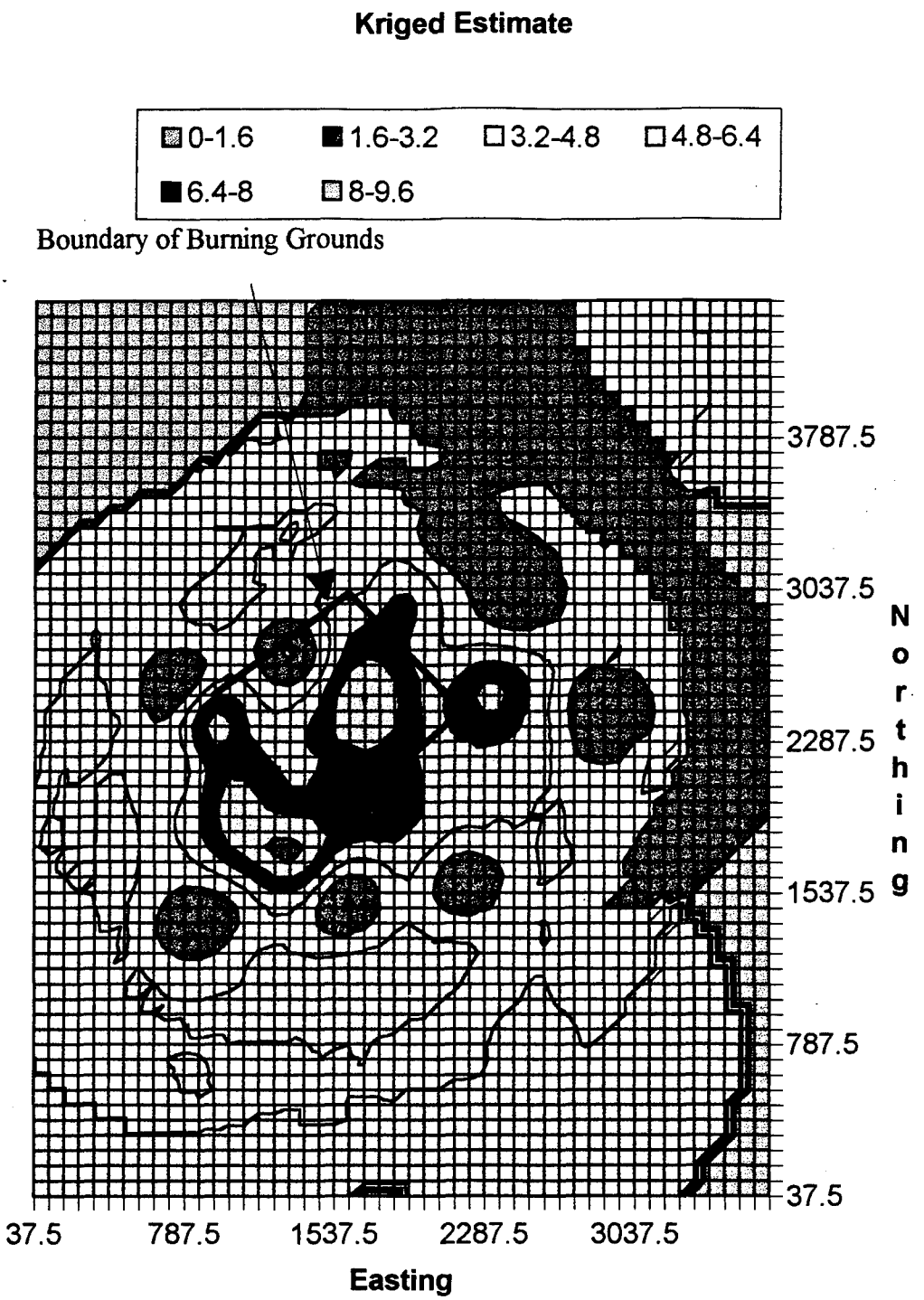

Monte Carlo Maximum Precision. The same technique used in the contaminated groundwater transport analysis was applied to determine the minimum number of simulations needed to adequately represent the conditions. Figure 39 presents the maximum precision plot of the mean simulated concentration for increasing simulations. As there were 3000 simulated nodes for each realization, statistically analyzing all the nodes and plotting the results was not feasible. Three randomly selected nodes, not to include sampling points, were used in the precision analysis, as shown in Figure 39. The figure shows that maximum precision was reached between 40 and 60 simulations for each of the three simulated nodes.

Figure 39. Monte Carlo maximum precision plot of mean concentration versus number of simulations.

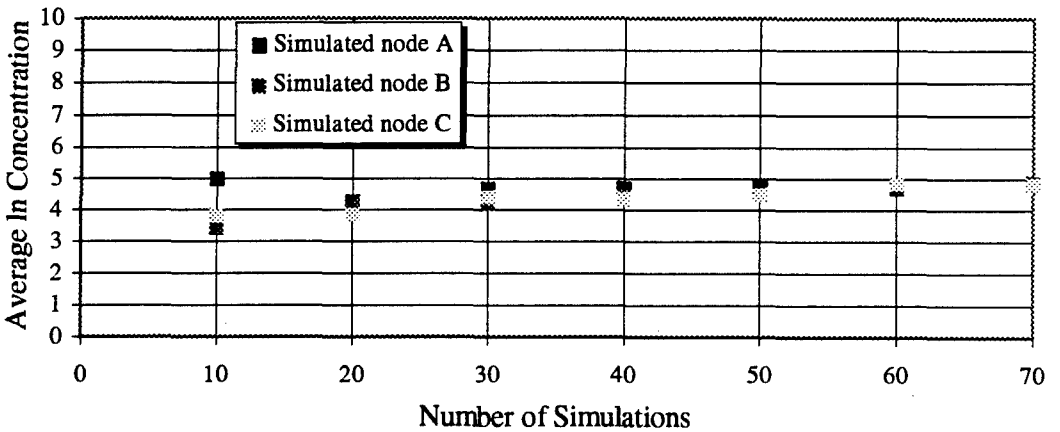

Another check was conducted using the standard deviations of the three nodes in the same fashion as the plot of the running means. A plot of the relationship (Figure 40) showed the standard deviations converging to one value at around 40 simulations but not as well as in Figure 39. Beyond 40 simulations the standard deviations diverged but still remained within acceptable tolerance limits.

Figure 40. Monte Carlo maximum precision plot of standard deviation of concentration versus number of simulations.

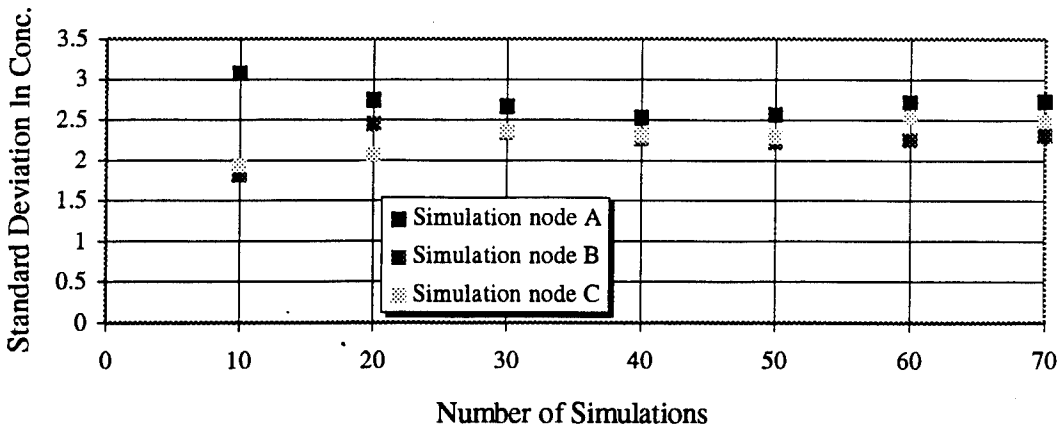

Statistically derived isoconcentration maps illustrated the upper boundaries of the 95% and 90% confidence intervals and the mean simulation concentrations were prepared. The plot of the simulated means, Figure 41, was very similar to the Kriged estimate in Figure 38, illustrating that the average of conditional simulations at a given location converges to the Kriging estimate and the variance converges to the kriging variance (Delhomme, 1979). This similarity lends itself to the verification of maximum precision and that 45 simulations were adequate to represent the conditions.

Figure 41. Isoconcentration map of the means from the conditional simulation realizations. The legend gives the TCE concentrations as log-normal transformed.

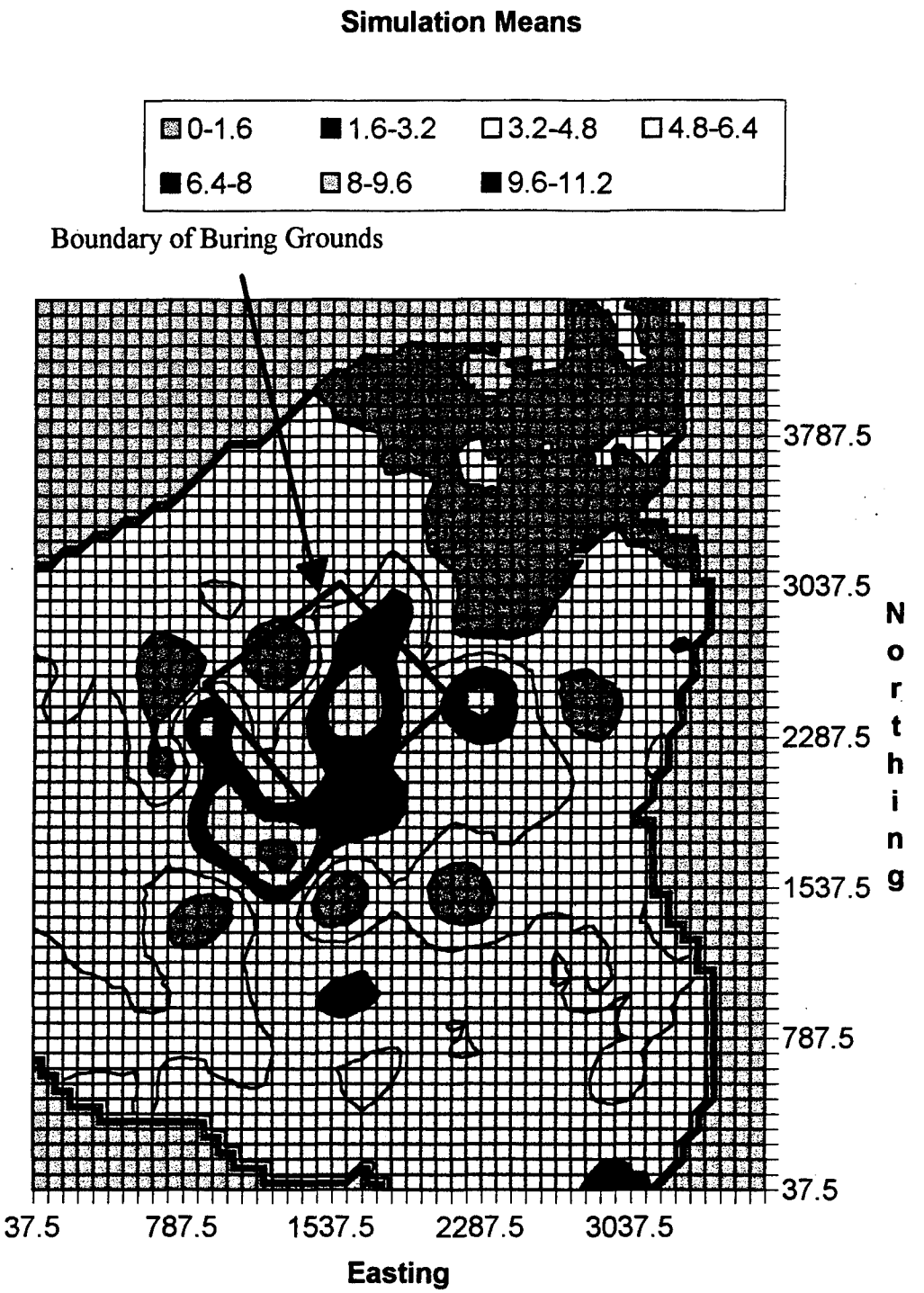

The objective of the conditional simulation was to identify statistical variance about an isoconcentration map of the contaminant plume. Isoconcentration maps were developed for the statistical upper boundary of the 95% confidence interval (UB 95 CI) and the upper boundary of the 90% confidence interval (UB 90 CI), shown in Figures 42 and 43, respectively. Both figures illustrate the concentration variation within the plume and the areal extent of the plume. Comparison of the two figures revealed that the areal spread of the respective plumes was the same for the UB 95 CI and UB 90 CI. Differences, however, did occur in these simulated plumes. Note that the higher contaminant concentrations were denser in Figure 42 (the UB 95 CI) than in Figure 43 (the UB 90 CI). This variation may be significant when determining remediation alternatives and attendant costs based on the size and strength of the contaminant plume.

Figure 42. Isoconcentration map of the UB 95 CI from the conditional simulation realizations. The legend gives the TCE concentrations as log-normal transformed.

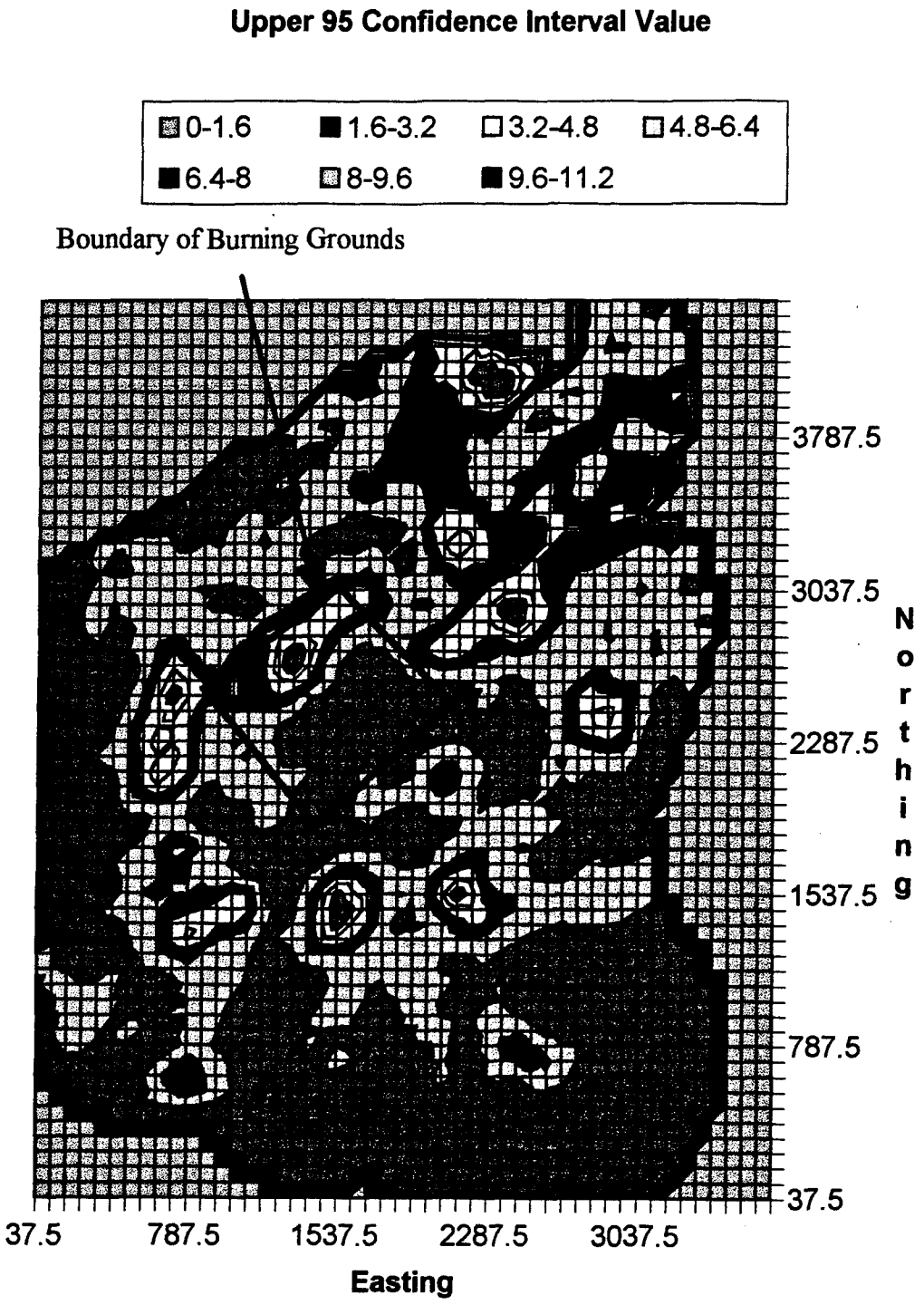

Figure 43. Isoconcentration map of the UB 90 CI from the conditional simulation realizations. The legend gives the TCE concentrations as log-normal transformed.

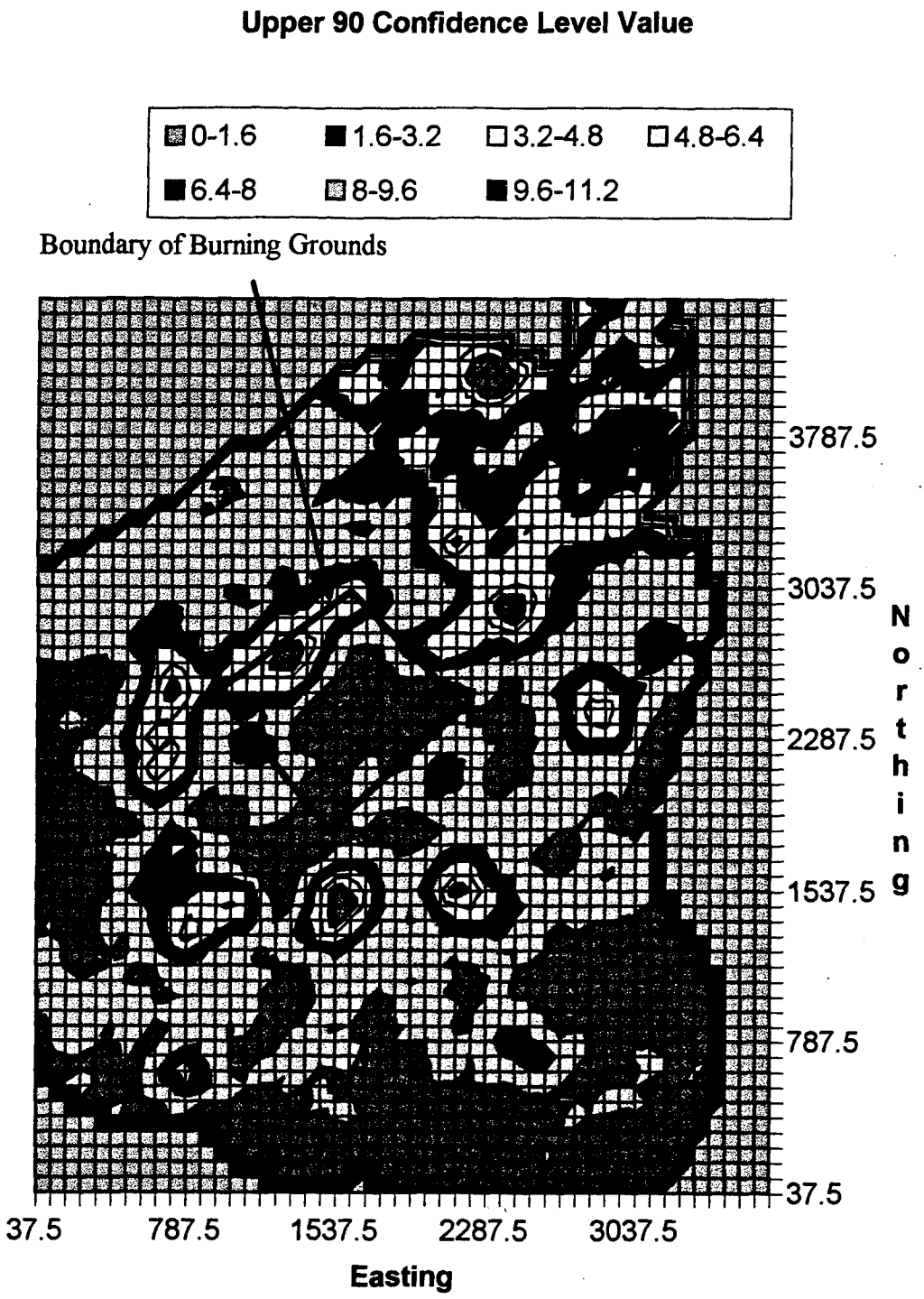

Remedial Action Costs

Groundwater Extraction. Costs for groundwater extraction and parameter inputs for CORA module 206 are summarized in Table 7. The left column of the table lists the input parameters required for this CORA cost module. Parameters having a large impact on the costs included: number of wells, pump rate and depth. The results from CORA are listed in the right column. For this module there were two costs associated with groundwater extraction, capital costs reflecting the construction costs associated with extration well emplacement and operational and maintenance cost (O&M) which were estimated for a one year period. These costs were calculated as a yearly recurring cost in the objective function during the decision tree analysis.

Table 7. CORA groundwater extraction cost module 206 summary table.

CORA Inputs		CORA Results	
Parameter	Value	Component	Cost ($)
Number of wells.	15	Capital cost	360,000
Pumping rate per well (gpm).	500	O&M cost	370,000
Well diameter (inches).	6		
Gravel packed wells?	yes		
Average depth of wells (ft).	75		
Transfer piping length (ft).	1000		
Pumping water level/well (ft).	55		
Average temperature (°F).	64		
Confidence level.	medium		
Level of protection.	none		

In-Situ Bioremediation. Table 8 presents the CORA parameters and results for this remediation alternative. Input parameters involving the area of contamination, initial concentration and oxygen demand increased the costs of bioremediation when their quantities were high. In this analysis hydrogen peroxide was used to deliver oxygen to the microorganisms causing the O&M costs to increase sharply over other alternatives. The capital costs for this alternative ($490,000) were a little higher than for groundwater extraction but the significant cost difference was between O&M costs, of $1.7 million annually for bioremediation versus $370,000 for the groundwater extraction.

Table 8. CORA in-situ bioremediation cost module 304 summary table.

CORA Inputs		CORA Results	
Parameter	Value	Component	Cost ($)
Area of contaminant (acres).	308	Capital cost	490,000
Thickness of contaminant (ft).	17	O&M cost	1,700,000
Initial TCE conc. (mg/kg).	12532		
Level of degradation (%).	100		
Oxygen demand (mg/mg)	3.5		
Soil bulk density (pcf).	99		
Percent COD leached.	30		
Efficiency of H_2O_2 (%).	30		
Remediation period (years).	10		
Sampling events/month.	1		
Number of sampling wells.	20		
Soil cores per year.	10		
Labor required (man-d/wk).	5		
Protection level.	none		
Average temperature (°F).	64		
Confidence level.	medium		

Discharge to Surface Water. Discharge into local drainage features was assumed for the treated groundwater due to the sites remote location and lack of accessibility to a permitted waste water treatment plant. Results presented in Table 9 were only the costs considering the actual discharge. Treatment costs were calculated separately for two different operations and are presented in Tables 10 and 11. The most significant costs associated with this module were the capital costs and cost incurred to get an NPDES permit for discharge. The majority of the capital startup costs were for materials to drain the treated water an estimated 3000 feet from the treatment site to Caddo Lake, as shown in the parameter inputs column of Table 9. These costs would not be incurred for the in-situ bioremediation alternative but would be a factor in groundwater extraction. They represent, therefore, an additional cost for that alternative.

Table 9. CORA discharge to surface water cost module 406 summary table.

CORA Inputs		CORA Results	
Parameter	Value	Component	Cost ($)
Transmission mode.	gravity	Base capital cost	200,000
Flow (gpm).	2000	NPDES permit	46,000
Length of pipe (ft).	3000	O&M cost	740
Depth of trench (ft).	6		
Is diffuser required?	no		
Protection level.	none		
Average temperature (°F).	64		
Confidence level.	medium		

Granular Activated Carbon Treatment. This was the more expensive treatment process of the two estimated and combined with the previously itemized extraction costs was the most expensive remediation alternative in the analysis. Results in Table 10 show that capital costs were $2.0 million while yearly O&M costs were $1.9 million. The O&M costs were strongly influenced by the asterisk-highlighted parameter, the carbon usage, that was estimated by CORA at about 1 million pounds per year which may be excessive.

Table 10. CORA granular activated carbon cost module 309 summary table.

CORA Inputs		CORA Results	
Parameter	Value	Component	Cost ($)
Water flow (gpm).	2000	Capital cost	2,000,000
Total organic carbon (ug/l).	10000	O&M cost	1,900,000
Protection level.	none		
Average temperature (°F).	64		
Confidence level.	medium		
Carbon used (lb/yr).	1132818*		

Air Stripping Treatment. The second of two treatment operations this system was much less costly than the activated carbon system. Presented in Table 11 are the input parameters required to develop the cost of the system. Parameters highlighted with an asterisk were calculated by CORA based on the input parameters. The resulting capital and operational cost were $400,000 and $110,000 respectively. The operational costs were on a yearly basis and were used in a recurring cost economic analysis to determine the total cost for this system for a 10 year operational period.

Table 11. CORA air stripping cost module 307 summary table.

CORA Inputs		CORA Results	
Parameter	Value	Component	Cost ($)
Water flow (gpm).	2000	Capital cost	400,000
Protection level.	none	O&M cost	110,000
Average temperature (°F).	64		
Confidence level.	medium		
Flow discharge (gpm).	2000*		
Air stripping towers number.	2*		
Overall packing depth (ft).	43*		
Tower diameter (ft).	11*		
Power required (kW).	101*		
Gas flow (cfm).	6030*		

* Calculated by CORA from input parameters.

Site Preparation. Site preparation costs were included into all the remediation alternatives. The assumption was that electrical power would be brought to the site from an existing electrical distribution system that existed nearby at other ammunition plant facilities. A key parameter input shown in Table 12 was the distance to the electrical distribution point, which CORA used to estimate the cost as $28,000. Capital costs were the only cost associated and included access to the distribution system and construction of an electrical drop on the site.

Table 12. CORA site preparation cost module summary table.

CORA Inputs		CORA Results	
Parameter	Value	Component	Cost ($)
Site clearing (acres).	0	Capital cost	28,000
Tree removal (acres).	0	O&M cost	0
Dust control area (acres).	0		
Local utility connection?	yes		
Distance to power point (ft).	2000		
Gas connection required?	no		
Water connection required?	no		
Access road required?	no		
Building demolition (cy).	0		
Average temperature (°F).	64		
Confidence level.	medium		

Failure Costs

Surface Water Diversion. This cost module was one of the three costs that made up the cost of failure determination, as discussed in Chapter III. The costs for surface water diversion, presented in Table 13, were based on the parameter inputs shown in the left column of the table. Key parameters included the length and width of the contaminated site as well as the 25 year storm rainfall in 24 hour period. The projected capital costs of $1.1 million were much higher than the attendant annual operational cost estimated at $4,700.

Table 13. CORA surface water diversion and collection cost module 105 summary table.

CORA Inputs		CORA Results	
Parameter	Value	Component	Cost ($)
Length of cont. site (ft).	1000	Capital cost	1,100,000
Width of cont. site (ft).	1000	O&M cost	4,700
25 yr., 24 hr rain (inches).	6		
Average temperature (°F).	64		
Confidence level.	low		
Protection level	none		

Site Access Restrictions. Assuming the contamination was transported beyond the boundaries of the ammunition plant, the potential for additional site security requirements was likely. Site security included the requirements listed in the parameter input column such as dimensions of the perimeter and guard requirements. As mentioned in Chapter III, the reasons for security varied but most likely would be required for protection of remediation equipment as well as securing the site from unwarranted access by the general public. Table 14 presents the results of the CORA estimation of $750,000 in yearly operational costs with no capital costs.

Table 14. CORA site access restrictions cost module 504 summary table.

CORA Inputs		CORA Results	
Parameter	Value	Component	Cost ($)
Site perimeter (ft).	10000	Capital cost	0
Permanent fencing?	no	O&M cost	750,000
Temporary fencing?	no		
Lighting required?	no		
Security guard required?	yes		
Access points required.	5		
Guards per access point.	1		
Number of shifts.	3		
Temporary guardhouses.	5		
Vehicles required.	3		
Confidence level.	low		

Municipal Water Supply. Input parameters as shown in Table 15 included pipeline length, well depth and number of residential and commercial connections. CORA estimated that the capital costs would be $6.8 million with yearly recurring costs of $54,000 per year (Table 15). It was assumed that if failure occurred, recurring costs would be realized over a 50 year period. That is, the new municipal water supply would serve the local community for 50 years and yearly costs would be incurred during that period.

Table 15. CORA municipal water supply cost module 502 summary table.

CORA Inputs		CORA Results	
Parameter	Value	Component	Cost ($)
Length of line (ft).	10000	Capital cost	6,800,000
Average well depth (ft)	100	O&M cost	54,000
Residential connections.	500		
Commercial connections.	100		
Total commercial flow (gpm).	50		
Average temperature (°F).	64		
Above grade protection.	none		
Below grade protection.	none		
Confidence level.	low		

Additional Groundwater Monitoring Well Cost

The cost determined in this model was that incurred per well constructed. The number of wells chosen for installation was then multiplied to this unit-cost estimate. The annual O&M costs were those associated with well upkeep and monitoring costs. The parameter input column of Table 16 shows the average depth of wells to be 50 feet with a quarterly monitoring frequency that tested for volatile organic compounds such as TCE. The estimated capital cost per well was $8,100 while O&M cost was $9,200 per well per year (Table 16).

Table 16. CORA groundwater monitoring cost module 503 summary table.

CORA Inputs		CORA Results	
Parameter	Value	Component	Cost ($)
Number of wells.	1	Capital cost	8,100
Average well depth (ft).	50	O&M cost	9,200
Number to monitor.	1		
Monitoring frequency (#/yr).	4		
Monitor HSLORG	yes		
Monitor VOA GC/MS	yes		
Average temperature (°F).	64		
Level of protection.	none		
Confidence level.	medium		

Existing Groundwater Monitoring Costs

Costs determined in this module were associated with current and future monitoring of existing monitoring wells. Since these wells were already constructed, only O&M costs were appropriate, as shown by the parameter input column in Table 17, where the number of wells constructed was set to zero. The monitoring number parameter was 40, corresponding to number of wells on the site, with a quarterly monitoring frequency for volatile organic compounds. CORA estimated that yearly recurring cost to monitor the wells was $280,000 as shown in Table 17.

Table 17. CORA groundwater monitoring cost module 503 summary table.

CORA Inputs		CORA Results	
Parameter	Value	Component	Cost ($)
Number of wells.	0	Capital cost	0
Average well depth (ft).	0	O&M cost	280,000
Number to monitor.	40		
Monitoring frequency (#/yr).	4		
Monitor HSLORG	yes		
Monitor VOA GC/MS	yes		
Average temperature (°F).	64		
Level of protection.	none		
Confidence level.	medium		

Estimated Cost Summary

The estimated costs are summarized in Table 18 for each of the alternatives evaluated in the decision analysis. The table was divided into three sections: costs incurred, potential costs for testing and potential costs for failure. Under the incurred costs column are the estimated costs to implement the corresponding alternative. Their costs were divided into capital costs and annual operation costs, as shown in Table 18. The estimated costs for additional testing were separated because these costs may or may not be incurred, depending if the additional testing alternative was chosen. The final cost category was the estimated costs for failure. If no action were taken and the contaminant reached the POC in concentrations greater than 5 ug/l, then these costs were realized.

Table 18. Summary of estimated costs for alternatives by cost type.

Type of Cost	Alternative Cost ($ x 10^6, capital cost/annual O&M cost)			
Costs Incurred	P&T 1	P&T 2	Bioremediation	No Action
Groundwater Extraction	.36/.37	.36/.37	-	-
In-Situ Bioremediation	-	-	.49/1.7	-
Surface Discharge	.25/.001	.25/.001	-	-
Activated Carbon Treatment	-	2.0/1.9	-	-
Air Stripping Treatment	.40/.11	-	-	-
Site Preparation	.03/0.0	.03/0.0	.03/0.0	-
Monitoring Groundwater	0.0/.28	0.0/.28	0.0/.28	0.0/.28
Potential Costs for Testing	P&T 1	P&T 2	Bioremediation	No Action
Additional monitoring/well	.008/.009	.008/.009	.008/.009	.008/.009
Potential Costs for Failure	P&T 1	P&T 2	Bioremediation	No Action
Surface Water Diversion	-	-	-	1.1/.005
Site Restrictions/Security	-	-	-	0.0/.75
Municipal Water Supply	-	-	-	6.8/.054
TOTALS	1.05/.77	2.65/2.56	.53/1.99	7.91/1.10

Decision Tree Analysis

The complete decision tree for the analysis is illustrated in the accompanying map file as Figure 56. The size of the trees precluded them from being illustrated on standard paper and they were plotted on larger sheets. Figure 56 presents the decision tree structure having the alternatives labeled and the objective function cost for each of the consequences realized.

To illustrate the results of the decision tree analysis, Figure 44 presents the tree in rolled-back form showing the estimated monetary values (EMV) for each of the decision alternatives. This decision tree is a collapsed version of the tree illustrated in Figure 56 and is different only in that the redundant sub-branches have been collapsed for clarity. Each of the end nodes in Figure 44 has either the "Remedial Action" sub-branch or "Take No Action" sub-branch, as illustrated in Figure 45, attached to those nodes. The collapsed sub-branches were the same throughout the decision tree and varied only with respect to the values for the objective junction cost variables and probability variables.

Referring to the first decision node in Figure 44 labeled "Contaminated Groundwater Problem", it can be seen that the optimum decision was to "Postpone Action" with a resulting EMV of $4.7 million dollars. The EMV should not be associated with the expected cost of consequences but is a relation of objective function cost and probability for the states of nature (Ossenbruggen, 1984). Actual costs are summarized in Chapter V for each of the consequences.

Figure 44. Decision tree for example problem with collapsed sub-branches showing expected monetary values for the decision alternatives.

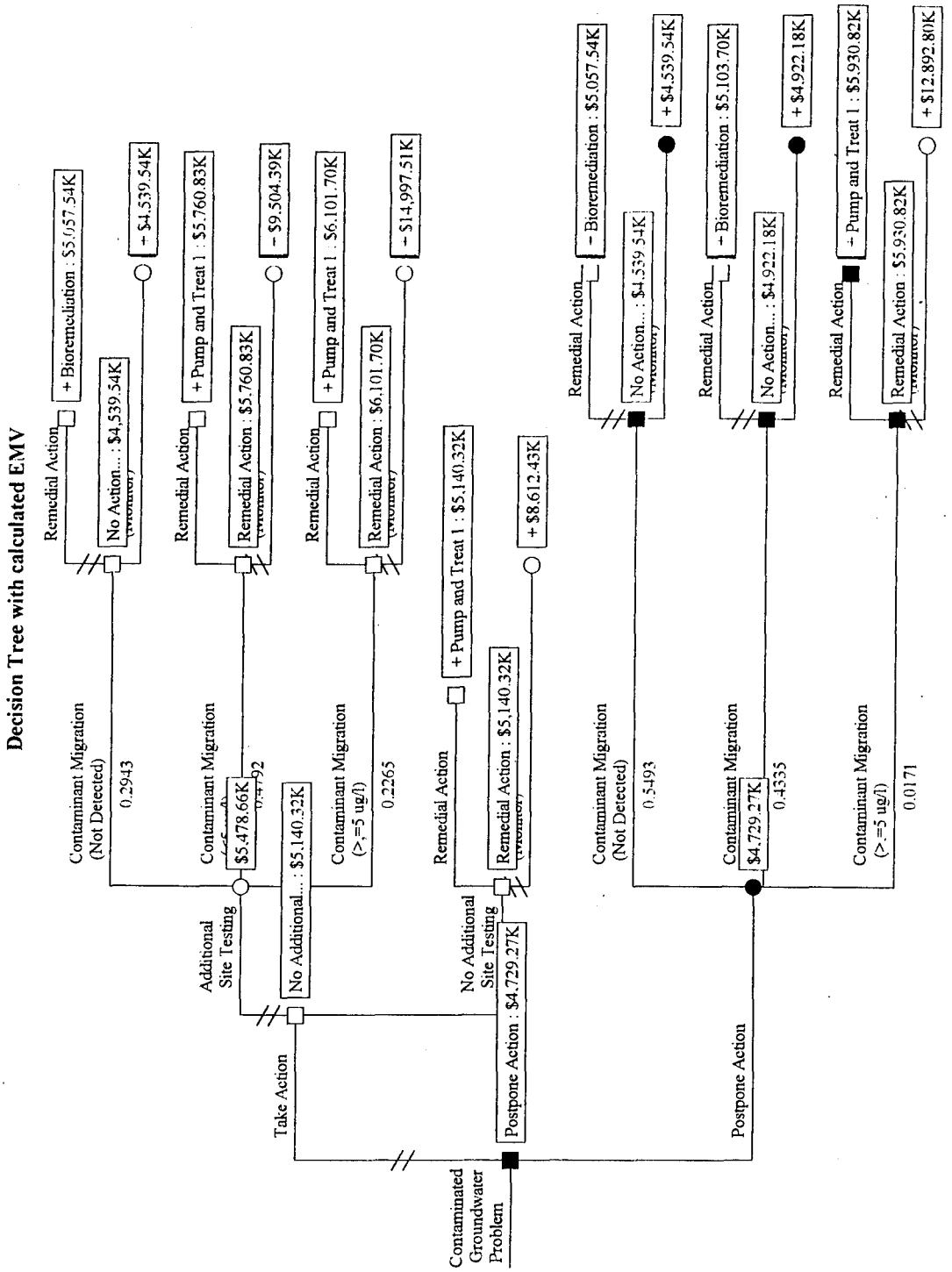

Figure 45. Detail of collapsed sub-branches not shown in Figure 44.

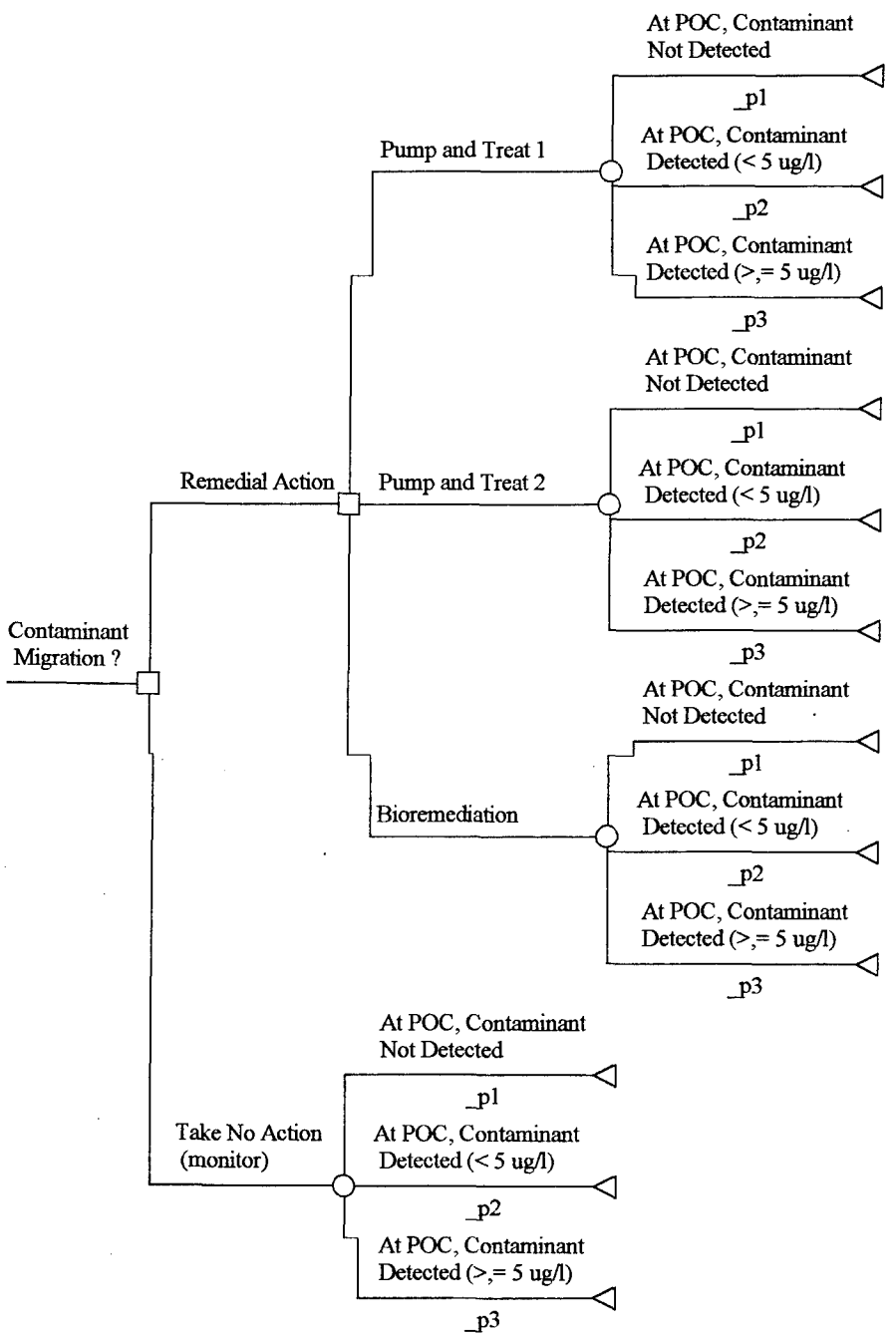

The next node on the "Postpone Action" sub-branch is a chance node representing the three possible test outcomes from the additional test wells. The probabilities for each of the three possible test results are shown in decimal form near the test branch label. There are three optimal decisions each corresponding to the test results. If the test well did not detect contamination, the optimal solution was to take no remedial action and continue monitoring (highlighted with darkened nodes). If the test well detected contamination but the concentration was below the MCL (5 ug/l) the optimal solution remained the same, the same conclusion was reached. Finally, if the test well detected contamination concentrations greater than or equal to 5 ug/l, then the optimum decision was to choose the pump and treat alternative with air stripping treatment of the groundwater.

Variable Sensitivity

Sensitivity analysis is an important part of any decision analysis process. As was discussed within the CORA cost results section, if the estimated cost of failure was inflated or, conversely, too low, then an effect on the optimum alternative derived in the decision tree analysis could result. A sensitivity analysis was conducted separately for the capital cost and operational costs at the root node (first decision branch) of the decision tree.

Output from this analysis can be the typical "variable versus expected value" plot or an alternative type of plot called the tornado diagram. Figure 46 illustrates the tornado diagram that was determined for the following capital cost variables within the objective

function: remedial action cost, cost of failure and additional testing cost. Tornado diagrams illustrate the variables with the greatest sensitivity to the expected monetary value (EMV) at the top and the least sensitive at the bottom. The horizontal axis in the figure represents the EMV value that was calculated in the decision tree. The optimum EMV calculated as $4729.27K was highlighted as a vertical dashed line in the figure.

Figure 46. Tornado diagram illustrating sensitivity for the capital cost variables of the objective function.

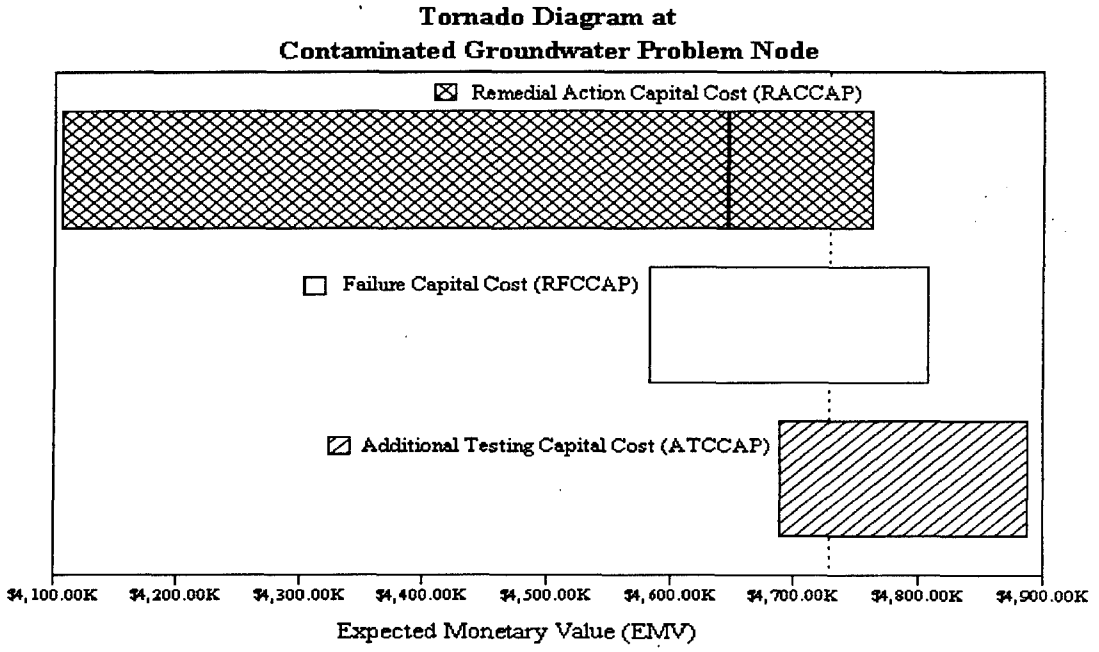

Sensitivity for remedial action capital costs was the most sensitive of the three variables evaluated and had the potential to change the decision from a postpone action alternative to one requiring immediate action. This is seen by the dark vertical line within the sensitivity block located at about $4650K EMV. The mark indicated that the optimum decision could change with a significant change in the variable's value. Another way of

showing this relationship is presented in Figure 47, a sensitivity plot of remedial action capital cost versus EMV.

Figure 47. Sensitivity analysis plot of remedial action capital cost.

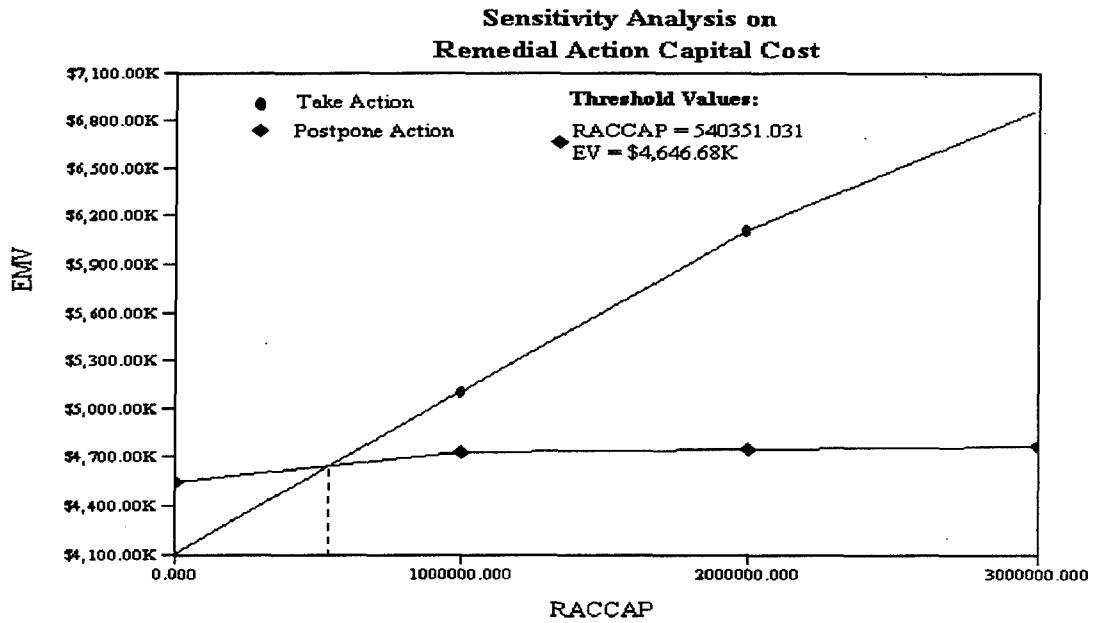

This figure shows that "postpone actions" is the optimal decision as long as the capital cost of remediation is greater than $540,351, as illustrated by the dashed vertical line to the line intersection. At or below this point the optimal decision would be to take action with a new EMV of $4646.68K.

The tornado diagram in Figure 46 showed no sensitivity to the failure and additional testing cost variables. Figures 48 and 49 present a sensitivity analysis for each individual variable. In Figure 48, failure capital costs ranging from zero to almost $14 million illustrated no intersection of the decision alternatives. The converging slope of the two lines was such that intersection would occur at a point beyond any reasonable estimation of failure costs.

Figure 48. Sensitivity analysis plot of failure capital cost.

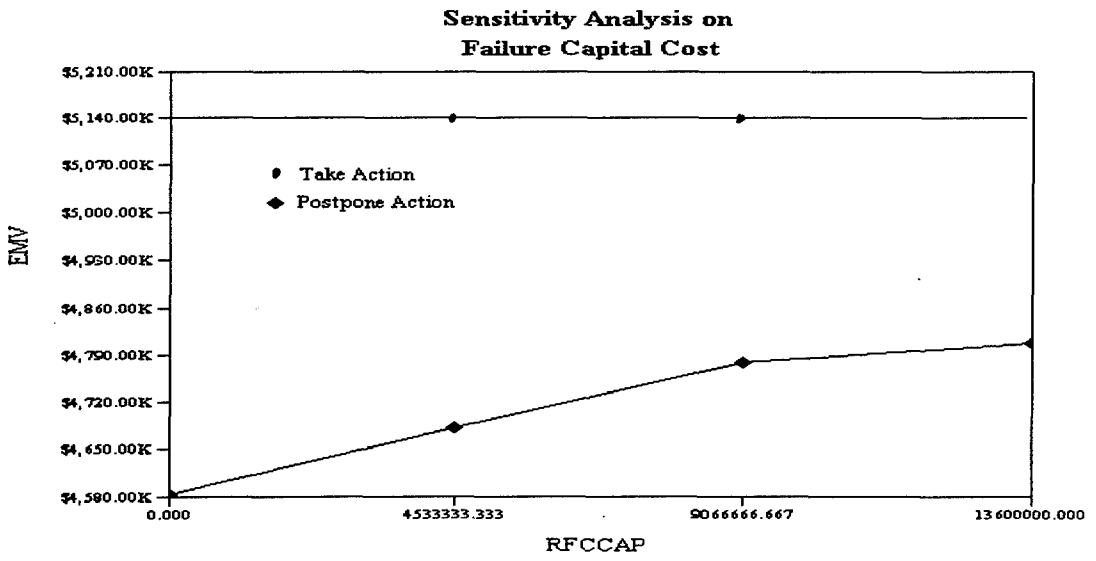

In Figure 49, the same sensitivity was illustrated for additional testing capital cost. Capital costs ranging from zero to $200,000 illustrated no intersection of the decision alternatives. Again, the converging slope of the two lines was such that intersection would occur beyond any reasonable estimation of failure costs.

Figure 49. Sensitivity analysis plot of additional testing capital cost.

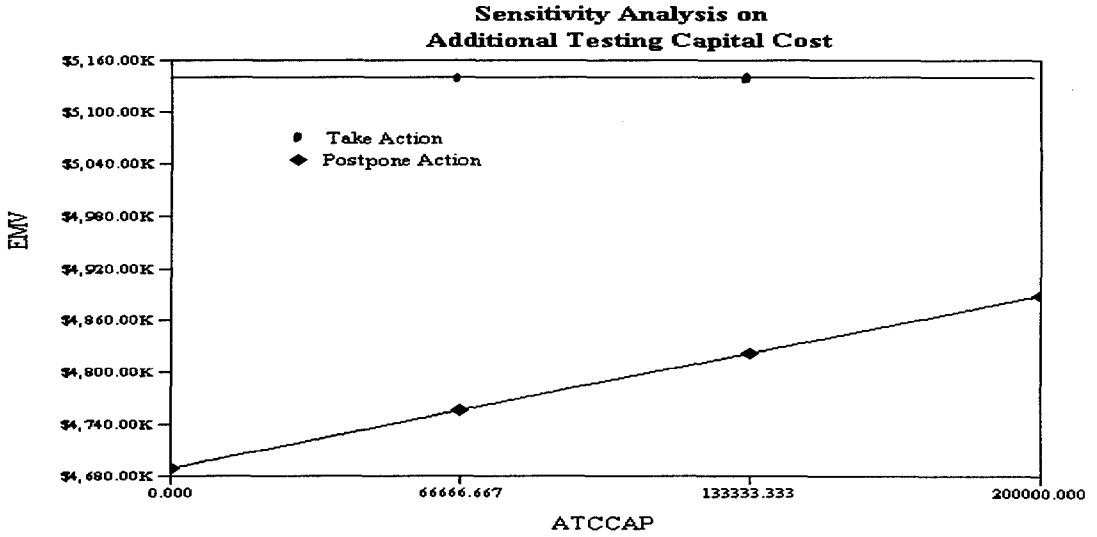

A similar sensitivity analysis was conducted with the operational and maintenance cost variables resulting in a tornado diagram illustrated in Figure 50. This diagram had the distinctive tornado shape, with monitoring costs as the most sensitive, indicating that an increase in the optimal EMV could change the decision alternative. Two variables, additional testing and remedial action operational costs, showed a potential to change the decision from a postpone action alternative to one requiring immediate action as highlighted by the dark vertical lines within their sensitivity boxes.

Figure 50. Tornado diagram illustrating sensitivity for the operational and maintenance cost variables of the objective function.

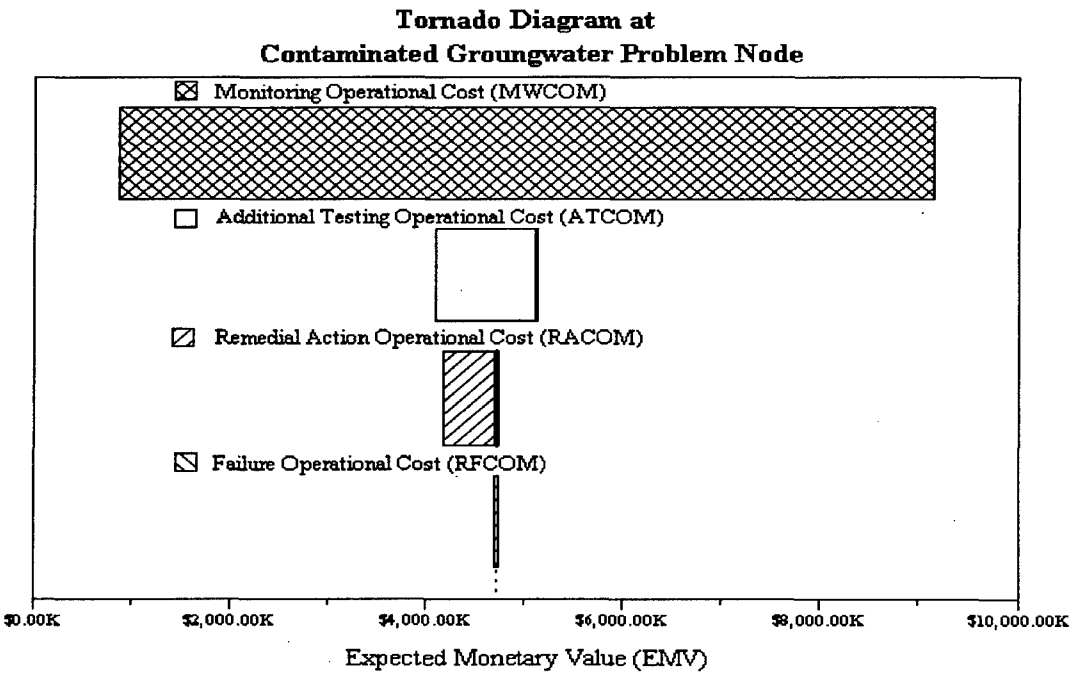

A separate sensitivity plot (Figure 51) showed that monitoring cost were very sensitive to changes in EMV but the decision alternatives intersected beyond $600,000. That is, any change in monitoring costs would not change the decision alternative but it would change

if the EMV was increased from $4.7 million to about $5.2 million. An increase in the EMV is only possible if the probabilities were changed and/or the all objective function variable values were increased. More important was the sensitivity of additional testing and remedial action costs.

Figure 51. Sensitivity analysis plot of monitoring operational cost.

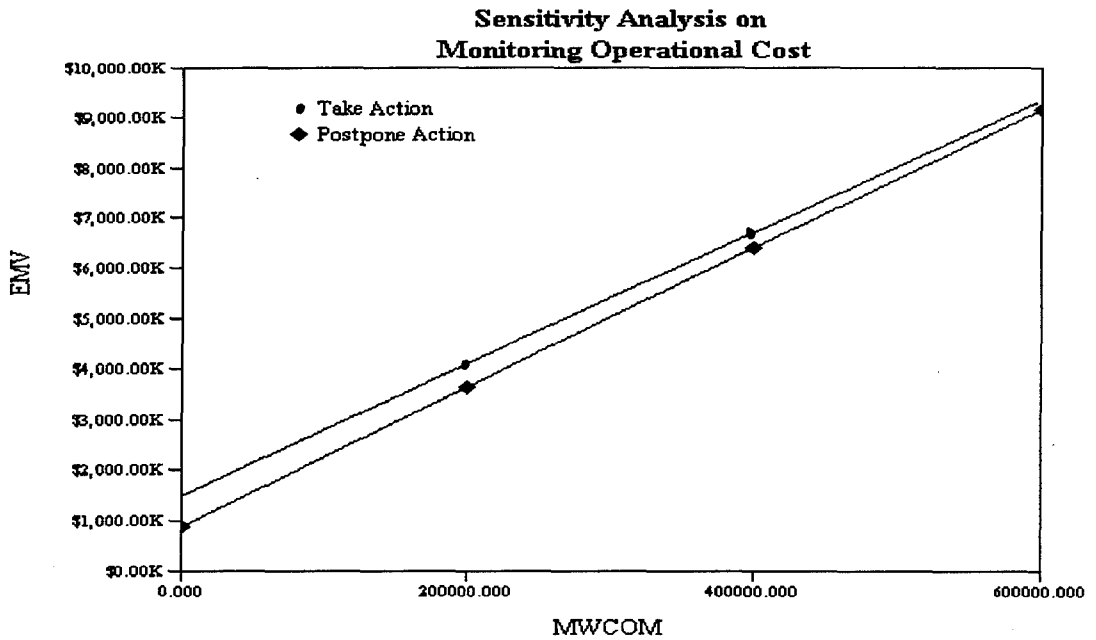

These two variables had the potential to change the optimum alternative. Figure 52 illustrates the additional testing sensitivity with a change in optimal alternative occurring at about $76,000 cost. This means that an increase in additional testing operational costs would result in a decision alternative change. Operational testing costs at or above $76,000 would change the optimum decision to the "take action alternative".

Figure 52. Sensitivity analysis plot of additional testing operational cost.

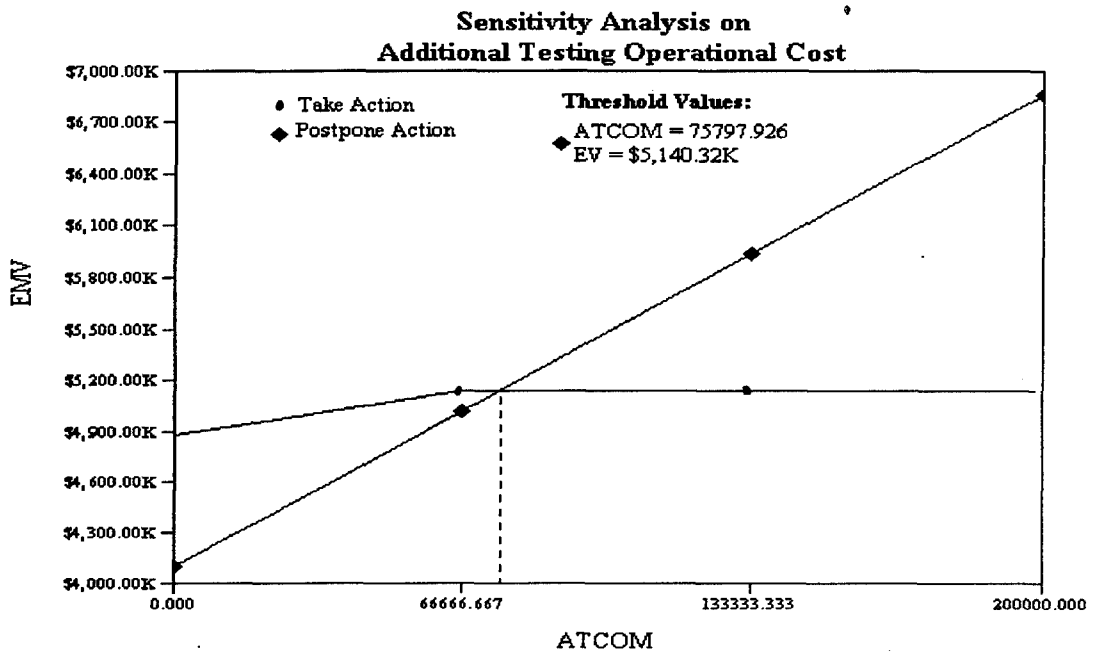

Remedial action operational cost sensitivity in Figure 53 showed that a decrease in cost to about $587,000 would cause a change in the optimum alternative.

Figure 53. Sensitivity analysis plot of remedial action operational cost.

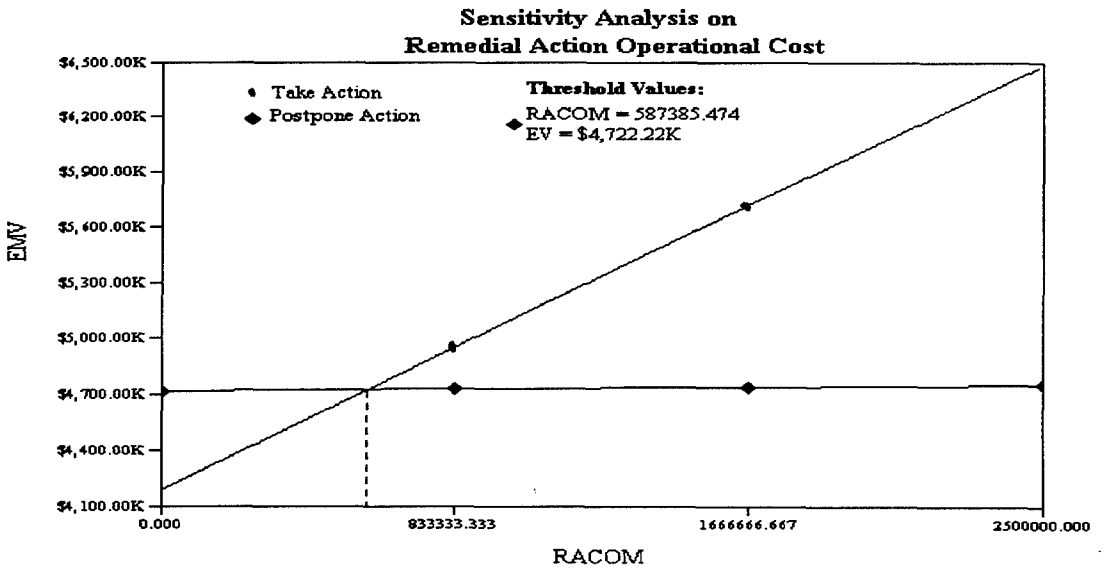

Once again, failure cost, which had the least confidence when estimating costs, was not sensitive to changes in cost as illustrated in Figure 54. The intersection of the two alternative cost sensitivity lines showed no convergence within a reasonable estimation range. Therefore the failure cost estimates appear to be reasonable and show no sensitivity to changes.

Figure 54. Sensitivity analysis plot of failure operational cost.

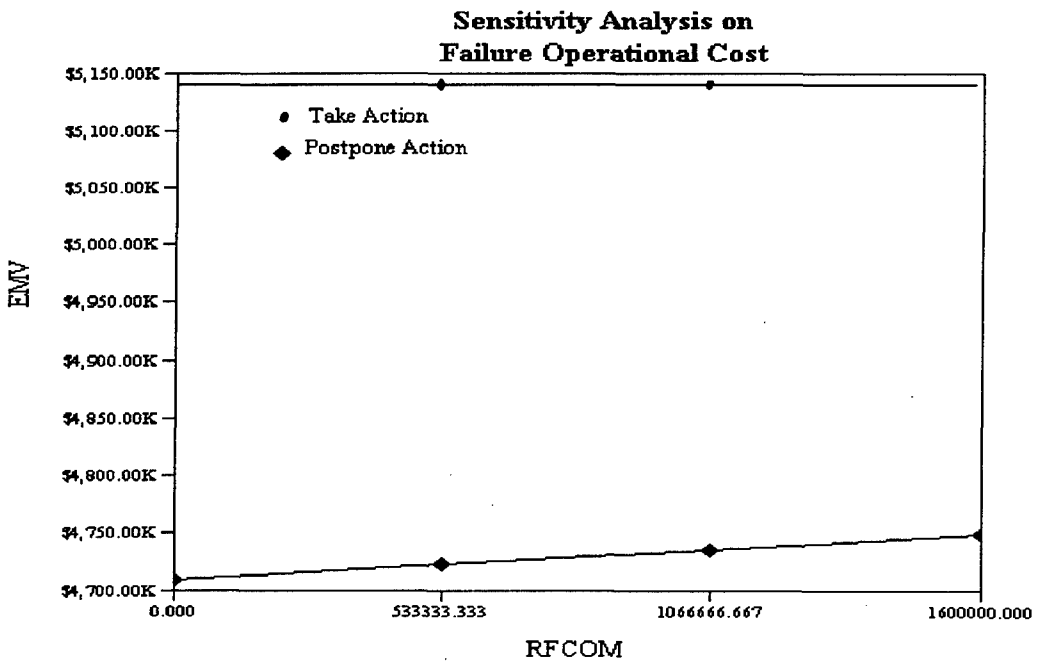

In summary, Table 19 presents the sensitivity analysis in a table for comparison of the objective function variables. The column titled "Range" shows the variable values for which the sensitivity analysis was conducted. The upper limit was about five times that of the estimated value determined using CORA. For variables that were sensitive to changes in the variable's value, the threshold value was presented in the table along with the threshold EMV.

Table 19. Summary table for objective function variables and their sensitivity to changes of their estimated costs.

			Thresholds, if Yes	
Variable	Range[1] ($x10^6$)	Sensitive	Value ($x10^6$)[2]	EMV ($x10^6$)
Remedial Action capital	0-3.0	yes	0.54	4.65
Remedial Action O&M	0-2.5	yes	0.59	4.72
Failure capital	0-13.6	no	-	-
Failure O&M	0-1.6	no	-	-
Additional Testing capital	0-0.20	no	-	-
Additional Testing O&M	0-0.20	yes	0.08	5.14
Monitoring O&M	0-0.60	no	-	-

1. This was the cost range used in the sensitivity analysis.
2. Value is the variable cost at which a change in the decision alternative would occur.

Chapter V

DISCUSSION OF RESULTS

Decision Tree Analysis

In Chapter II an example problem was introduced to which the decision analysis methodology was to be applied. Given the complexity of the situation and the decisions required, a decision tree analysis was utilized to evaluate the various decisions that were made in choosing the best alternative to remediate the contamination problem at the ammunition plant. The decision tree shown in Figure 55 is the same as in Figure 44 from Chapter IV, representing a collapsed version of the full tree presented in Figure 56.

The decision tree illustrated in Figure 55 is shown in rolled-back form. That is, the decision tree calculations were completed and illustrated the estimated monetary value (EMV) for each of the alternatives within the tree, thus highlighting the optimal decision alternatives. The darkened nodes highlight the optimal decision path for the analysis. The first decision within the decision tree was to "Take Action" or "Postpone Action". Calculation of the EMVs revealed that postponement of action was the best alternative with an EMV of $4,729.27 K. As discussed in Chapters III and IV, postponement of action by 10 years had a significant reduction in the probability that contaminant reached the plane of compliance (POC). That is, the greatest probability of contaminant occurrence was within the first 10 years, after which the probability decreased significantly. This decision alternative inherently included an additional testing phase that acted as an early warning system should contaminant migrate towards the POC

within the 10 year postponement period, thus initiating revised actions based on new migration data.

Following the "Postpone Action" branch, there are three probability branches emerging from the circular chance node. This sub-branch utilized Bayesian analysis to revise probabilities of contaminant transport based on additional monitoring wells. At this point within the decision tree, future actions were dependent upon the monitoring results from the additional wells. For two possible testing outcomes labeled "contaminant migration not detected" and "detected in amounts < 5 ug/l", the optimal decision alternative calculated was to take no remedial action. The "No Action" decision had an EMV of $4,539.54 K and $4,992.18 K for "No Detected Contamination" and "Detected Contamination < 5 ug/l", respectively. If contamination was detected in amounts greater than 5 ug/l, then the decision analysis shows that "Remedial Action" was the best alternative. The best remedial action alternative was determined to be the pump and treat technique utilizing an air stripping operation to treat the groundwater, assuming that the vapor emissions were not treated. This alternative had a calculated EMV of $5,930.82 K.

The utility of the decision tree analysis did not stop with just providing the best decision alternative. It was also used in evaluating decision alternatives under varying situations, commonly called "war gaming". Suppose for example that the alternative of "Postponing Action" was not an option. It can be seen in Figure 51 that at each of the decision nodes within the tree, the decision alternatives that were not the original optimal choice have a double hatch mark on their respective branch.

Figure 55. Decision tree of example problem with collapsed sub-branches showing expected monetary values for decision alternatives.

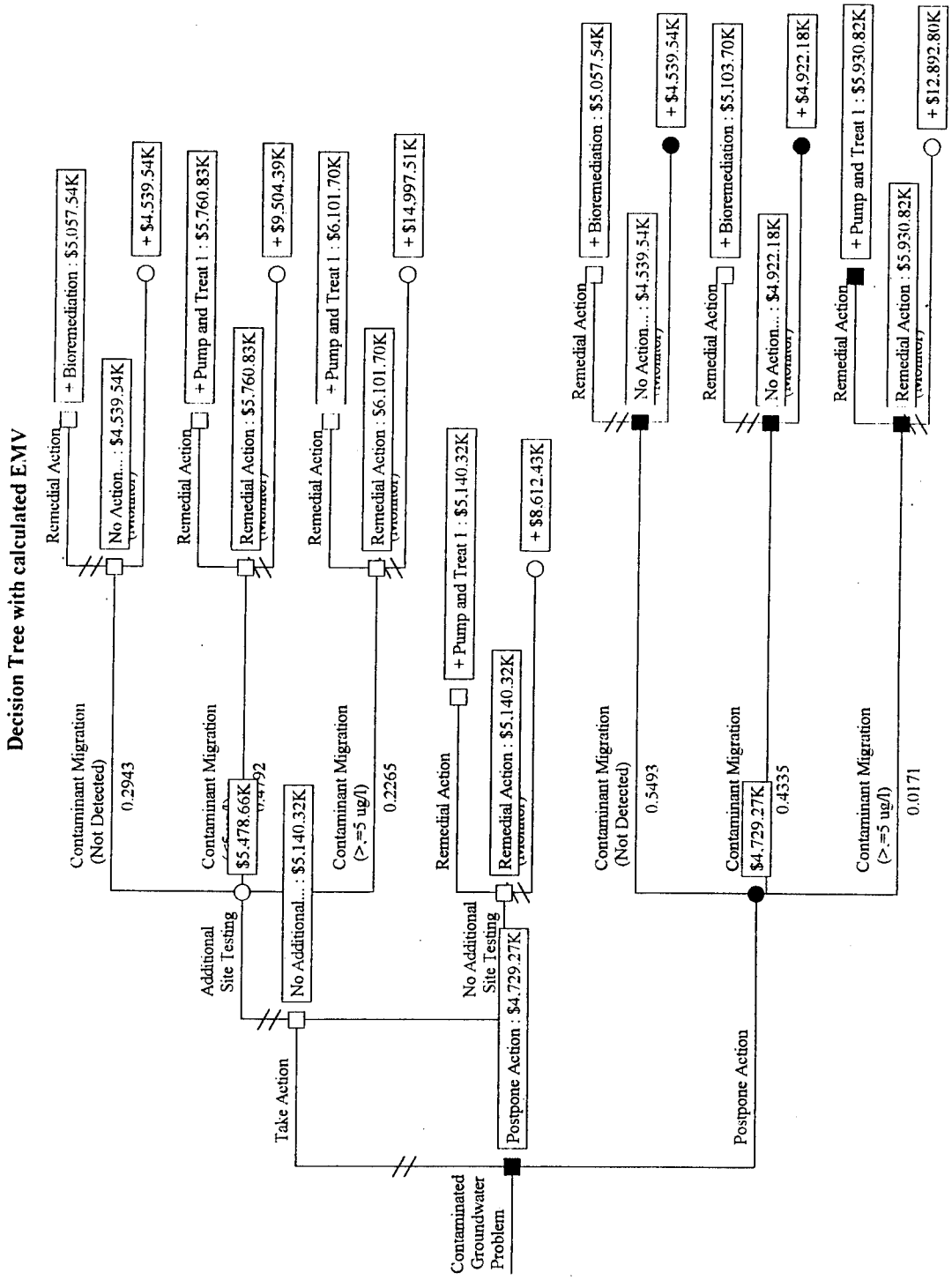

Using the hypothetical example that postponing action was not an acceptable alternative, the remaining decision alternative branch was analyzed. Within this decision branch there were two alternatives, "Additional Site Testing" or "No Additional Site Testing". The optimal decision alternative of the two was the branch without a double hatch. That is, the "No Additional Site Testing" alternative was preferred. The subsequent optimal decision alternative within this sub-branch was the remedial action alternative of pumping and treatment utilizing an air stripping operation, having an EMV of $5,140.32 K. From this alternative analysis it can be seen that the decision tree analysis was very useful in evaluating decisions under varying "war gaming" scenarios.

Probabilities of Decision Tree Analysis

The state of nature probabilities and the revised probabilities resulted from the stochastic Monte Carlo contaminant transport analysis conducted early in the decision analysis methodology process. This analysis was essential to assign probabilities of occurrence to the three states of nature that were used in the decision tree analysis. Probabilities for the three states of nature: contaminant not detected at the POC (S_1), contaminant detected at POC with concentration < 5 ug/l (S_2) and contaminant detected at POC with concentration ≥ 5 ug/l (S_3) are shown in Table 20. The table illustrates that the probability of contaminant occurrence at the POC decreased with time with more information. Therefore, an increased certainty was brought to the decision tree analysis through the contaminant transport analysis and the Bayesian analysis. Prior to the transport analysis the probability for any one state of nature to occur was 33.3% since the

sum of the three probabilities must equal 100%. After conducting the contaminant transport analysis, the probabilities were revised to 52, 35 and 13% for (S_1), (S_2) and (S_3), respectively and were employed in the "take action" decision alternative branch (see Table 20).

Table 20. Prior and revised probabilities utilized within the decision tree analysis.

Decision Tree Analysis		Probability (%)		
Decision Alternative	Test Result	S_1	S_2	S_3
Take action	No additional testing	52	35	13
Take action with testing	No detection of TCE	100	0	0
	Detection of TCE < 5 ug/l	46	42	12
	Detection of TCE ≥ 5 ug/l	0	67	33
Postpone Action 10 yrs	No detection of TCE	100	0	0
	Detection of TCE < 5 ug/l	95	4.5	.5
	Detection of TCE ≥ 5 ug/l	0	86	14

Combining the transport and the Bayesian analysis, the probabilities were further refined for the states of nature. From Table 20 the revised probabilities under the "Take Action" alternative were significantly different when compared to the prior probabilities without additional testing data. The prior probability of POC contamination of 13% was higher than the revised probability of 0% for the "No Contaminant Detected" test result. Revised and prior probabilities were similar at 12% and 13%, respectively, for the "Detection < 5 ug/l" test result. Revised probabilities increased to 33% if detection is ≥ 5 ug/l in the additional monitoring well.

Within the "Take Action" branch of the decision tree, the optimal alternative calculated was not to do the additional testing but to take remedial action. This decision

illustrates how the methodology takes into consideration not only the enhanced probabilities from Bayes analysis but also considers the cost and benefit that additional testing provided. The additional testing alternative had a higher EMV then the take action branch, thus precluding it as an optimal decision alternative. The higher EMV of additional testing resulted from the probability of S_3 occurring, given detection of contaminant < 5 ug/l, which was 12%. This probability combined with the objective function cost was great enough to make the EMV for the take no action alternative higher than the remedial action alternative. The lower EMV for remedial action did not lower the higher overall EMV for the additional testing sub-branch of the decision tree, thus the take action branch, having a lower EMV, was the optimal alternative.

Probabilities associated with the postpone action branch were revised from the prior probabilities for the states of nature for years 10-19. These probabilities were illustrated as curve B in Figure 32 of Chapter IV. The revised probabilities for the postpone action alternative were low enough in S_3 that the remedial action alternative was calculated as the optimal alternative only if the contaminant was detected in quantities ≥ 5 ug/l in the additional monitoring wells.

Expected Monetary Value in Decision Analysis

The contaminant transport and Bayesian analysis were important to developing prior and revised probabilities for the states of nature within the decision analysis. Conditional simulation and cost estimation were important to determining the EMVs that were calculated within the decision analysis and were used to determine the optimal

alternative. Conditional simulation was used to define the size and strength of the contaminant plume that existed beneath the burning grounds using spatial statistics developed from monitoring data. These two parameters were used in the cost estimation program CORA to estimate the cost for remedial action and failure.

From the conditional simulation results shown in Chapter IV, remedial action alternatives were developed for the decision analysis. Three alternatives were used to demonstrate the methodology. Two of the alternatives utilized pump and treat technology with varying treatment operations. Pump and treat #1 used an air stripping operation to remove the TCE from groundwater. This option was inexpensive when compared to pump and treat #2 which used granulated activated carbon to treat groundwater. The third alternative utilized in-situ biodegradation technology. This technique was also expensive due to the size of the plume and use of hydrogen peroxide to deliver oxygen to the microorganisms.

The groundwater extraction operations were much less expensive than in-situ bioremediation due the remediation scheme and number of extraction wells, with first year operating costs of $980,000 versus $2.19 million, respectively. The hydraulic barrier approach previously discussed in Chapter III was taken to be the primary reason for these decreased costs. This scheme was much cheaper and more practical than installing extration wells in a grid network over the entire site. The bioremediation scheme involved inoculating the contaminated aquifer with microorganisms and providing them nutrients and oxygen. This alternative was expensive due to the use of hydrogen peroxide as a delivery agent for the oxygen and the size and strength of the plume.

The objective function costs for the various decision alternatives within the decision tree are illustrated in Table 21. Within the decision tree there were three main decision alternatives under the column labeled "Decision Alternatives". Each of these alternatives had sub-decision branches involving remedial or no action. These decision alternatives were labeled individually under the "Decision Alternative Objective Function Cost" column. The table illustrates the objective function cost for all possible outcomes within the decision tree. The cost difference experienced between the non-testing alternative and the testing alternatives were the additional costs incurred for installing the additional monitoring wells and associated lab analysis costs. Comparison of the alternatives to postpone and take action with testing reveals some costs remain the same and others differ. The reason the cost varied for S_3 was due to the discount rate effect on the operation and maintenance costs given a 10 year delay. That is, the cost of operations will be higher in 10 years due to inflation. Cost for the other two states of nature were not different due to an assumption that capital costs had been committed for reaction if contaminant was detected in amounts ≥ 5 ug/l in the additional monitoring wells.

Illustration of the expected monetary values calculated during the decision tree analysis are presented in Table 22. The table is similar to Table 21, with the same decision alternative columns, except the replacement of the S_x column with Z_x, the outcome from additional testing. This is because the EMV is a calculation of the S_x probability multiplied by its respective objective function cost. Since there was no additional testing within one of the decision alternatives Z_x does not apply for that alternative.

Table 21. Objective function costs for the remedial action and no action alternatives.

		Decision Alternative Objective Function Cost ($x • 10^6)			
Decision Alternative	S_x^*	P&T 1	P&T 2	Biorem.	None
Take action with additional test	S_1/Z_x	5.57	7.17	5.06	4.54
	S_2/Z_x	5.57	7.17	5.06	11.3
	S_3/Z_x	7.18	21.3	15.2	22.4
Take action with no testing	S_1	4.90	6.50	4.38	3.86
	S_2	4.90	6.50	4.38	10.7
	S_3	6.75	20.9	14.8	21.8
Postpone action (testing inherent)	S_1/Z_x	5.57	7.17	5.06	4.54
	S_2/Z_x	5.57	7.17	5.06	11.3
	S_3/Z_x	8.13	22.3	16.2	22.4

* S_x represents the three states of nature and Z_x represents the three test results defined as:
Z_1 - additional testing does not detect contaminant
Z_2 - additional testing detects contaminant with concentration < 5 ug/l
Z_3 - additional testing detects contaminant with concentration ≥ 5 ug/l

It can be seen from Table 22 that for the decision alternative "Take Action" and "Conduct Additional Testing", the optimal sub-branch decision alternative for a test resulting in Z_1 was take no remedial action, having an EMV of 4.54. The EMV for the optimal alternative was lower than the other EMVs within the same row. If the test results were either Z_2 or Z_3, then the optimal sub-branch decision would be pump and treat remediation scheme one (P&T 1). From the table, the decision alternative to take action with no testing showed the optimal sub-branch decision for P&T 1 with an EMV of 5.14 which was less than the other EMVs. The "Postpone Action" alternative was similar to the other alternative involving additional testing. From the table, the optimum sub-branch alternatives for Z_1, Z_2 and Z_3 were no remedial action (4.54), no remedial action (4.92) and P&T 1 (5.93), respectively.

Calculation of the EMVs for the main decision alternatives involving testing was the same as for sub-branches involving a chance node with states of nature. In this case the optimal EMV was multiplied by the probability of Z_x. For example, the EMV for the alternative "Postpone Action" was calculated as $\$4.73 \times 10^6$ (see Figure 55). The calculation is as follows:

Z_1: $EMV_{Z1} = \$4.54 \times 10^6$ and $P_{Z1} = .5493$
Z_2: $EMV_{Z2} = \$4.92 \times 10^6$ and $P_{Z2} = .4335$
Z_3: $EMV_{Z3} = \$5.93 \times 10^6$ and $P_{Z3} = .0171$

$$EMV = (EMV_{Z1} \bullet P_{Z1}) + (EMV_{Z2} \bullet P_{Z2}) + (EMV_{Z3} \bullet P_{Z3}) \quad (42)$$

Table 22. Expected monetary value for decision alternatives within the decision tree.

		Sub-branch Decision Alternative EMVs ($\$x \bullet 10^6$)			
Decision Alternative	Z_x^*	P&T 1	P&T 2	Biorem.	None
Take action with additional test	Z_1	5.57	7.17	5.06	**4.54**
	Z_2	**5.76**	8.83	6.25	9.50
	Z_3	**6.10**	11.8	8.41	15.0
Take action with no testing	na	**5.14**	8.38	5.74	8.61
Postpone action (testing inherent)	Z_1	5.57	7.17	5.06	**4.54**
	Z_2	5.58	7.24	5.10	**4.92**
* Refer to Z_x definition in Table 21.	Z_3	**5.93**	9.29	6.61	12.9

Sensitivity Analysis

The original motivation to conduct a sensitivity analysis was a lack of confidence in the estimated costs for failure that were used in the objective function. After conducting the sensitivity analysis it was found that the decision analysis was not sensitive

to failure costs at the decision point to postpone or take action (see Figures 44, 46, 48 and 52). Objective function cost variables that were sensitive include remedial action capital cost (RACCAP), additional testing operational cost (ATCOM) and remedial action operational cost (RACOM). The sensitivity plot for RACCAP (see Figure 45) illustrates that the optimal decision could change if RACCAP went below $540,351. The lowest RACCAP value, for P&T 1, was estimated by CORA to be nearly $1 million. Therefore, it is unlikely that remedial action capital costs will go below the threshold value. If RACCAP did go below the threshold value, then the optimal decision alternative would change to "Take Action".

The other objective function variable encompassing remediation costs, the operation and maintenance cost, showed sensitivity with a threshold value of about $590,000 (see Figure 51). The likelihood that the optimal alternative would change was less for remedial action O&M (RACOM) costs than it was for its capital costs. RACOMs threshold value is about 20% of the lowest estimated RACOM value. That is, the lowest estimated RACOM value was a little over $3 million and the likelihood that it would reduce to $590,000 appears small.

In Figure 50 the additional testing O&M cost (ATCOM) showed sensitivity with a threshold value of about $76,000. Again, the likelihood that the optimal alternative would change appears small since the ATCOM for the present optimal alternative, postpone action, is about $45,000. However, if seven or more additional monitoring wells were installed versus the estimated three, then the optimal alternative could change. This is based on the estimation that ATCOM is $9,200 per well per year.

The results discussed in this chapter were strongly based on the assumptions made throughout the analysis involving transport, conditional simulation and the optimization equation. Additionally, as mentioned in Chapter II, the data utilized in this analysis was representative of the upper portions of the Wilcox aquifer. If data were made available that could change a previously made assumption, then the analysis would need to be evaluated to determine the effect on the results. For example, if the physical parameters for TCE were to change, then the significance of these changes on the current results should be determined. In other words, the results of this analysis are based on the data and assumptions presented in this analysis.

Chapter VI

CONCLUSIONS

Methodology Summary

This study was conducted to provide a decision analysis methodology for military commanders and their staffs when confronted with an environmental contamination problem. The methodology was based on an established problem-solving foundation that was adapted to incorporate uncertainty analysis of imperfect data and quantify the uncertainty with respect to time. The uncertainty output was then used in conjunction with a decision optimization model for utilization in a decision tree analysis.

The uncertainty analysis used existing contaminant transport models in stochastic fashion to develop time versus concentration break-through curves. The break-through curves were then used to develop probabilities of occurrence for contaminant reaching the plane of compliance (POC) within specified time periods. These probabilities were utilized in the optimization model to calculate the expected monetary value for the decision alternatives. To further refine the contaminant transport probabilities, a Bayesian analysis was conducted to determine the revised probabilities given uncertainties associated with laboratory testing. These revised probabilities were used in the decision tree sub-branches involving additional testing in the same fashion that the prior probabilities were used.

The areal extent and concentration distribution of the contaminant plume was defined by using conditional simulation. These plume characteristics were important in

developing the remediation schemes and their costs. Three remediation schemes were used in this analysis: pump and treat groundwater with air stripping, pump and treat groundwater with activated carbon and in-situ bioremediation. Each of the these remediation strategies required that the plume size and concentration be known to estimate attendant costs. Their costs, as well as monitoring, additional testing and failure costs were estimated using the CORA expert system. The costs developed by CORA were used in the objective function of the decision model.

The objective function, equation (1) of Chapter II, was a cost minimization model that incorporated remediation, monitoring, additional testing and failure costs. This equation was used to calculate the cost of each consequence within the decision tree. The objective function cost combined with the probabilities, developed in the uncertainty analysis, were used to determine the expected monetary value for each of the decision alternatives. The decision alternative with the least expected monetary value was the optimum alternative.

Summary of Findings

Transport Modeling

The following findings were made from contaminant transport modeling through the unsaturated and saturated zones.

- Mass loading of TCE into the underlying aquifer was modeled as 631 kg/yr for the upper boundary 95% confidence interval and 267 kg/yr for the mean value.
- Reliability of the saturated zone transport analysis was illustrated by the calibration modeling of contaminant transport to a existing monitoring well

which had similar concentrations within the same order of magnitude (see Table 6).

- The probability distribution of contamination at the POC with a specific time period varied greatly due to biodegradation and/or migration of the contaminant into deeper un-monitored zones within the aquifer (see Figure 31).

Bayesian Analysis

The Bayesian analysis revealed that additional knowledge did improve probabilities over the prior probabilities (see Table 20, Chapter V). However, the "additional testing" decision alternative was not the optimum alternative given if action was taken immediately, which meant that revised probabilities were not enough to have an effect on the optimum expected monetary value in all cases.

Conditional Simulation

Findings from the conditional simulation analysis include the following:

- Conditional simulation realizations (Figure 37) produced noticeable differences in concentration variation over short distances as compared to the kriging estimate (Figure 38) and the U.S. Army Corps of Engineers' isoconcentration map (Figure 12).
- The difference between the UB 95 CI and UB 90 CI isoconcentration maps was that the contaminant concentration density varied (Figures 42 and 43, respectively). The areal extent (size) of the plumes did not vary between the two figures.
- Mean concentration and plume area for the UB 95 CI was 12,532 ug/l and 308 acres, respectively. The mean concentration for the UB 90 CI was 11683 ug/l and the area was the same as the UB 95 CI.

Decision Analysis

Findings from the decision analysis include the following:

- Decision analysis provided a link between the economic framework and the technical analysis.
- The method was flexible to varying situations by:
  - ◊ the ability to implement the analytical tool(s) that fit the situation
  - ◊ integrating a Bayesian framework, as presented in this thesis
  - ◊ incorporating a utility function that caters to a risk-averse decision maker
- It was found that "Postpone Action" was the optimum decision for the particular example used. This resulted from having the lowest expected monetary value ($4,729.27 K) and means that, given the available information it was statistically the best decision alternative. Caution must be taken in the fact that this decision was based on monitoring data from the upper portions of the aquifer, which means that this may not be the optimum decision given additional information from lower portions of the aquifer.

Methodology Fulfills Need

The decision analysis methodology presented in this thesis has demonstrated its utility in environmental decision analysis under conditions of uncertainty. Environmental decision analysis is a very complex and dynamic process that requires a methodology that can concisely illustrate the problem and adapt to changes in conditions and uncertainty. The methodology provided a link between uncertainty analysis and a decision optimization model which can be applied to strategic, operational or tactical level decision making. Both governmental or private users can benefit from the methodology. The methodology was not limited to the tools used in the example problem but is flexible to varying situations in which the user determines what tools are appropriate.

Adaptability

The utility of the methodology is in its capability to be used in varying situations. The methodology is not limited to groundwater contamination as it was applied in the example problem. The technique can be applied to other environmental contamination problems that invariably involve some level of uncertainty similar to the example problem. Typically groundwater contamination remediation involves much uncertainty with respect to contamination conditions and hydrogeological conditions, as illustrated. With wide spread occurrence of groundwater contamination, it was appropriate to use such an example for presentation of the methodology. Had the example problem involved heavy metal contamination, the decision analysis methodology would not have changed, only the tools utilized to quantify uncertainty and characterize the problem.

REFERENCES

American Petroleum Institute Decision Support System for Exposure and Risk Assessment (APIDSS) version 1.0 (1994). Prepared under contract by: Du Pont Environmental Remediation Services, Woodward-Clyde Consultants.

ArcUSA computer software. Copy right 1992. Environmental Systems Research Institute, Inc.

ASCE Task Committee (1988). Review of geostatistics in geohydrology. I: Basic concepts. Journal of Hydraulic Engineering, 116(5), 612-658.

Baird, B.F. (1978). Introduction to Decision Analysis. Belmont, California: Wadsworth Publishing.

Brown, G.C., Brigadier General (1993). The Army gets greener. The Military Engineer, 85(555), 64-66.

Callahan, M.A. (1979). Water related fate of 129 priority pollutants. U.S. Environmental Protection Agency, Athens GA, EPA-600/3-85-038.

Chechile, R.A. (1991). Probability, utility and decision trees in environmental decision analysis. Environmental Decision Making, A Multidisciplinary Perspective. New York: Van Nostrand Reinhold.

CH2M Hill (1990). Cost of remedial action model users manual, version 3.0. Office of Solid Waste and Emergency Response, U.S. EPA.

Clark, I. (1979). Practical Geostatistics. London, England: Applied Science Publishers.

Cooper, R.M. and Istok, J.D. (1988). Geostatistics applied to groundwater contamination. I: Methodology. Journal of Environmental Engineering, 114(2), 270-299.

Cressie, N.A. (1991). Statistics for Spatial Data. New York: John Wiley and Sons, Inc.

Cushing, E.M., Boswell, E.H., & Hosman, R.L. (1964). General geology of the Mississippi embayment: U.S. Geological Survey Professional Paper 448-B.

Dean, J.D., Huyakorn, P.S., Donigian, A.S., Voos, K.A., Schanz, R.W., Meeks, Y.J. and Carsel, R.F. (1989). Risk of Unsaturated/Saturated Transport and Transformation of Chemical Concentrations (RUSTIC), Volume I: Theory ad Code Verification. Environmental Research Laboratory, Office of Research and Development, U.S. EPA. EPA 600/3-89/048a.

REFERENCES

Decision Analysis by TreeAge (DATA) (1994). Decision analysis software developed by TreeAge Software, Inc.

Delhomme, J.P. (1978). Kriging in the hydrosciences. Advances in Water Resources, 1(5), 251-266.

Delhomme, J.P. (1979). Spatial variability and uncertainty in groundwater flow parameters: A geostatistical approach. Water Resources Research, 15(2), 269-280.

Deutsch, C.V. (1989). DECLUS: a FORTRAN 77 program for determining optimum spatial declustering weights. Computers & Geosciences, 15(3), 325-332.

Deutsch, C.V. and Journel, A.G. (1992). GSLIB Geostatistical Software Library and User's Guide. New York: Oxford University Press.

Englund, E. and Sparks, A. (1991). Geostatistical Environmental Assessment Software, User's Guide. Environmental Monitoring Systems Laboratory, Office of Research and Development, U.S. EPA. EPA 600/8-91/008.

Environmental Protection Agency (EPA) (1987a). Data Quality Objectives for Remedial Activities: Development Process. Office of Emergency and Remedial Response and Office of Waste Programs Enforcement. EPA/540/G-87/003.

Environmental Protection Agency (EPA) (1987b). Processes, Coefficients and Models for Simulating Toxic Organics and Heavy Metals in Surface Waters. Environmental Research Laboratory, Athens Ga. EPA PB87-213880.

Fetter, C.W. (1980). Applied Hydrogeology. Columbus, Ohio: Charles E. Merrill Publishing Co.

Fisher, W.L. & McGowen, J.H. (1969). Depositional systems in Wilcox Group (Eocene) of Texas and their occurrence of oil and gas. The American Association of Petroleum Geologists Bulletin, 53(1), 30-54.

Freeze, R.A. and Cherry, J.A. (1979). Groundwater. Englewood Cliffs, New Jersey: Prentice-Hall, Inc.

Freeze, R.A., Massmann, J., Smith, L., Sperling, T., & James, B. (1990). Hydrogeological Decision Analysis: 1. A Framework. Ground Water Journal, 28(5), 738-764.

REFERENCES

Freeze, R.A., Massmann, J., Smith, L., Sperling, T., & James, B. (1992). Hydrogeological Decision Analysis: 4. The concept of data worth and its use in the development of site investigation strategies. Ground Water Journal, 30(4), 574-587.

Golden, M.L., Peer, A.C., Brown, S.E. Jr. (1994). Soil Survey of Harrison County, Texas: Soil Conservation Service, U.S. Department of Agriculture.

Gorelick, S.M., Voss, C.I., Gill, P.E., Murray, W., Saunders, M.A. and Wright, M.H. (1984). Aquifer reclamation design: The use of contaminant transport simulation combined with nonlinear programming. Water Resources Research. 20(4), 415-427.

Green, M.G., & Marr, A.J. (1990). Closure of an Unlined Evaporation Pond: a Case History. Bulletin of the Association of Engineering Geologists, 27(2), 235-243.

Hellman, T.M. and Hawkins D.A. (1988). How clean is clean? The need for action. Hazardous Waste Site Management: Water Quality Issues. Washington, D.C.: National Academy Press.

Hohn, M.E. (1988). Geostatistics and Petroleum Geology. New York: Van Nostrand Reinhold.

Hosman, R.L., Long, A.T., Lambert, T.W., & others (1968). Tertiary aquifers in the Mississippi Embayment: U.S. Geological Survey Professional Paper 448-D.

Hosman, R.L., & Weiss, J.S. (1991). Geohydrologic units of the Mississippi embayment and Texas coastal uplands aquifer systems, South-central United States: U.S. Geological Survey Professional Paper 1416-B.

Howard, P.H., Sage, G.W., Jarvis, W.F. and Gray, D.A. (1990). Handbook of Environmental Fate and Exposure Data for Organic Compounds. Chelsea, Michigan: Lewis Publishing.

Journel, A.G. and Huijbregts, C. (1978). Mining Geostatistics. London, England: Academic Press.

Jury, W.A., Spencer, W.F. and Farmer, W.J. (1983). Behavior assessment model for trace organics in soil - 1. Model description. Journal of Environmental Quality, 12, 558-564.

Jury, W.A., Russo, D., Streile, G., Hesham, E.A. (1990). Evaluation of Organic Chemicals Residing Below the Soil Surface. Water Resources Research, 26(1), 13-20.

REFERENCES

Karickhoff, S.W., Brown, D.S. and Scott, T.A. (1979). Sorption of hydrophobic pollutants on natural sediments. Water Research, 13, 241-248.

Massmann, J., Freeze, R.A., Smith, L., Sperling, T., & James, B. (1991). Hydrogeological Decision Analysis: 2. Applications to groundwater contamination. Ground Water Journal, 29(4), 536-548.

Matheron, G. (1971). The Theory of Regionalized Variables and Its Applications. Fontainbleau, France: Les Cahiers du Centre de Morphologie Mathematique de Fontainebleau.

Matheron, G. (1973). The intrinsic random functions and their applications. Advances in Applied Probability, 5, 438-468.

Matson, G.C. (1916). The Caddo Oil and Gas Field, Louisiana and Texas: U.S. Geological Survey Bulletin 619.

MAPEXPERT computer software. Copy right 1993. DeLorme Mapping Company.

Medina, M.A., Butcher, J.B. and Marin, C.M. (1989). Monte Carlo analysis and bayesian decision theory for assessing the effects of waste sites on groundwater, II: Applications. Journal of Contaminant Hydrology, 5, 15-31.

Ossenbruggen, P. J. (1984). Systems Analysis for Civil Engineers. New York, New York: John Wiley and Sons.

Press, S.J. (1989). Bayesian Statistics: Principles, Models and Applications. New York: John Wiley and Sons.

Sawyer, C.N., McCarty, P.L., Parkin, G.F. (1994). Chemistry for Environmental Engineering. New York: McGraw-Hill, Inc.

Standard Methods (1989). Standard Methods for the Examination of Water and Wastewater. American Public Health Association, American Water Works Association and Water Pollution Control Federation. Baltimore, Maryland: Port City Press.

Sullivan, K. (1984). Summary of Henry's Law Constants. Used by Hydro Group.

U.S. Army (1994). Field Manual 100-1, The Army. Department of Army.

U.S. Army (1993). Field Manual 100-5, Operations. Department of Army.

REFERENCES

U.S. Army Corps of Engineers (USACE) Tulsa District (1993). Data summary report of investigation results from 1976 through 1992 for Burning Ground 3 & the unlined evaporation pond. Longhorn Army Ammunition Plant, Karnack, Texas.

U.S. Geological Survey (1986). USGS open file report STATPAC, Using spatial statistics programs. Lakewood, Colorado.

Verschueren, K. (1983). "Handbook of Environmental Data on Organic Chemicals." New York. Van Nostrand Reinhold.

Weast, R. (1980). "Handbook of Chemistry and Physics," 60th edition. CRC Press, Inc.

APPENDIX A

Additional discussion of the geostatistical methods

applied and tools utilized for: Data Assessment,

Data Spatial Variance Analysis and Sample Data Declustering.

Tool Utilized

The tool used in the data assessment step of the geostatistical analysis was Geostatistical Environmental Assessment Software (Geo-EAS) version 1.2.1 (Englund and Sparks, 1991). It is a collection of interactive software tools for performing two-dimensional kriging of a regionalized variable. (Englund and Sparks, 1991). Geo-EAS software and documentation was developed by the U.S. EPA utilizing public domain software.

The Geo-EAS program used for data assessment was the univariate statistics program called STAT1. The menu driven program provides the user with the following statistical information:

Data Observations

- Number of observations
- Number of missing observations
- Number of retained observations

Data Statistics

- Mean
- Variance
- Standard Deviation
- Percent Coefficient Variation
- Lower data limit
- Upper data limit

Histogram

- Plot of histogram
- Skewness
- Kurtosis

Probability

- Plot of probability
- 25th percentile value
- Median value
- 75th percentile value

Methods Applied

A data file containing the monitoring well coordinates and measured concentrations from 1993 was analyzed utilizing STAT1 to determine the univariate statistics for the measured TCE concentrations. STAT1 has a convenient feature that allows the user to choose a log option for the data. This feature transforms the data values into natural log numbers and then analyzes the transformed data. An statistical analysis was conducted using both the non-transformed and transformed TCE concentrations.

Results of Data Assessment

The following table summarizes the statistics of the sample data for both the measured concentrations (ug/l) and the log-normal transformed measured concentrations. The sample size was 37 monitoring wells that had measured TCE concentrations measuring from 5-18,300 ug/l. Statistical analysis calculated the mean as 1800.3 and median as 150.0 with a standard deviation of 4115.8. To measures for distribution normality, skewness and kurtosis, had values of 3.12 and 12.13 respectively. Normally distributed data should have skewness close to zero and kurtosis near one. The transformed concentration statistics does have a near normal distribution with skewness equal to .11 and kurtosis equal to 1.90 (see Table A-1).

Table A-1. Statistical analysis of measured data and log-normal converted concentrations.

Sample size is 37	TCE concentration (ug/l)	log-normal TCE conc. (ln ug/l)
Minimum concentration	5	1.609
Maximum concentration	18,300	9.814
Standard Deviation	4115.8	2.585
Mean	1800.3	5.058
Median	150.0	5.011
95% Confidence Interval	-	-
lower limit	428.0	4.196
upper limit	3172.6	5.919
Skewness	3.12	.11
Kurtosis	12.13	1.90

Another STAT1 tool used to determine the distribution of the data was a cumulative distribution plot as shown in Figures A-1 and A-2. The distribution presented in Figure A-1 was for the non-transformed TCE data, which illustrates the data's skewed distribution. The log-normal transformed data plotted in Figure A-2 represents a near normal distribution which is better suited to geostatistical analysis. The data illustrates a linear cumulative distribution from the transformed concentrations of 1.7-9.8.

Figure A-1. Cumulative distribution plot of 1993 measured monitoring well concentrations that are not log-normal transformed.

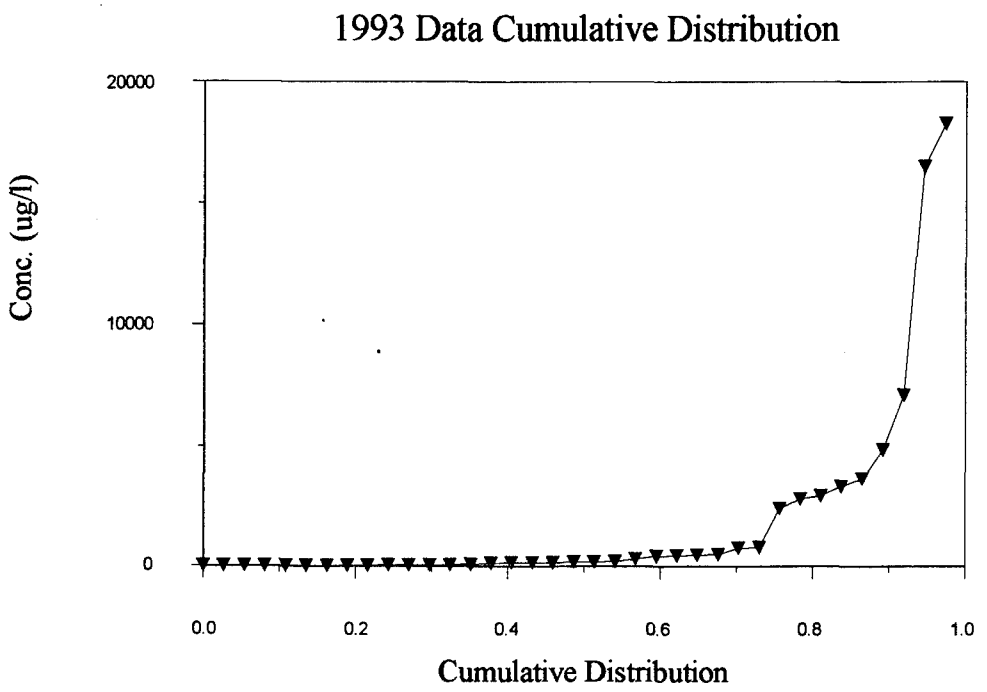

Figure A-2. Cumulative distribution plot of 1993 measured monitoring well concentrations that are log-normal transformed.

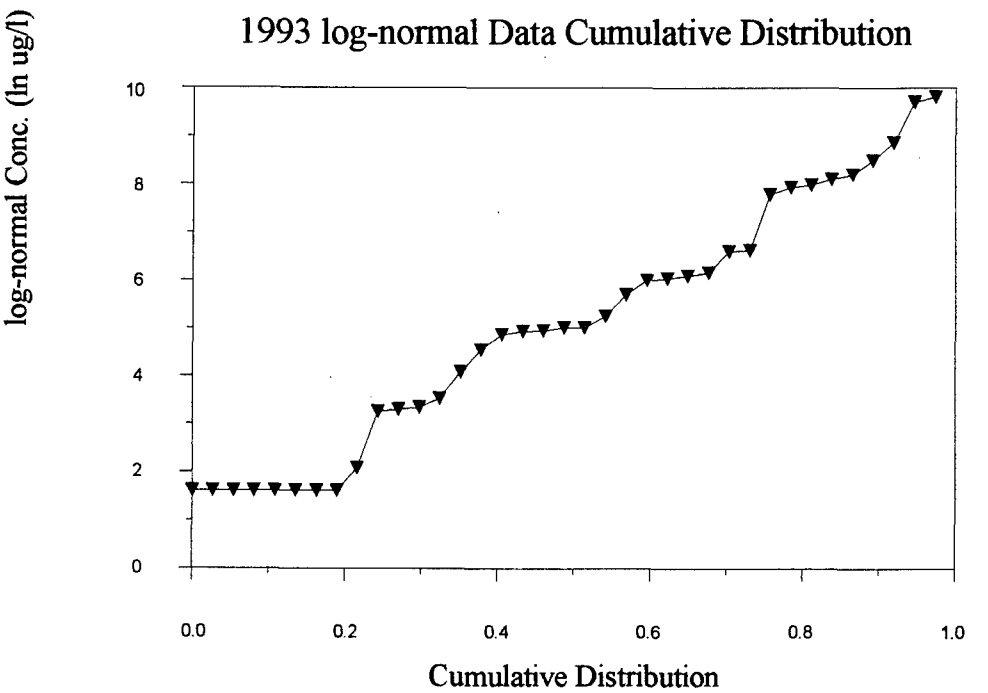

Methods Applied

Figure A-3 is an example of a linear model with a nugget effect. The variability of the nugget effect (C_0) is due to sampling error, analysis error and structure affects (if spatial structure with a range less than the smallest **h** is present) (Cooper and Istok, 1988). Note that the variogram is equal to the slope multiplied by the range (h) for the linear model.

Figure A-3. Simple linear model and nugget effect (Cooper and Istok, 1988).

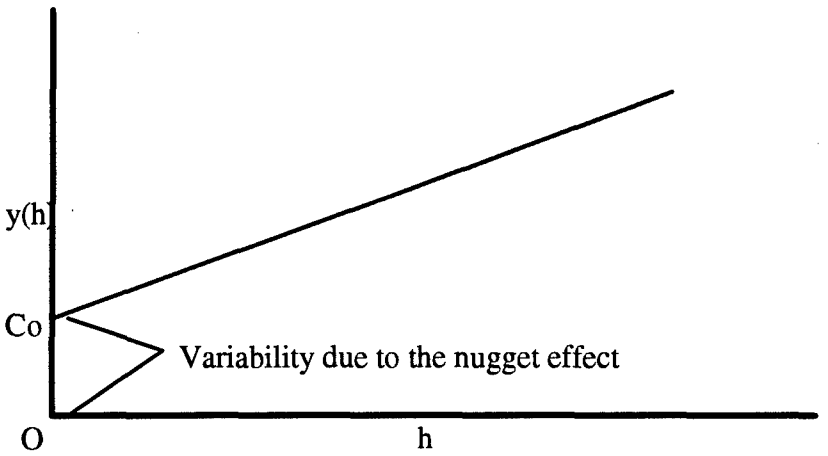

The type of model is usually obvious from the experimental variogram provided enough data points were collected (Cooper and Istok, 1988). Listed below were the guidelines used to ensure a best fit of the model to the experimental variogram. The technique used to determine if the variogram model was representative of the true variogram was a cross-validation procedure incorporated into Geo-EAS. This program

determined how well the fitted variogram predicted the observed values at the monitoring well locations. Cross-validation should not be used solely for verifying good fit of the model variogram nor should variogram parameters be changed to achieve a good cross-validation (Deutsch and Journel, 1992). The following were evaluation criteria used to determine the acceptability of the variogram model (USGS STATPAC, 1986):

- Mean kriging error should be close to zero.
- Standard deviation of the kriging errors should be lower than the standard deviation of the regionalized variable.
- Standard deviation of the standardized errors should be close to unity.
- The standardized errors should be independent of the kriged values (Journel and Huijbregts, 1978).
- The standardized errors should be independent of their location as expressed by their x- and y-coordinates.
- The kriged value should be positively correlated with the observed value of the regionalized variable.
- It is important for the final theoretical variogram model to closely approximate the observed variogram of the data.

Tool Utilized

Two programs, PREVAR and VARIO, from the Geo-EAS package were used to develop the experimental variogram and to fit a model to the variogram. A third program, called XVALID, was utilized to validate the variogram model utilizing the previously listed guidelines.

PREVAR is a preprocessor program for the program VARIO (Englund and Sparks, 1991). Because variogram calculations use the distance and relative direction between pairs of points in the sampled area, PREVAR computes these so that variogram

parameters may be changed and variogram recalculated more quickly in VARIO (Englund and Sparks, 1991). The output from PREVAR is a pairs comparison file containing the input data file contents along with distances and relative directions between pairs of sample points (Englund and Sparks, 1991). This information was then used by the program VARIO to calculate variogram values.

VARIO is a two-dimensional variogram analysis and modeling program (Englund and Sparks, 1991). Using the pairs comparison file developed by PREVAR, it calculates the variogram values and other statistics for a specified set of pair distance intervals (Englund and Sparks, 1991). Tolerances may be specified for pair direction and lag distance intervals (Englund and Sparks, 1991). Plots of variogram values vs. distance can be displayed as well as several graphs of the individual lag results such as lag-histograms, box plots, postplots and lag-scatter plots (Englund and Sparks, 1991). Variograms may be fitted with a model of up to four nested variogram structures (Englund and Sparks, 1991).

XVALID stands for "cross-validation" that involves estimating values at each sampled location in an area by kriging with the neighboring sample values (Englund and Sparks, 1991). The estimates are compared to the original observations in order to test if the hypothetical variogram model and neighborhood search parameters will accurately reproduce the spatial variability of the sampled observations (Englund and Sparks, 1991). The evaluation criteria listed in the guidelines list were also calculated.

Variogram Results

Within the spatial variance analysis there were two objectives: Develop the experimental variogram that is representative of the true variogram and fit a model to the experimental variogram. Developing the variogram entailed not only statistics of the spatial data but also requires knowledge of the geology for the site. The resulting experimental variogram presented in Figure A-4 illustrates the spatial variable variance in the vertical axis with respect to distance, in feet, between the variables in the horizontal axis. The experimental variogram showed a variance ceiling of about 7.5 beyond the range of 400 feet. Between the origin and 400 feet, the structure was not well defined due to the complexity of the geology and the sparse sampling data. This hindered the variograms capability to detect variation within the incremental lag spacing that was set at 290 feet. Changing the incremental lag spacing 290 feet to 200 feet, this assisted in defining the structure near the origin. Figure A-5 presents the new experimental variogram showing two points between the origin and 400 feet. The reduction in the incremental lag spacing caused greater scatter in variance at further points in Figure A-5 than in Figure A-4. This highlights the importance of conducting several iterations of variogram development.

Both of these experimental variograms were utilized in the model variogram development as discussed in Chapter III. Figure A-4 assisted in determining the variogram sill with its relatively good structure beyond 400 feet and Figure A-5 was important to verify the lower end structure with additional variance points less than 400

feet. These lower end points assisted in defining the model variogram shape and verification of a nugget effect.

In the example problem an assumption was made that the variogram was isotropic with no anisotropic structures within the aquifer. Given the complexity and randomness of the depositional structures within the aquifer, modeling the random anisotropic structures would be futile and was beyond the presentation of the methodology in this thesis. Therefore, the experimental variograms developed were considered omni-directional as illustrated in Figures A-4 and A-5 by the Direction and Tolerance parameters set at 0.0 and 90°, respectively.

Figure A-4. Experimental variogram for log-normal sample data with a maximum lag of 1200 feet and an incremental lag spacing of 290 feet.

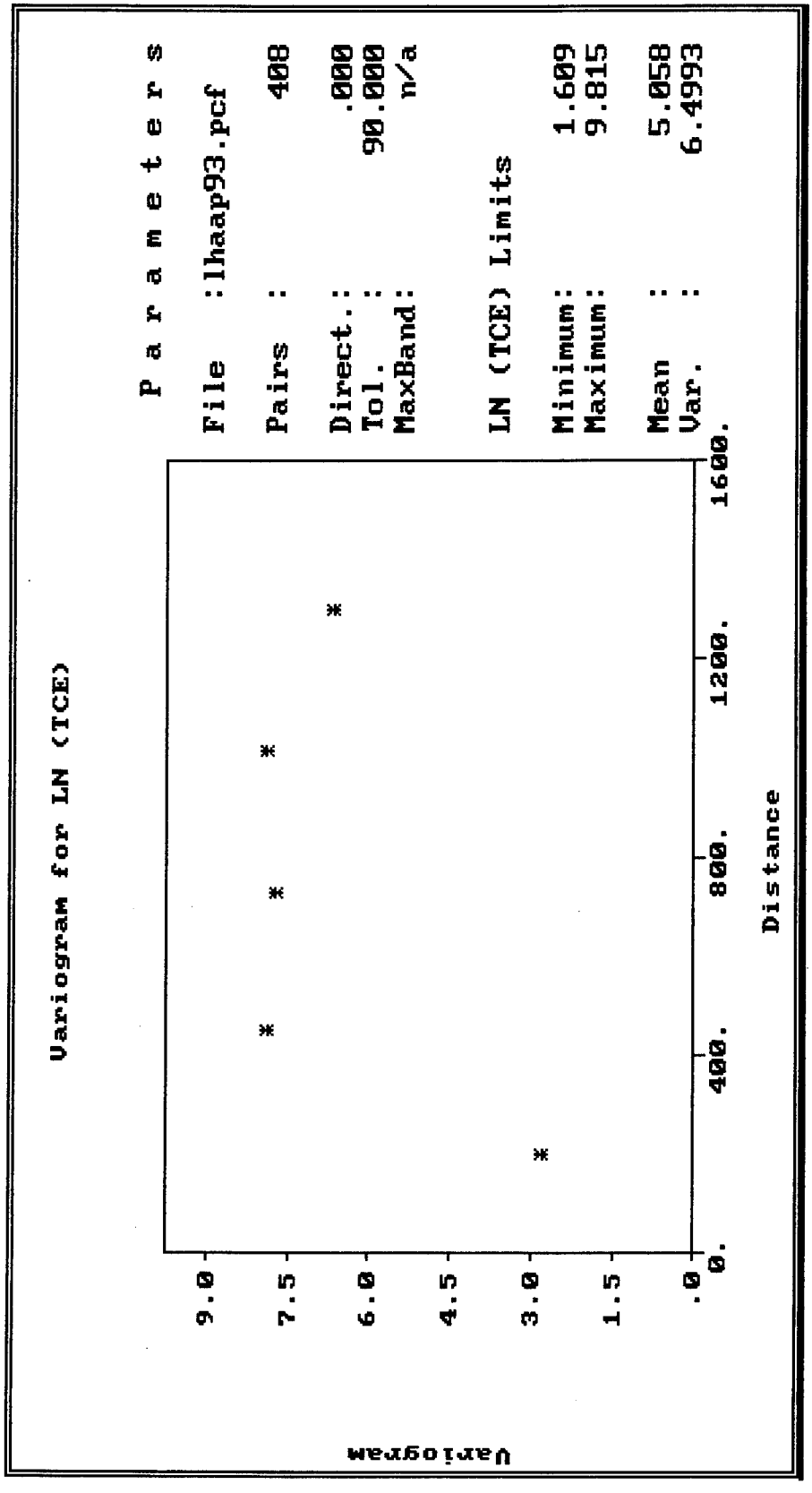

Figure A-5. Experimental variogram for log-normal sample data with a maximum lag of 1200 feet and an incremental lag spacing of 200 feet.

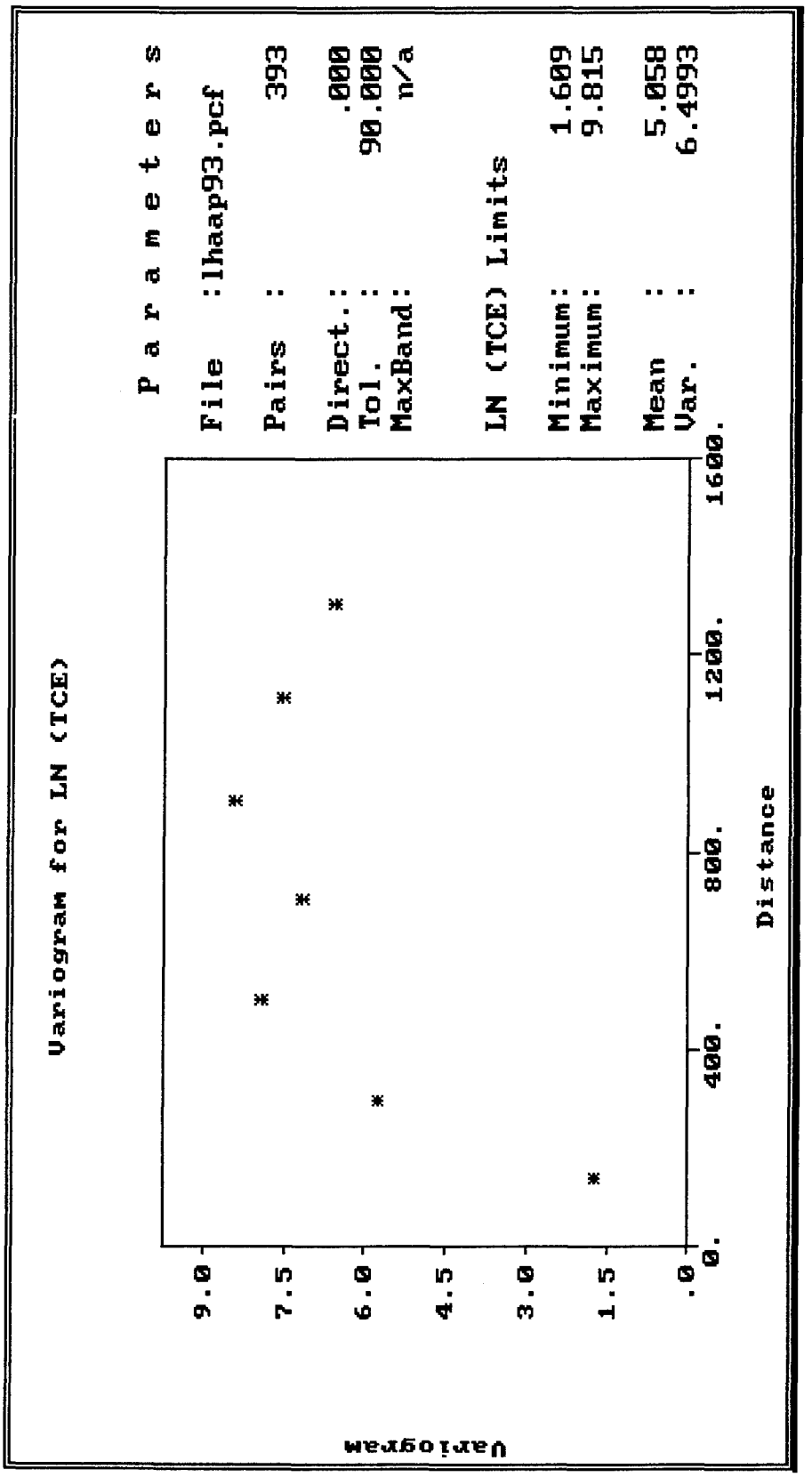

Variogram Cross-Validation

Using the evaluation criteria outlined early in the appendix and in Chapter III, the following results were found during the cross-validation analysis.

- Mean kriging error should be close to zero.

  The mean kriging error was equal to .283 (see Table A-2).

- Standard deviation of the kriging errors should be lower than the standard deviation of the regionalized variable.

  Standard deviation of the kriged errors is 2.384 which was lower than the standard deviation of the regionalized variable of 2.585 (see Table A-2).

- Standard deviation of the standardized errors should be close to unity or 1.0.

  The standardized errors standard deviation was .836 (see Table A-2).

- The standardized errors (zscore) should be independent of the kriged values (Journel and Huijbregts, 1978).

  Figure A-6 illustrates a scatter plot of zscore (y-axis) and the kriged values (zstar on x-axis), which showed little correlation. The correlation coefficient .247 indicated some correlation but was too low to indicate any correlation.

- The standardized errors (zscore) should be independent of their location as expressed by their x- and y-coordinates.

  Figure A-7 illustrating a scatter plot of zscore (y-axis) with both the x- and y-coordinates, easting and northing respectively, showed very little correlation. The correlation coefficients were .048 and .099 for easting and northing respectively.

- The kriged value should be positively correlated with the observed value of the regionalized variable.

  Figure A-8 illustrated in a scatter plot that the kriged value had some correlation with the observed value. The correlation value was low at .431 but high enough to show correlation.

- It is important for the final theoretical variogram model to closely approximate the observed variogram of the data.

  Figures 35 and 36 from Chapter IV illustrated close approximation of the variogram model to the experimental variogram.

Table A-2 summarizes the XVALID results illustrating the mean and standard deviation for the variable, kriged estimate, kriging error and kriging standardized error. The significance of these values were given in the previous summary paragraph.

Table A-2. Cross-validation results table for the model variogram.

	Mean	Standard Deviation
Variable sample point value (Z)	5.058	2.585
Kriged estimate at sample point (Z^*)	5.443	1.586
Kriging error	.283	2.384
Kriging standardized error	2.082	.836

The following four figures are the correlation plots used in the validation of the variogram model. Figure A-6 presented the correlation of kriging standardized error to the kriged estimate for TCE concentrations. The calculated correlation coefficient was .247 indicating some correlation but was not significant. If correlation were zero then the slope of the line in the figure would be zero and few points should occur on the line. Figures A-7 and A-8 are correlation plots of the kriging standardized error to the East and North coordinates. These figures are the same as Figure A-6 in that they exhibited no correlation as shown by the correlation coefficient and the zero slope of the line. Figure A-9 presents the correlation of the kriged estimate (Zstar) to the log-normal transformed measured TCE concentration. The correlation was positive with a line slope of .264 and coefficient of .431.

Figure A-6. Scatter plot of the standardized errors (zscore) versus the kriged values (zstar).

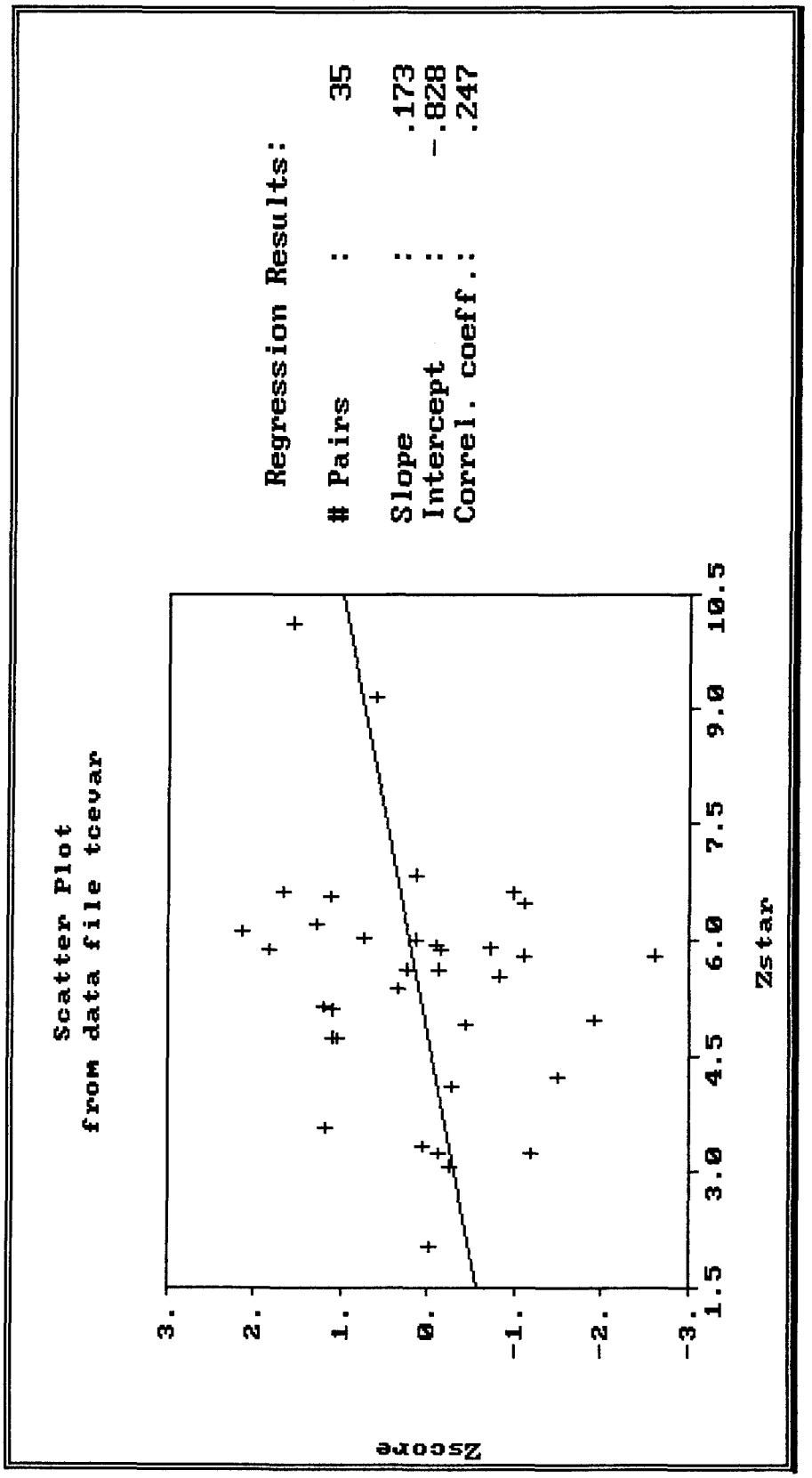

Figure A-7. Scatter plot of the standardized errors (zscore) versus the x-coordinate (easting).

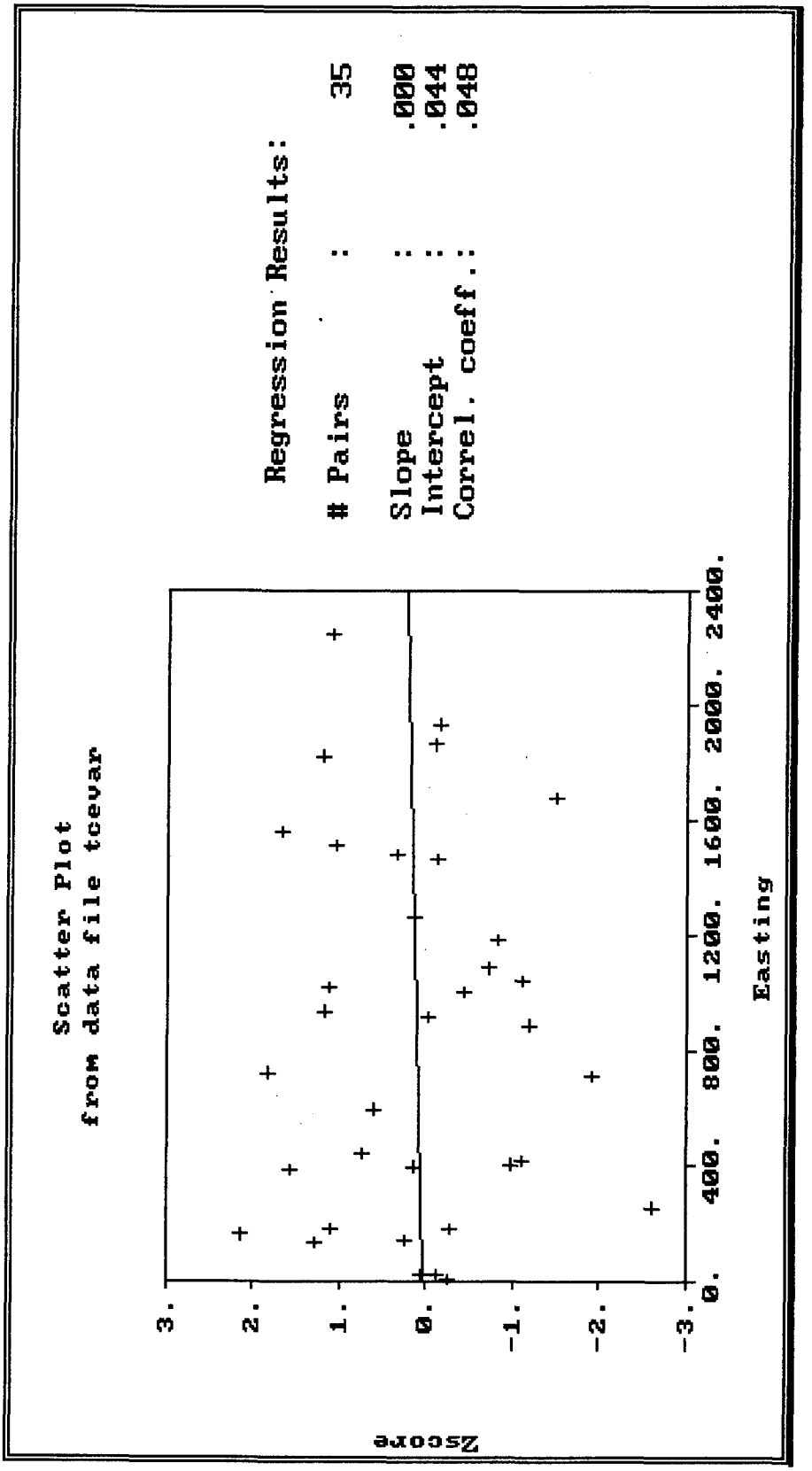

Figure A-8. Scatter plot of the standardized errors (zscore) versus the y-coordinate (northing).

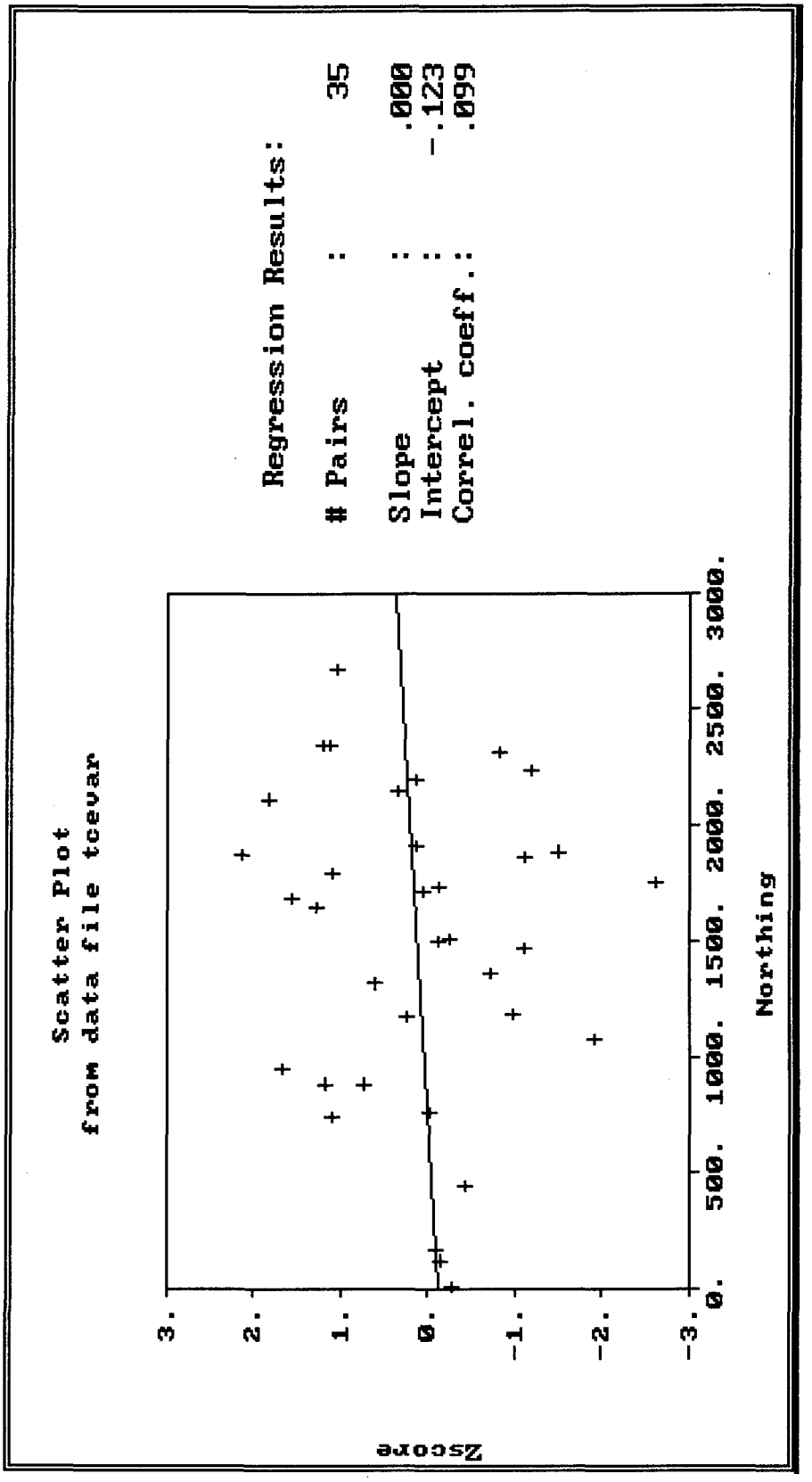

Figure A-9. Scatter plot of the kriged values (zstar) versus the sample point values (TCE).

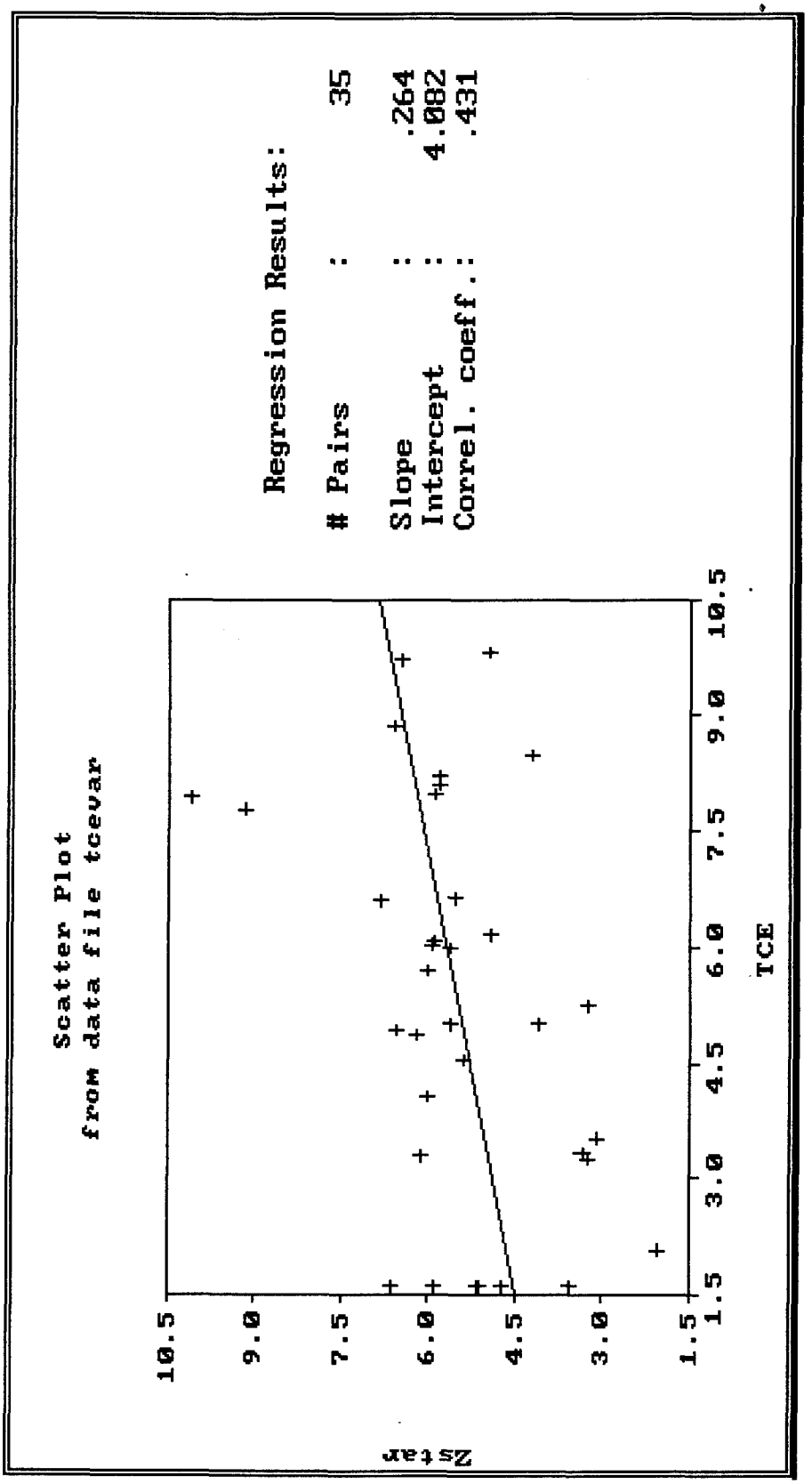

Sample Data Declustering

Tool Utilized and Methods Applied

The program DECLUS (Deutsch, 1989) provides an algorithm for determining three-dimensional declustering weights in cases where the sample site clusters are known to be clustered preferentially in either high or low valued-areas (Deutsch and Journel, 1992). Since the monitoring wells were installed to locate the contaminant plume, the resulting monitoring data would be skewed with contaminant concentration measurements. The DECLUS program takes this into account and assigns weights to the sample data based on their clustering. That is, a sample point that was located away from other sample points would have a higher weight than one located in a cluster of sample points.

Results of Declustering

Using the same sample data from the monitoring wells, DECLUS calculated the decluster weights for each of the sample points as summarized in Table A-3. In addition to the declustering weights shown in the table, the measured TCE concentration and log-normal transformed concentrations were given for each monitoring well. From Table A-4 the decluster weights for MW-10, MW-12 and MW-14 were less than one due to their clustered location as shown in Figure 9 of Chapter II. Other wells that were not clustered but isolated by great distances, such as C-6, C-7 and C-10, had decluster weights greater

than one and in some cases greater than two or three as seen in Table A-4. Therefore the isolated sampling data was given a higher weighting than the clustered data.

Table (4-4). Table of sample point values and their corresponding weights.

Monitoring Well	Measured Conc. (ug/l)	Transformed Conc. (ln ug/l)	Decluster Weight
C-01	475	6.1633	1.3638
C-02	26	3.2581	0.8355
C-03	5	1.6094	0.6831
C-04	5	1.6094	0.9578
C-05	5	1.6094	1.8407
C-06	139	4.9345	3.0989
C-07	150	5.0106	1.6535
C-08	5	1.6094	1.0196
C-09	420	6.0403	2.0121
C-10	440	6.0868	2.1174
MW-1	16500	9.7111	0.6750
MW-3	740	6.6067	0.6783
MW-4	760	6.6333	0.6766
MW-5	140	4.9416	0.6965
MW-6	190	5.247	0.7055
MW-7	18300	9.8147	0.7857
MW-8	7100	8.8679	0.7245
MW-9	3325	8.1092	0.7232
MW-10	130	4.8675	0.7966
MW-11	300	5.7038	0.7844
MW-12	3650	8.2025	0.7902
MW-13	28	3.3322	0.8458
MW-14	2800	7.9374	0.7426
MW-16	27	3.2958	0.8383
MW-17	34	3.5264	0.8051
MW-18	150	5.0106	0.7380
MW-19	59	4.0775	0.9607
MW-20	8	2.0794	1.0449
MW-21	4850	8.4867	0.6834
MW-22	406	6.0064	0.7362
MW-23	2930	7.9828	0.6774
102	5	1.6094	0.9515
109	94	4.5433	0.6810
124	5	1.6094	0.7387
126	5	1.6094	1.1484
129	2400	7.7832	0.7121
130	5	1.6094	1.0668

VITA

Todd A. Wang

Candidate for the Degree of

Master of Science

Thesis: A MULTILEVEL DECISION ANALYSIS METHOD FOR REMEDIATION OF CONTAMINATED SITES UNDER CONDITIONS OF UNCERTAINTY

Major Field: Environmental Engineering

Biographical:

[redacted], the son of John and Eileen Wang.

Civilian Education: Graduated from Liberal High School, Liberal, Kansas in May 1981; received Associate of Science degree from Dodge City Community College, Dodge City, Kansas in May 1983; received Bachelor of Science degree in Geological Engineering from Colorado School of Mines, Golden, Colorado in December 1986. Will complete the requirements for a Master of Science degree in Environmental Engineering from Oklahoma State University, Stillwater, Oklahoma in December 1995.

Military Education: Graduated from the United States Army Engineer Officers Basic Course, Fort Belvoir, Virginia in June 1987. Graduated from the United States Army Engineer Officers Advance Course, Fort Leonard Wood, Missouri in August 1991. Graduated from the United States Army Combined Arms Service and Staff School, Fort Leavenworth, Kansas in May 1994.

Experience: Served as a platoon leader, company executive officer and battalion staff officer for the 43rd Engineer Combat Battalion, Fort Benning, Georgia. Led and planned military operations with the battalion in overseas deployments to Honduras, Costa Rica and Saudi Arabia. Served as a company commander and battalion staff officer for the 536th Engineer Combat Battalion, Fort Kobbe, Republic of Panama. Led and planned military operations with the battalion in deployments throughout Central and South America.

Professional Memberships: Society of American Military Engineers.

Figure 56. Decision Tree of Example Problem

(2)

ble Problem Showing all Sub-branches

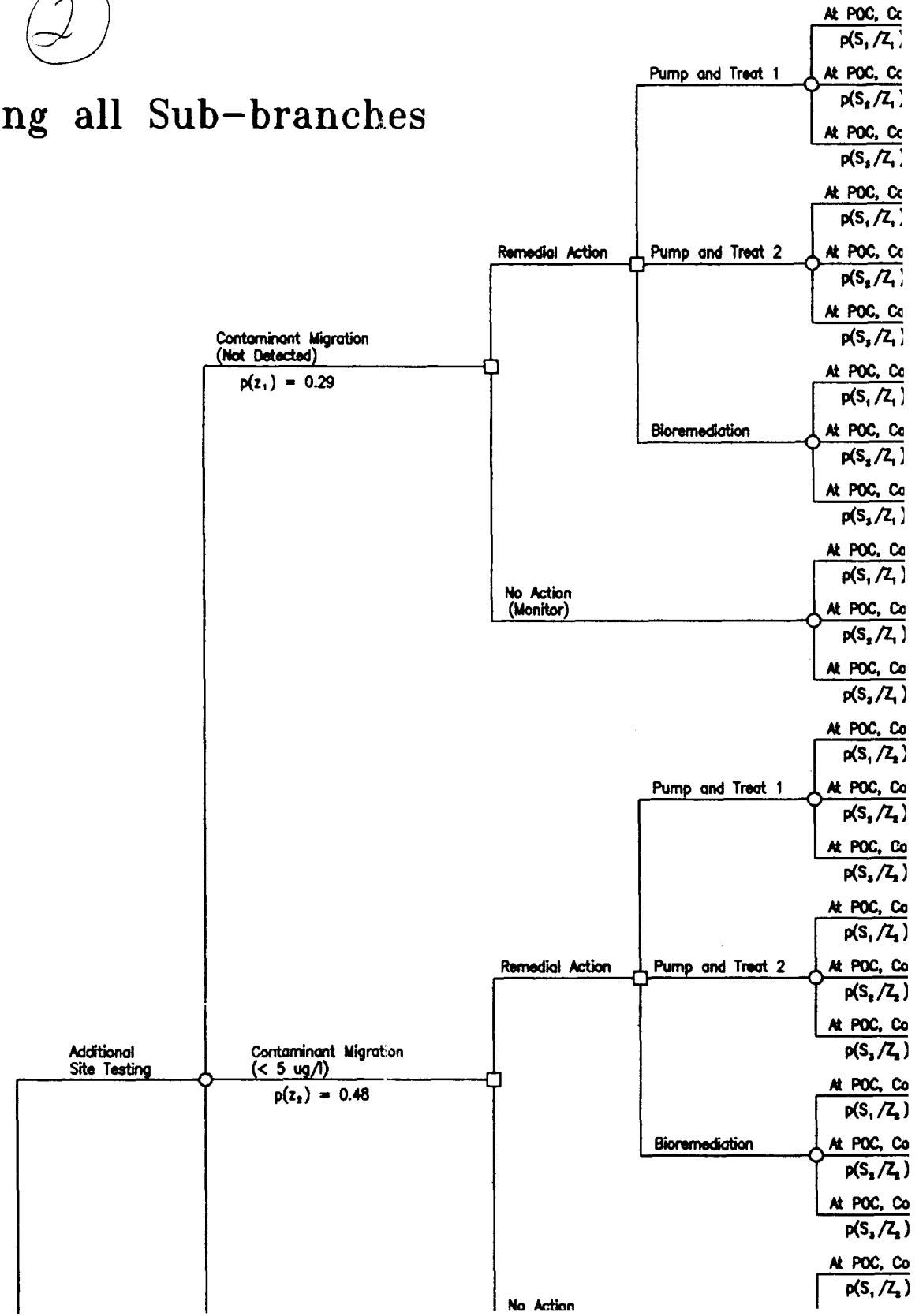

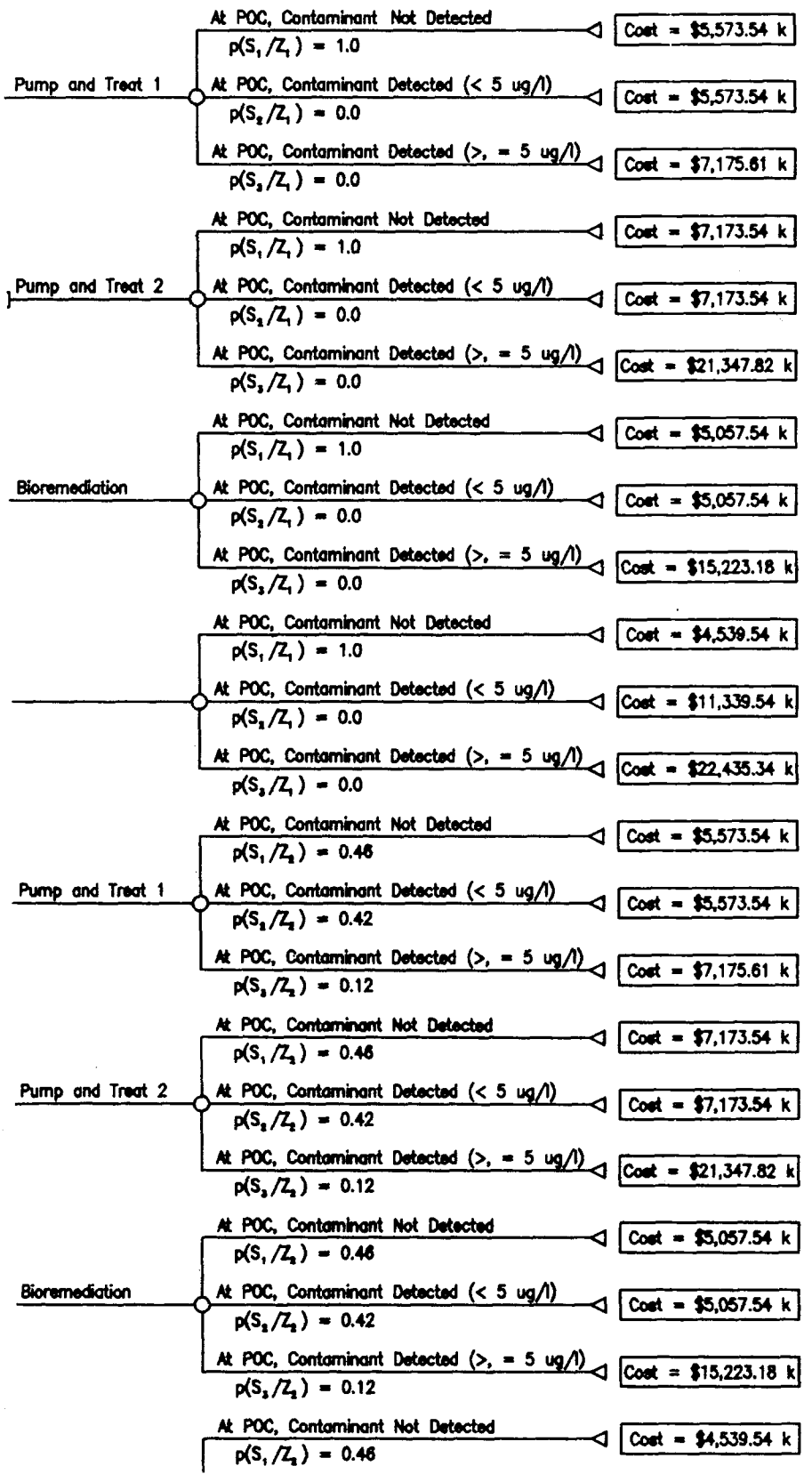
Pump and Treat 1
At POC, Contaminant Not Detected
p(S1/Z1) = 1.0
Cost = $5,573.54 k
At POC, Contaminant Detected (< 5 ug/l)
p(S2/Z1) = 0.0
Cost = $5,573.54 k
At POC, Contaminant Detected (>, = 5 ug/l)
p(S3/Z1) = 0.0
Cost = $7,175.61 k
Pump and Treat 2
At POC, Contaminant Not Detected
p(S1/Z1) = 1.0
Cost = $7,173.54 k
At POC, Contaminant Detected (< 5 ug/l)
p(S2/Z1) = 0.0
Cost = $7,173.54 k
At POC, Contaminant Detected (>, = 5 ug/l)
p(S3/Z1) = 0.0
Cost = $21,347.82 k
Bioremediation
At POC, Contaminant Not Detected
p(S1/Z1) = 1.0
Cost = $5,057.54 k
At POC, Contaminant Detected (< 5 ug/l)
p(S2/Z1) = 0.0
Cost = $5,057.54 k
At POC, Contaminant Detected (>, = 5 ug/l)
p(S3/Z1) = 0.0
Cost = $15,223.18 k
At POC, Contaminant Not Detected
p(S1/Z1) = 1.0
Cost = $4,539.54 k
At POC, Contaminant Detected (< 5 ug/l)
p(S2/Z1) = 0.0
Cost = $11,339.54 k
At POC, Contaminant Detected (>, = 5 ug/l)
p(S3/Z1) = 0.0
Cost = $22,435.34 k
Pump and Treat 1
At POC, Contaminant Not Detected
p(S1/Z2) = 0.46
Cost = $5,573.54 k
At POC, Contaminant Detected (< 5 ug/l)
p(S2/Z2) = 0.42
Cost = $5,573.54 k
At POC, Contaminant Detected (>, = 5 ug/l)
p(S3/Z2) = 0.12
Cost = $7,175.61 k
Pump and Treat 2
At POC, Contaminant Not Detected
p(S1/Z2) = 0.46
Cost = $7,173.54 k
At POC, Contaminant Detected (< 5 ug/l)
p(S2/Z2) = 0.42
Cost = $7,173.54 k
At POC, Contaminant Detected (>, = 5 ug/l)
p(S3/Z2) = 0.12
Cost = $21,347.82 k
Bioremediation
At POC, Contaminant Not Detected
p(S1/Z2) = 0.46
Cost = $5,057.54 k
At POC, Contaminant Detected (< 5 ug/l)
p(S2/Z2) = 0.42
Cost = $5,057.54 k
At POC, Contaminant Detected (>, = 5 ug/l)
p(S3/Z2) = 0.12
Cost = $15,223.18 k
At POC, Contaminant Not Detected
p(S1/Z2) = 0.46
Cost = $4,539.54 k

(3)

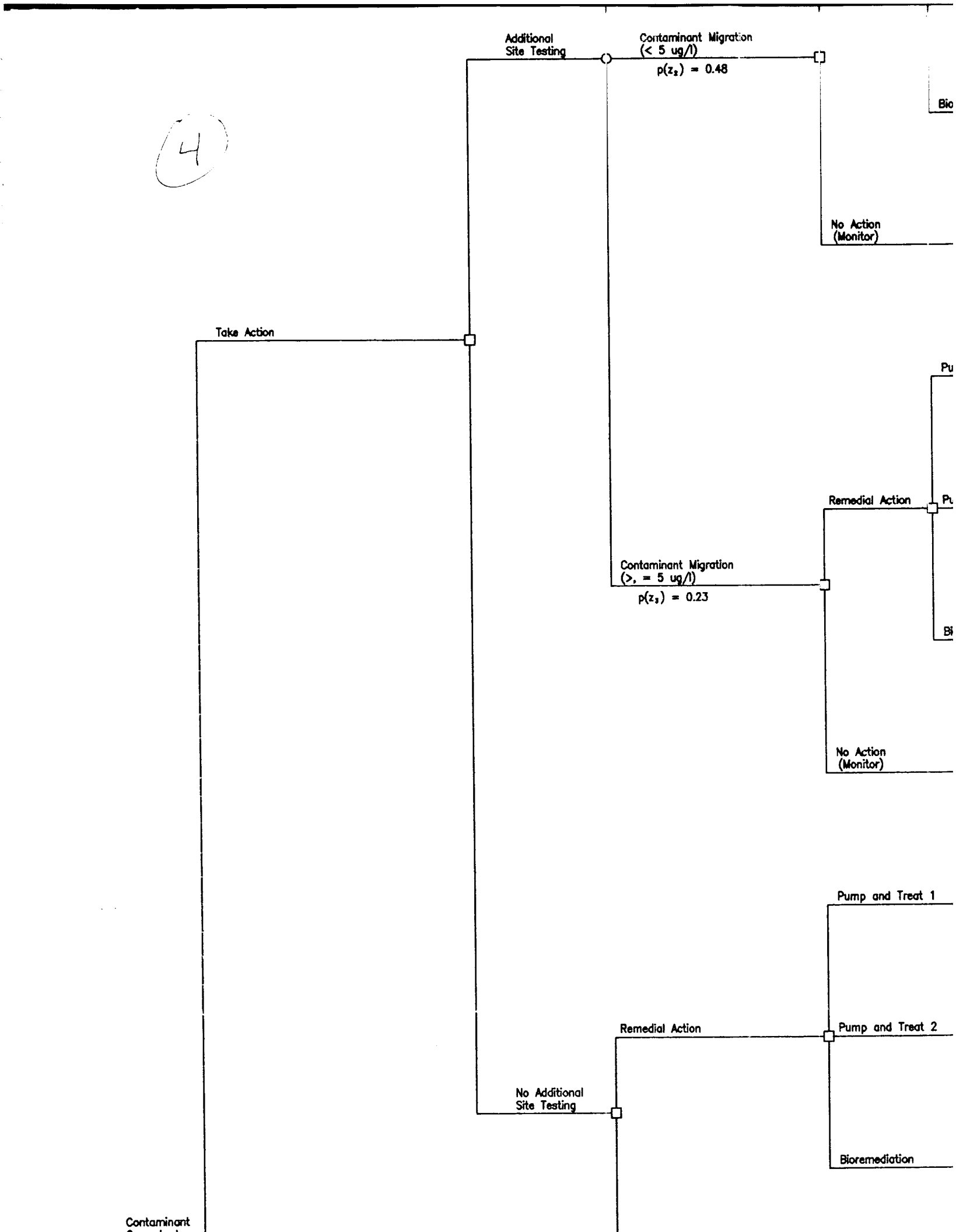
4
Additional Site Testing
Contaminant Migration (< 5 ug/l)
p(z₂) = 0.48
No Action (Monitor)
Take Action
Remedial Action
Contaminant Migration (>, = 5 ug/l)
p(z₃) = 0.23
No Action (Monitor)
Pump and Treat 1
Remedial Action
Pump and Treat 2
No Additional Site Testing
Bioremediation

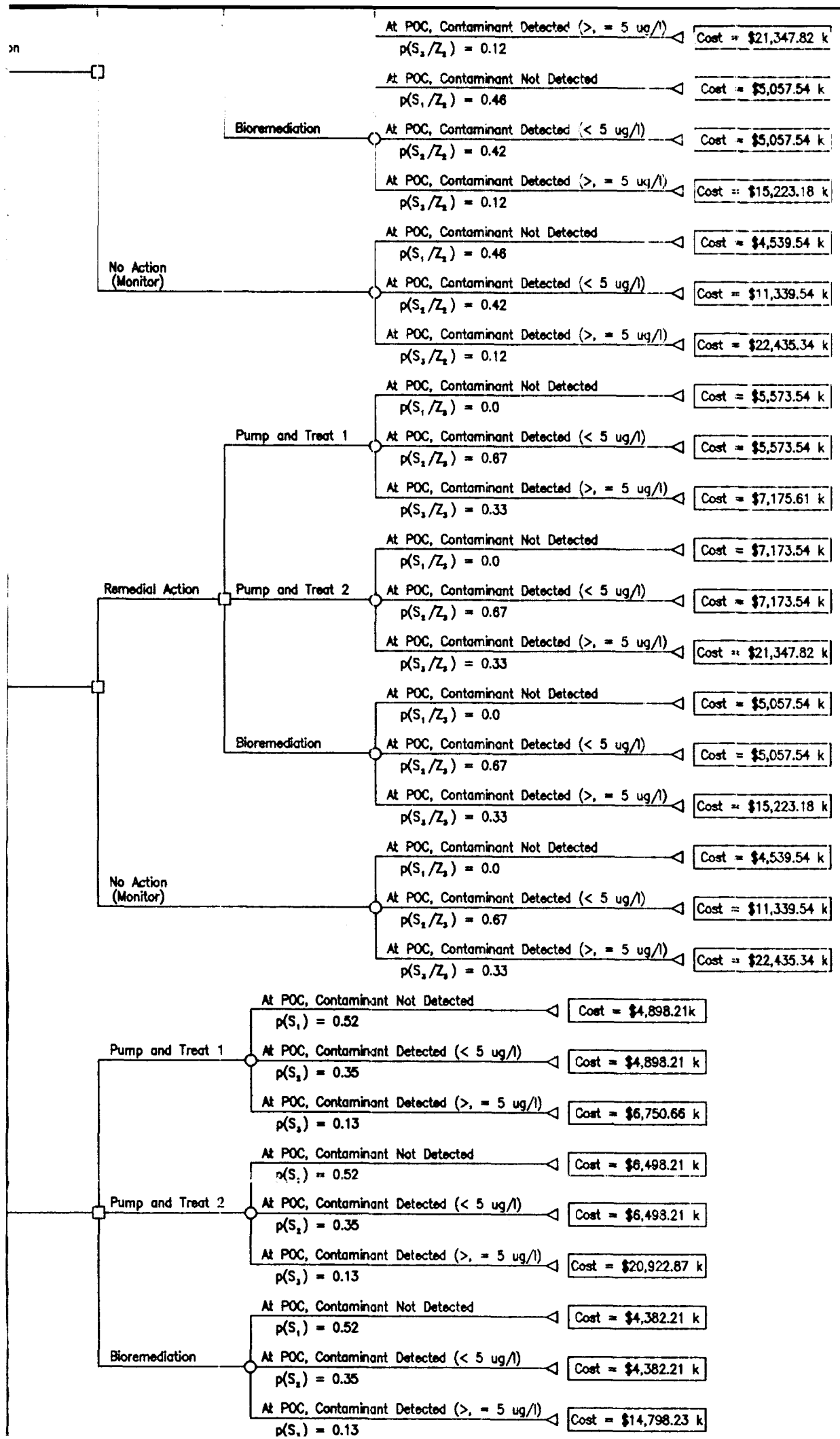
At POC, Contaminant Detected (>, = 5 ug/l)
p(S3/Z1) = 0.12
Cost = $21,347.82 k
At POC, Contaminant Not Detected
p(S1/Z1) = 0.46
Cost = $5,057.54 k
Bioremediation
At POC, Contaminant Detected (< 5 ug/l)
p(S2/Z1) = 0.42
Cost = $5,057.54 k
At POC, Contaminant Detected (>, = 5 ug/l)
p(S3/Z1) = 0.12
Cost = $15,223.18 k
At POC, Contaminant Not Detected
p(S1/Z2) = 0.46
Cost = $4,539.54 k
No Action (Monitor)
At POC, Contaminant Detected (< 5 ug/l)
p(S2/Z2) = 0.42
Cost = $11,339.54 k
At POC, Contaminant Detected (>, = 5 ug/l)
p(S3/Z2) = 0.12
Cost = $22,435.34 k
At POC, Contaminant Not Detected
p(S1/Z3) = 0.0
Cost = $5,573.54 k
Pump and Treat 1
At POC, Contaminant Detected (< 5 ug/l)
p(S2/Z3) = 0.67
Cost = $5,573.54 k
At POC, Contaminant Detected (>, = 5 ug/l)
p(S3/Z3) = 0.33
Cost = $7,175.61 k
At POC, Contaminant Not Detected
p(S1/Z3) = 0.0
Cost = $7,173.54 k
Remedial Action
Pump and Treat 2
At POC, Contaminant Detected (< 5 ug/l)
p(S2/Z3) = 0.67
Cost = $7,173.54 k
At POC, Contaminant Detected (>, = 5 ug/l)
p(S3/Z3) = 0.33
Cost = $21,347.82 k
At POC, Contaminant Not Detected
p(S1/Z3) = 0.0
Cost = $5,057.54 k
Bioremediation
At POC, Contaminant Detected (< 5 ug/l)
p(S2/Z3) = 0.67
Cost = $5,057.54 k
At POC, Contaminant Detected (>, = 5 ug/l)
p(S3/Z3) = 0.33
Cost = $15,223.18 k
At POC, Contaminant Not Detected
p(S1/Z3) = 0.0
Cost = $4,539.54 k
No Action (Monitor)
At POC, Contaminant Detected (< 5 ug/l)
p(S2/Z3) = 0.67
Cost = $11,339.54 k
At POC, Contaminant Detected (>, = 5 ug/l)
p(S3/Z3) = 0.33
Cost = $22,435.34 k
At POC, Contaminant Not Detected
p(S1) = 0.52
Cost = $4,898.21k
Pump and Treat 1
At POC, Contaminant Detected (< 5 ug/l)
p(S2) = 0.35
Cost = $4,898.21 k
At POC, Contaminant Detected (>, = 5 ug/l)
p(S3) = 0.13
Cost = $6,750.66 k
At POC, Contaminant Not Detected
p(S1) = 0.52
Cost = $6,498.21 k
Pump and Treat 2
At POC, Contaminant Detected (< 5 ug/l)
p(S2) = 0.35
Cost = $6,498.21 k
At POC, Contaminant Detected (>, = 5 ug/l)
p(S3) = 0.13
Cost = $20,922.87 k
At POC, Contaminant Not Detected
p(S1) = 0.52
Cost = $4,382.21 k
Bioremediation
At POC, Contaminant Detected (< 5 ug/l)
p(S2) = 0.35
Cost = $4,382.21 k
At POC, Contaminant Detected (>, = 5 ug/l)
p(S3) = 0.13
Cost = $14,798.23 k

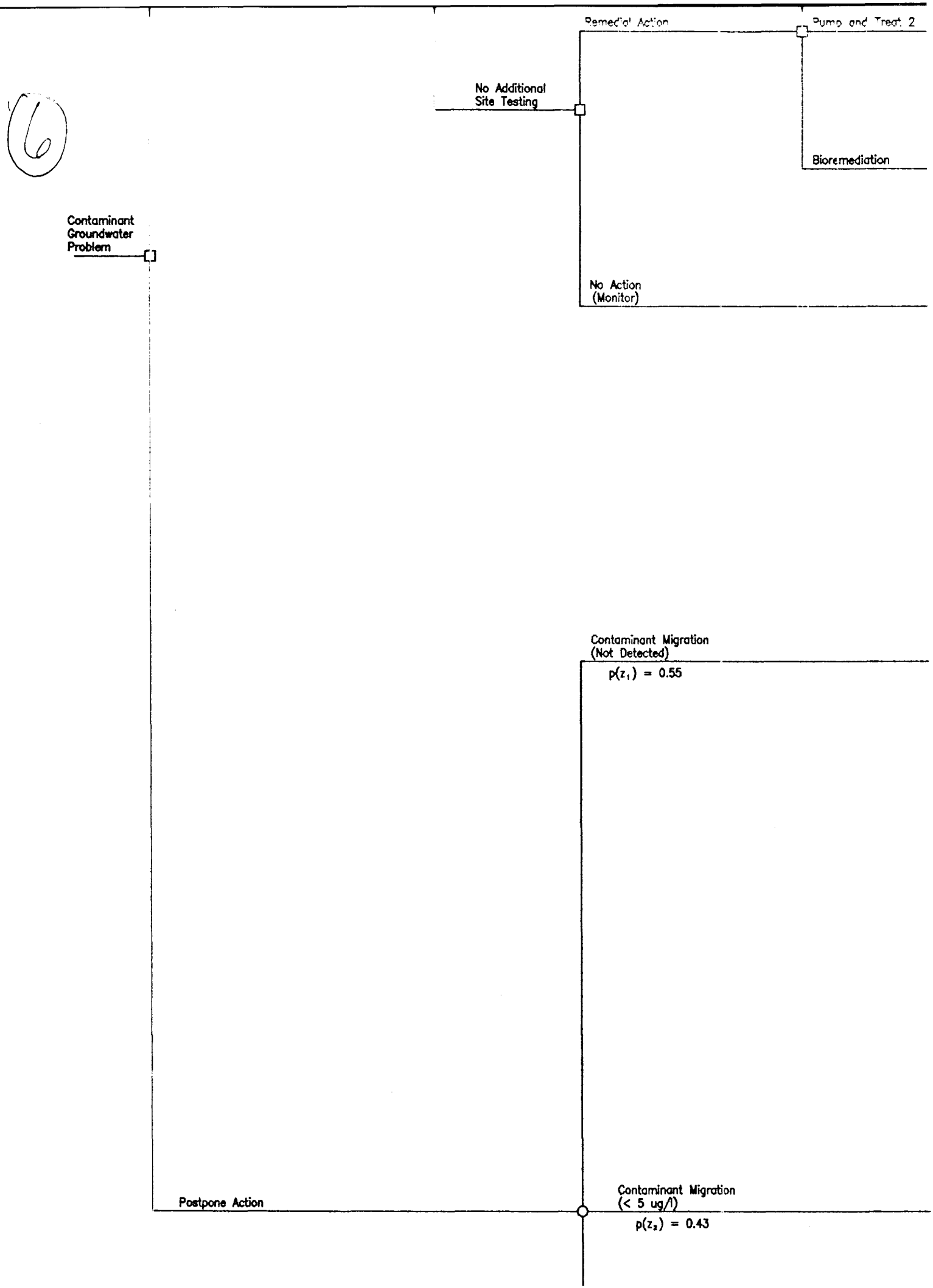
6
Remedial Action
Pump and Treat 2
No Additional
Site Testing
Bioremediation
Contaminant
Groundwater
Problem
No Action
(Monitor)
Contaminant Migration
(Not Detected)
$p(z_1) = 0.55$
Postpone Action
Contaminant Migration
(< 5 ug/l)
$p(z_2) = 0.43$

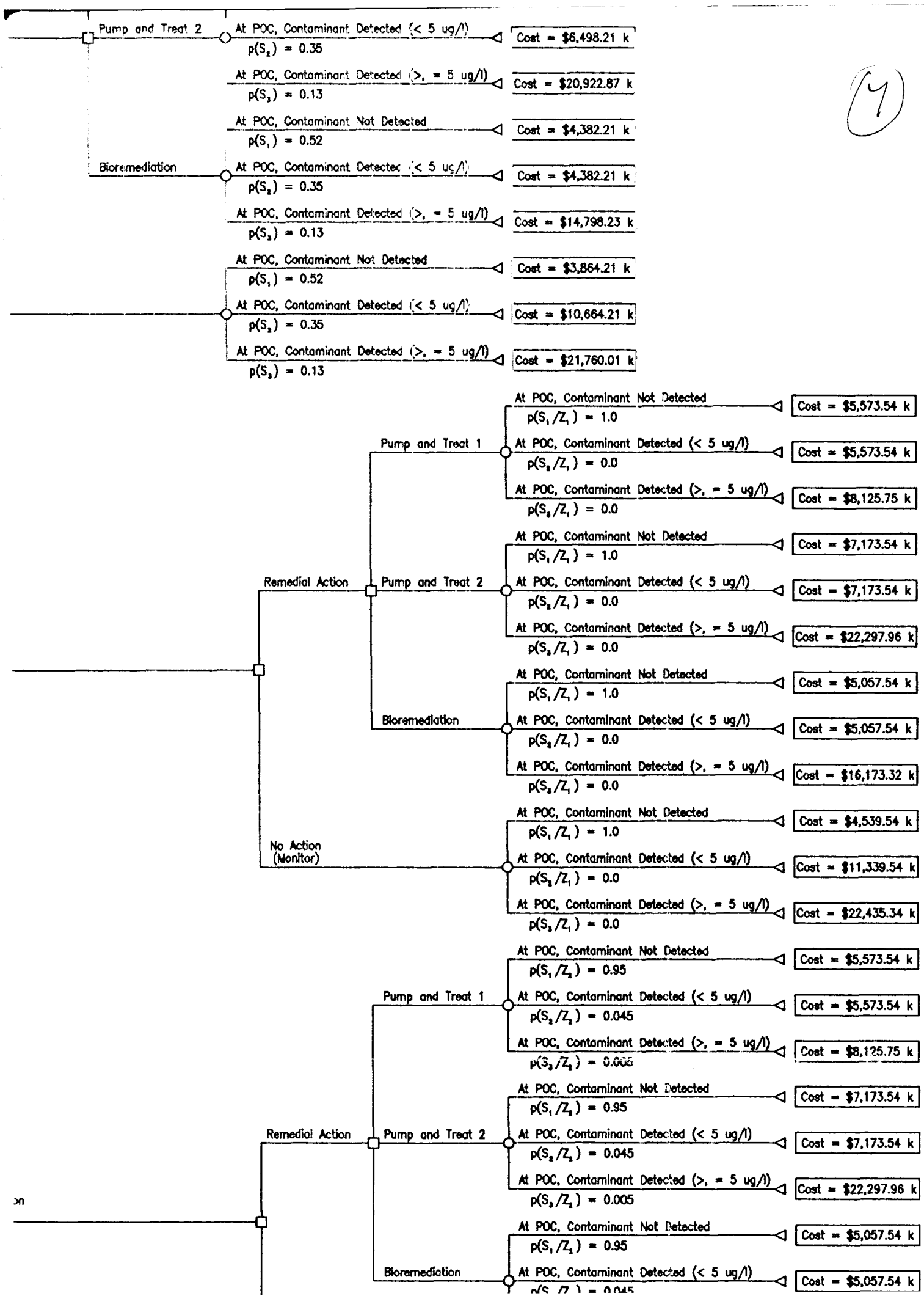
Pump and Treat 2
At POC, Contaminant Detected (< 5 ug/l)
p(S1) = 0.35
Cost = $6,498.21 k
At POC, Contaminant Detected (>, = 5 ug/l)
p(S3) = 0.13
Cost = $20,922.87 k
At POC, Contaminant Not Detected
p(S1) = 0.52
Cost = $4,382.21 k
Bioremediation
At POC, Contaminant Detected (< 5 ug/l)
p(S2) = 0.35
Cost = $4,382.21 k
At POC, Contaminant Detected (>, = 5 ug/l)
p(S3) = 0.13
Cost = $14,798.23 k
At POC, Contaminant Not Detected
p(S1) = 0.52
Cost = $3,864.21 k
At POC, Contaminant Detected (< 5 ug/l)
p(S2) = 0.35
Cost = $10,664.21 k
At POC, Contaminant Detected (>, = 5 ug/l)
p(S3) = 0.13
Cost = $21,760.01 k
Remedial Action
Pump and Treat 1
At POC, Contaminant Not Detected
p(S1/Z1) = 1.0
Cost = $5,573.54 k
At POC, Contaminant Detected (< 5 ug/l)
p(S2/Z1) = 0.0
Cost = $5,573.54 k
At POC, Contaminant Detected (>, = 5 ug/l)
p(S3/Z1) = 0.0
Cost = $8,125.75 k
Pump and Treat 2
At POC, Contaminant Not Detected
p(S1/Z1) = 1.0
Cost = $7,173.54 k
At POC, Contaminant Detected (< 5 ug/l)
p(S2/Z1) = 0.0
Cost = $7,173.54 k
At POC, Contaminant Detected (>, = 5 ug/l)
p(S3/Z1) = 0.0
Cost = $22,297.96 k
Bioremediation
At POC, Contaminant Not Detected
p(S1/Z1) = 1.0
Cost = $5,057.54 k
At POC, Contaminant Detected (< 5 ug/l)
p(S2/Z1) = 0.0
Cost = $5,057.54 k
At POC, Contaminant Detected (>, = 5 ug/l)
p(S3/Z1) = 0.0
Cost = $16,173.32 k
No Action
(Monitor)
At POC, Contaminant Not Detected
p(S1/Z1) = 1.0
Cost = $4,539.54 k
At POC, Contaminant Detected (< 5 ug/l)
p(S2/Z1) = 0.0
Cost = $11,339.54 k
At POC, Contaminant Detected (>, = 5 ug/l)
p(S3/Z1) = 0.0
Cost = $22,435.34 k
Remedial Action
Pump and Treat 1
At POC, Contaminant Not Detected
p(S1/Z2) = 0.95
Cost = $5,573.54 k
At POC, Contaminant Detected (< 5 ug/l)
p(S2/Z2) = 0.045
Cost = $5,573.54 k
At POC, Contaminant Detected (>, = 5 ug/l)
p(S3/Z2) = 0.005
Cost = $8,125.75 k
Pump and Treat 2
At POC, Contaminant Not Detected
p(S1/Z2) = 0.95
Cost = $7,173.54 k
At POC, Contaminant Detected (< 5 ug/l)
p(S2/Z2) = 0.045
Cost = $7,173.54 k
At POC, Contaminant Detected (>, = 5 ug/l)
p(S3/Z2) = 0.005
Cost = $22,297.96 k
Bioremediation
At POC, Contaminant Not Detected
p(S1/Z2) = 0.95
Cost = $5,057.54 k
At POC, Contaminant Detected (< 5 ug/l)
p(S2/Z2) = 0.045
Cost = $5,057.54 k

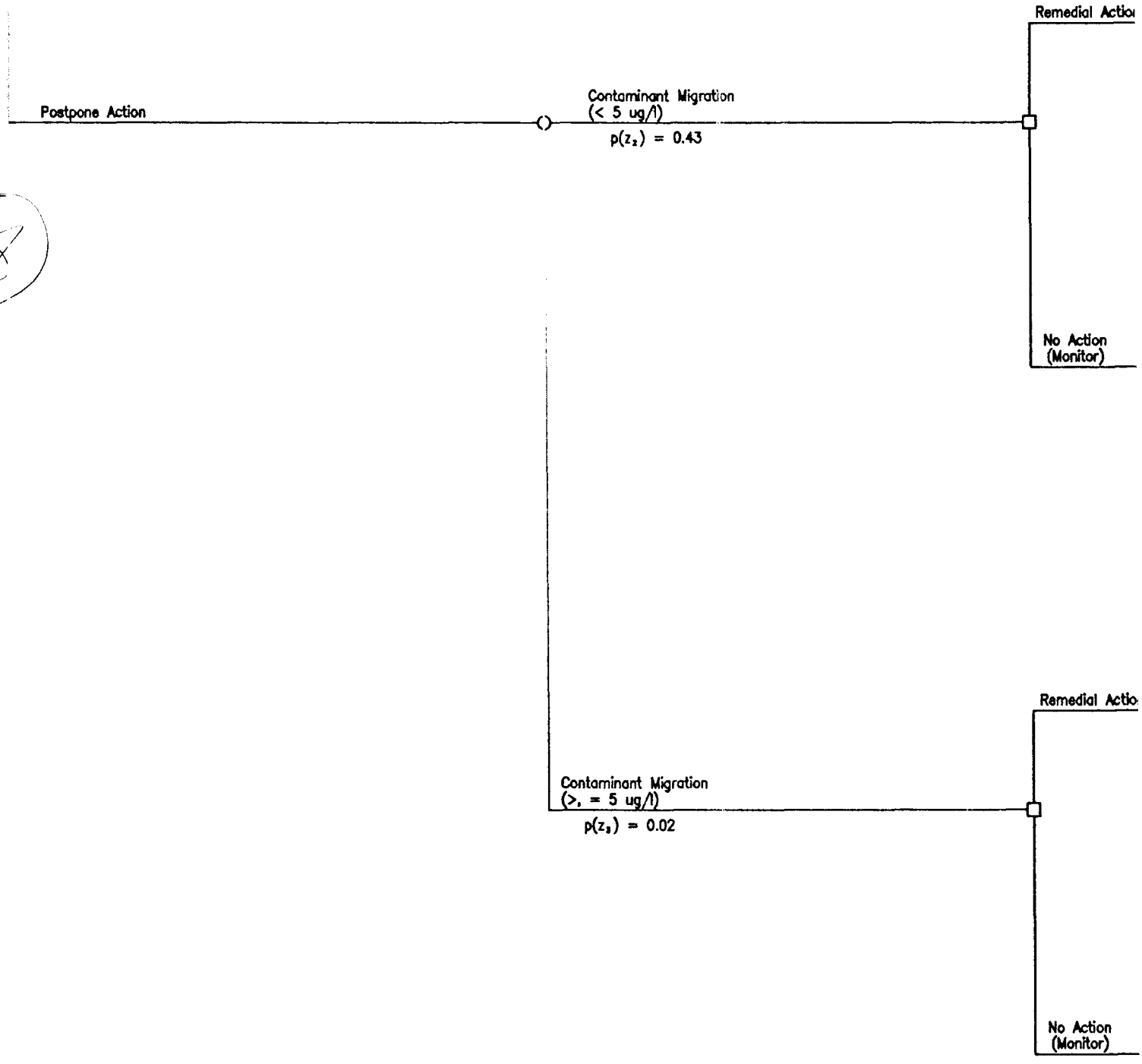
Remedial Actio
Postpone Action
Contaminant Migration
(< 5 ug/l)
p(z2) = 0.43
No Action
(Monitor)
Remedial Actio
Contaminant Migration
(>, = 5 ug/l)
p(z1) = 0.02
No Action
(Monitor)

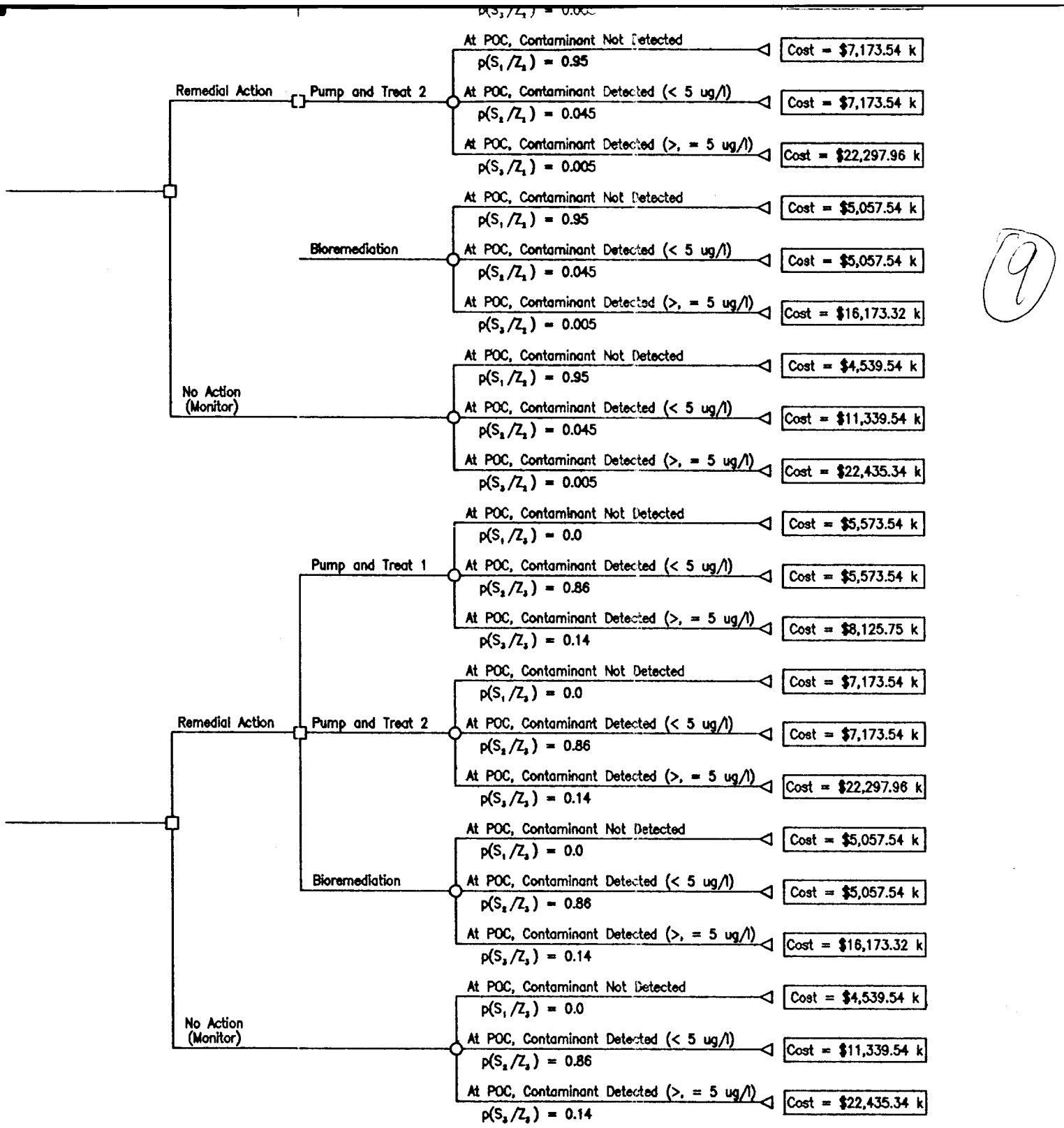
Remedial Action
Pump and Treat 2
At POC, Contaminant Not Detected
p(S1 /Z1) = 0.95
Cost = $7,173.54 k
At POC, Contaminant Detected (< 5 ug/l)
p(S2 /Z1) = 0.045
Cost = $7,173.54 k
At POC, Contaminant Detected (>, = 5 ug/l)
p(S3 /Z1) = 0.005
Cost = $22,297.96 k
Bioremediation
At POC, Contaminant Not Detected
p(S1 /Z2) = 0.95
Cost = $5,057.54 k
At POC, Contaminant Detected (< 5 ug/l)
p(S2 /Z2) = 0.045
Cost = $5,057.54 k
At POC, Contaminant Detected (>, = 5 ug/l)
p(S3 /Z2) = 0.005
Cost = $16,173.32 k
No Action
(Monitor)
At POC, Contaminant Not Detected
p(S1 /Z3) = 0.95
Cost = $4,539.54 k
At POC, Contaminant Detected (< 5 ug/l)
p(S2 /Z3) = 0.045
Cost = $11,339.54 k
At POC, Contaminant Detected (>, = 5 ug/l)
p(S3 /Z3) = 0.005
Cost = $22,435.34 k
Remedial Action
Pump and Treat 1
At POC, Contaminant Not Detected
p(S1 /Z1) = 0.0
Cost = $5,573.54 k
At POC, Contaminant Detected (< 5 ug/l)
p(S2 /Z1) = 0.86
Cost = $5,573.54 k
At POC, Contaminant Detected (>, = 5 ug/l)
p(S3 /Z1) = 0.14
Cost = $8,125.75 k
Pump and Treat 2
At POC, Contaminant Not Detected
p(S1 /Z2) = 0.0
Cost = $7,173.54 k
At POC, Contaminant Detected (< 5 ug/l)
p(S2 /Z2) = 0.86
Cost = $7,173.54 k
At POC, Contaminant Detected (>, = 5 ug/l)
p(S3 /Z2) = 0.14
Cost = $22,297.96 k
Bioremediation
At POC, Contaminant Not Detected
p(S1 /Z3) = 0.0
Cost = $5,057.54 k
At POC, Contaminant Detected (< 5 ug/l)
p(S2 /Z3) = 0.86
Cost = $5,057.54 k
At POC, Contaminant Detected (>, = 5 ug/l)
p(S3 /Z3) = 0.14
Cost = $16,173.32 k
No Action
(Monitor)
At POC, Contaminant Not Detected
p(S1 /Z3) = 0.0
Cost = $4,539.54 k
At POC, Contaminant Detected (< 5 ug/l)
p(S2 /Z3) = 0.86
Cost = $11,339.54 k
At POC, Contaminant Detected (>, = 5 ug/l)
p(S3 /Z3) = 0.14
Cost = $22,435.34 k